U.PORTO

FEUP FACULDADE DE ENGENHARIA
UNIVERSIDADE DO PORTO

Development of Hydroxyapatite-Based Hybrid Materials for Biomedical Applications

Ph.D. Dissertation
in
Chemical and Biological Engineering
by

Gabriela Ruphuy Chan

Supervisors:
Maria Filomena Filipe Barreiro
Madalena Maria Gomes de Queiroz Dias

Laboratory of Separation and Reaction Engineering
Associate laboratory LSRE/LCM
Faculty of Engineering
University of Porto

October 2016

This work was in part financed by ProjectPOCI-01-0145-FEDER-006984 – Associate Laboratory LSRE-LCM – funded by FEDER – Fundo Europeu de Desenvolvimento Regional – through COMPETE2020 – Programa Operacional Competitividade e Internacionalização (POCI) e by national funds through FCT – Fundação para a Ciência e a Tecnologia.

Statement

This thesis includes experimental results obtained by Mariana Souto-Lopes, within the scope of her PhD studies, under the supervision of Prof. Maria Helena Fernandes and Christiane Salgado. The results correspond to the microbiological assay and the cytotoxicity test described from Sections 5.2.6.6 to 5.2.6.9. The analysis of such results was done in collaboration with Mariana as well. The experiments were carried out at the Laboratory for Bone Metabolism and Regeneration, Faculty of Dental Medicine of the University of Porto (FMDUP), Porto, Portugal.

Gabriela Ruphuy Prof. Filomena Barreiro Prof. Madalena Dias

To my parents and siblings

Nothing in life is to be feared, it is only to be understood.

Now is the time to understand more, so that we may fear less

Marie Skłodowska Curie

Acknowledgments

To the Laboratory of Separation and Reaction Engineering (LSRE), in the person of Professor Madalena Dias, for having provided the facilities and technical conditions needed to perform this work. To EStiG-IPB, in the person of Professor Luís Pais, for the support given during my long stays at LSRE-IPB.

I deeply thank my supervisor, Professor Filomena Barreiro, for her constant guidance, confidence and encouragement throughout this whole journey. Thank you for giving me the opportunity to pursuit and achieve this goal, for all the constructive criticism that helped me become a better scientist, and for your friendship.

I wish to profoundly thank my co-supervisor, Professor Madalena Dias, for her continuous support, advice, and motivation along the performance of this work.

I sincerely thank Professor Jose Carlos Lopes for his valuable advice and constructive criticism that contributed to the development of this work and to my scientific growth.

I would like to express my gratitude to Professor Fernando Monteiro for his advice and encouragement, and for his willingness to help always when needed.

To Mariana Lopes, Professor Maria Helena Fernandes and Christiane Salgado for their contribution for this thesis with the microbiological and cytotoxicity assays.

To my colleagues and friends at LSRE. To Marina for her help and friendship since I first arrived to LSRE-FEUP. I thank Marcelo for his friendship and scientific discussions. To Nelson, Rómulo, Carlos Teixeira, Joana, Cláudio, Carlos Fonte, Enis, Pelin, Anna, Jacqueline, Franzisca and Tobias, for their motivation and great moments that we shared during years. Thanks to Ricardo Santos for his assistance when needed. To Isabel Fernandes, Ainara Saralegi, Patrícia Costa, Yaidelin Manrique, Diana Paiva for their help in different stages of this work.

I wish to deeply thank to my parents and my siblings for their unconditional love, support and encouragement that helped me achieve this goal.

I would like to thank Jan for his patience and continuous encouragement, and to my friends Marina Manic, Marina Torres, Natalia, Víctor, Gabriela, Isabel, Karla, Melissa, Carolina, Fabián, Lautaro and Johanna for their constant motivation and friendship along these years.

I acknowledge Universidad de Costa Rica (UCR), Ministerio de Ciencia, Tecnología y Telecomunicaciones de Costa Rica (MICITT) and Consejo Nacional para Investigaciones Científicas y Tecnológicas (CONICIT) for my scholarship. I wish to thank Laboratorio Nacional de Nanotecnología (LANOTEC) in the person of Dr. José Vega-Baudrit for the help provided in the beginning of this work.

I acknowledge Fluidinova S.A., for providing the *nanoXIM-CarePaste* and *nanoXIM-HAp102* used in this work.

I thank everyone who directly or indirectly contributed to the accomplishment of this goal.

Abstract

This work comprises the development of hybrid inorganic-organic materials based on highly pure nano-hydroxyapatite (n-HAp). Chitosan (CS) was selected as the organic component, in order to develop n-HAp/CS products mimicking bone composition. The following main processing stages were considered: (1) dispersion preparation in which n-HAp is incorporated into the chitosan solution; (2) phase separation/solvent elimination in which the fixation of structural forms takes place; (3) purification and potential sterilization procedures.

Dispersion preparation is a key step since it implies the inclusion of HAp nanoparticles into the chitosan solution. This stage was carried out by physically mixing the HAp nanoparticles with the chitosan solution. The effect of different parameters on the resulting particle size and electrostatic stability (zeta potential) of the dispersions was studied. Results reflected that chitosan acts as a good stabilizer (zeta potential $>+30$ mV) of HAp nanoparticles in slightly acidic environment (pH 5.5), and such good stability was proven to be consistent along time. Taken into consideration these results, a method for the preparation of n-HAp/CS dispersions by fast stirring (ultraturrax) was developed. With mixing times <100 ms, the used fast stirring set up allowed the production of highly homogeneous and stable n-HAp/CS dispersions (pH 5.5), and it was determined that using HAp/CS weight ratio of 70/30 and n-HAp concentration of 20 g/l, the produced dispersions were suitable materials for the production of n-HAp/CS hybrids in different forms.

In the phase separation/solvent elimination stage, two different structural forms were developed: microparticles and scaffolds. Spray drying was used to produce the hybrid n-HAp/CS microparticles. The effect of pH of the n-HAp/CS dispersion (5.5 and 7.0) and the presence of KCl on the final n-HAp/CS microparticle's properties were studied. It was evidenced that KCl has no beneficial effect on the stability of the n-HAp/CS dispersions, and it appeared as a contaminant on the formed microparticles. Moreover, the generated microparticles presented differences depending on the pH at which the n-HAp/CS dispersion was prepared. Doughnut-like n-HApCS-5.5 microparticles (15.8-µm average size in volume) were found preferred over n-HApCS-7.0 microparticles, which require one step more in the productive process and presented a tendency to form large agglomerates. The produced microparticles are advantageous, as they allow HAp's superior properties at the nanoscale to be preserved in the form of microparticles that are suitable materials to develop injectable systems, drug delivery systems, or be shaped into solid substrates with increased surface area.

A simple 3-step production process was developed to produce n-HAp/CS hybrid materials in the form of scaffolds. The process consists in: (1) n-HAp/CS dispersion preparation; (2) freeze-drying stage to fix scaffold shape; and (3) supercritical CO_2 ($scCO_2$) extraction to remove acetic acid and promote sterilization. It was shown that $scCO_2$ extraction step is a suitable purification procedure since it allowed the successful removal of acetic acid, with the advantage of not compromising the microarchitecture achieved by freeze-drying unlike other tested methods based on neutralization with alkaline solutions. The produced scaffolds were sterile and exhibited suitable properties for non-load bearing bone graft applications; therefore, the developed 3-step process has great potential to produce ready-to-use n-HAp/CS scaffolds mimicking bone composition and structure.

Given the achieved results, three different n-HAp/CS hybrid products were successfully produced: dispersions, powder (microparticles), and scaffolds. The generated n-HAp/CS hybrid materials mimic bone composition, are composed of highly pure HAp nanoparticles, and displayed suitable properties for different potential applications.

Resumo

Este trabalho compreende o desenvolvimento de materiais híbridos inorgânico-orgânico baseados em nano-hidroxiapatite (n-HAp) de elevada pureza. Para este fim, escolheu-se para componente orgânico o quitosano (CS), de modo a produzir materiais híbridos n-HAp/CS que reproduzam a composição óssea utilizando as seguintes etapas de processamento: (1) preparação das dispersões base por incorporação da n-HAp numa solução de quitosano; (2) fixação da forma dos materiais por processos de separação de fase/eliminação de solvente; (3) purificação final e potencial esterilização dos materiais.

A preparação da dispersão é um passo importante, implicando a introdução das nanopartículas de HAp numa solução de quitosano. Esta etapa foi realizada utilizando o método da mistura simples. Foi estudado o efeito de diferentes parâmetros no tamanho de partícula e na estabilidade eletrostática (potencial zeta) das dispersões. Os resultados indicaram que o quitosano atua como agente estabilizador (potencial zeta >+30 mV) das nanopartículas de HAp em ambiente ácido (pH 5.5) e que este efeito se mantêm ao longo do tempo. Considerando estes resultados, desenvolveu-se um método para preparação das dispersões n- HAp/CS por mistura rápida (ultraturrax). Utilizando tempos de mistura <100 ms, foi possível obter dispersões (pH 5.5) homogéneas e estáveis. Com base na configuração de mistura rápida desenvolvida, determinou-se que as dispersões produzidas com HAp/CS de 70/30 e uma concentração de 20 g/l, eram adequadas para a produção de diferentes formas de materiais híbridos n-HAp/CS.

Foram desenvolvidas duas formas estruturais diferentes por separação de fases/eliminação de solvente: micropartículas e scaffolds. As micropartículas foram produzidas pela tecnologia de spraydrying. Foi estudado o efeito do pH das dispersões de n-HAp/CS (5.5 e 7.0) e da presença de KCl nas propriedades finais das micropartículas. Evidenciou-se que o KCl não beneficia a estabilidade das dispersões aparecendo como um contaminante nas micropartículas produzidas. Além disso, as micropartículas apresentaram diferenças em função do pH usado para a preparação das dispersões. As micropartículas n-HApCS-5.5 (tamanho médio 15.8 μm em volume) apresentaram forma de donut e vantagens sobre as micropartículas n-HApCS-7.0, as quais requerem um passo adicional na preparação e mostraram tendência para formação de aglomerados de grandes dimensões. As micropartículas formadas permitiram preservar as propriedades superiores da HAp nanométrica utilizada. Estas apresentam potencial para serem utilizadas no desenvolvimento de sistemas injetáveis de libertação controlada, ou moldadas em formas sólidas com área superficial incrementada.

Para a produção de scaffolds, foi desenvolvido um processo simples em 3 passos: (1) a preparação da dispersão n-HAp/CS; (2) liofilização para a fixação estrutural; e (3) extração com CO2 supercrítico (scCO2) para a remoção do ácido acético remanescente do processo de liofilização e esterilização simultânea. Demonstrou-se que a extração com scCO2 é um método de purificação vantajoso visto que possibilitou a remoção do ácido acético com sucesso sem comprometer a integridade estrutural do scaffold obtida durante o processo de liofilização, contrariamente aos métodos baseados em neutralização com soluções alcalinas. Os scaffolds produzidos apresentaram propriedades adequadas para aplicações como enxertos ósseos de baixa solicitação de carga. Assim, o processo de 3 passos desenvolvido apresenta elevado potencial para a produção de scaffolds prontos a usar, que reproduzem a composição e estrutura óssea.

Em síntese, os resultados obtidos permitiram o desenvolvimento de três produtos híbridos n-HAp/CS: dispersões, pós (micropartículas), e scaffolds. Os materiais híbridos obtidos simulam a composição óssea, são compostos por nano-partículas de hidroxiapatite de elevada pureza, e possuem propriedades adequadas a diferentes aplicações.

Resumen

Este trabajo comprende el desenvolvimiento de materiales híbridos inorgánico-orgánico con base en nano-hidroxiapatita (n-HAp) de alta pureza. Para ello, se eligió quitosano (CS) como componente orgánico de modo que los materiales híbridos n-HAp/CS fueron producidos con base en las siguientes etapas principales: (1) preparación de dispersiones, en la cual la n-HAp entra en contacto con el quitosano; (2) separación de fases/eliminación de solvente, en la cual el material adquiere una forma estructural determinada; (3) procedimientos de purificación y esterilización.

La etapa de preparación de la dispersión es clave, dado que implica la incorporación de la HAp en la solución de quitosano. Esta etapa se llevó a cabo mezclando físicamente las nanopartículas de HAp con la solución de quitosano. Se estudió el efecto de diferentes parámetros en el tamaño de partícula y la estabilidad electroestática (potencial zeta) de las dispersiones en cuestión. Los resultados revelaron que el quitosano actúa como buen agente estabilizador (potencial zeta $> +30$ mV) de las nanopartículas de HAp en medios ligeramente ácidos (pH 5.5), y tal estabilidad es consistente a lo largo del tiempo. Tomando en cuenta estos resultados, se desarrolló un método para la preparación de dispersiones n-HAp/CS mediante mezcla rápida (ultraturrax). Con tiempos de mezcla $<$100 ms, la configuración usada permitió la producción de dispersiones (pH 5.5) altamente homogéneas y estables. Asimismo, se determinó que, con una proporción másica HAp/CS de 70/30 y una concentración de n-HAp de 20 g/l, las dispersiones obtenidas son apropiadas para la producción de diferentes formas de materiales híbridos n-HAp/CS.

Por consiguiente, en la etapa de separación de fases/eliminación de solvente se produjeron dos formas diferentes de híbridos: micropartículas y *scaffolds*. Las micropartículas fueron producidas por *spray-drying*. Se estudió el efecto del pH de las dispersiones (5.5 y 7.0) y la presencia de KCl en las propiedades finales de las micropartículas. Se evidenció que el KCl no favorece la estabilidad de las dispersiones, e incluso aparece como un contaminante en las micropartículas. Por otra parte, las micropartículas producidas mostraron diferencias dependiendo del pH al cual fueron preparadas las dispersiones. Las micropartículas n-HApCS-5.5, con 15.8 μm de tamaño medio en volumen y morfología de dona, se fueron preferidas que las n-HApCS-7.0, las cuales requieren de un paso extra en el proceso de producción y además presentan tendencia a formar aglomerados de gran tamaño. Las micropartículas obtenidas tienen la ventaja de que permiten conservar las propiedades superiores de la HAp nanométrica en la forma de micropartículas, que son materiales apropiados para el desenvolvimiento de sistemas inyectables, de liberación controlada de fármacos, o pueden ser moldeadas en sustratos sólidos con alta área superficial.

Para la producción de materiales híbridos n-HAp/CS en la forma de *scaffolds* se desarrolló un proceso simple de 3 pasos, el cual consiste en: (1) preparación de las dispersiones; (2) liofilización para fijar la forma del *scaffold*; (3) extracción con CO_2 supercrítico ($scCO_2$) para remover el ácido acético residual y promover la esterilización. Se probó que la extracción con $scCO_2$ es un método de purificación adecuado dado que fue posible remover exitosamente el ácido acético, con la ventaja de que no se compromete la forma estructural fijada durante la liofilización, a diferencia de los otros métodos con base en neutralización con solución alcalina. Se comprobó la esterilidad de los *scaffolds* producidos, así como la idoneidad de sus propiedades para ser usados como injertos óseos que no requieren soporte de carga. Así, el proceso de 3 pasos desarrollado mostró gran potencial para la producción de *scaffolds* n-HAp/CS listos para usar, y que simulan la composición y estructura del hueso natural.

En síntesis, los resultados obtenidos permitieron el desarrollo de tres materiales híbridos n-HAp/CS diferentes: dispersiones, polvo (micropartículas), y scaffolds. Estos materiales imitan la composición ósea, están compuestos de HAp de alta pureza, y presentan propiedades apropiadas para diferentes potenciales aplicaciones.

Table of Contents

List of Figures

List of Tables

Notation

Abbreviations

HAp	Hydroxyapatite
n-HAp	Nano hydroxyapatite
CS	Chitosan
Ca-P	Calcium phosphates
PLA	Poly(L-lactic acid)
PGA	Poly(glycolic acid)
PLGA	Copolymers of poly(L-lactic acid) and poly(glycolic acid)
β-TCP	β-tricalcium phosphate
GAG	Glycosaminoglycans
RNA	Ribonucleic acid
DNA	Deoxyribonucleic acid
EtO	Ethylene oxide
$scCO_2$	Supercritical carbon dioxide
PBS	Phosphate buffer solution
EDTA	Ethylenediaminetetraacetic acid
BHI	Brain heart infusion
MEM	Minimum essential medium
α-MEM	Minimum essential medium, alpha modification
FDA	Food and Drug Administration
IUPAC	International Union of Pure and Applied Chemistry
MSCs	Mesenchymal stem cells
ECM	Extracellular matrix
DBM	Demineralized bone matrix

DD	Degree of deacetylation
IPNs	Interpenetrating polymer networks
TIPS	Thermally induced phase separation
DLS	Dynamic light scattering
LD	Laser diffraction spectroscopy
ELS	Electrophoretic light scattering
PCS	Photo correlation spectroscopy
PIDS	Polarisation intensity differential scattering
SD	Standard deviation
PSD	Particle size distribution
FTIR	Fourier transform infrared
SEM	Scanning electron microscopy
EDS	Energy-dispersive X-ray spectroscopy
TG	Thermogravimetry
DSC	Differential scanning calorimetry
AAS	Atomic Absorption Spectroscopy

Nomenclature

V_T	Total potential energy $[J]$
V_A	Attractive energy $[J]$
V_R	Repulsive energy $[J]$
V_S	Potential energy due to the solvent $[J]$
D_{part}	Particle diameter $[nm]$
L_{part}	Particle length $[nm]$

V_{part}	Particle volume $[m^3]$
N_{part}	Number of particles
Δx_{part}	Distance between particles $[nm]$
E_{abs}	Energy absorbed $[J]$
E_{loss}	Energy loss $[J]$
E_{in}	Energy input $[J]$
C_P	Heat capacity $[J \cdot K^{-1}]$
C_{HAp}	Concentration of hydroxyapatite $[g \cdot l^{-1}]$
m_{HAp}	Mass of hydroxyapatite $[g]$
ρ_{HAp}	Density of hydroxyapatite $[g \cdot cm^{-3}]$
M_{HAp}	Molar mass of hydroxyapatite $[g \cdot mol^{-1}]$
m_{dis}	Mass of dispersion $[g]$
ρ_{dis}	Density of dispersion $[g \cdot cm^{-3}]$
V_{dis}	Dispersion volume $[m^3]$
T	Temperature $[^{\circ}C]$
P	Pressure $[MPa]$
Q	Flow rate $[ml \cdot \min^{-1}]$
$t_{reaction}$	Reaction time $[s]$
$\dot{V}_{pump}$	Pump speed rate $[ml \cdot \min^{-1}]$
P_{output}	Power output $[J \cdot s^{-1}]$

1 Introduction

Bone, teeth, cartilage and skin, wood, nacre, crustacean carapaces and mollusc shells, are some of the many examples of hybrid materials that have existed in nature for millions of years. All of them exhibit extraordinary properties that cannot be attained by the individual components themselves, motivating many scientists to develop synthetic hybrid materials mimicking nature.

Hybrids are often produced in nature as hierarchical structures in which particulate, fibrous, and porous structural features are present at different scale. As a matter of fact, nature has the remarkable ability to combine organic and inorganic components at the nanoscale, producing smart materials in such a level of integration that allows, not only the accommodation of a maximum of elementary functions in a small volume, but also the optimization of complementary possibilities, functions and hierarchies [1, 2].

The possibility to produce materials with combined properties of their components is a very ancient challenge. From the Egyptian inks to the green ceramics of China, man has embraced the task of designing and processing hybrid materials for ages. One beautiful example is the Maya blue, a robust pigment used by Mayas in their Ancient paintings, which combines the colour of an organic pigment (natural blue indigo) with the resistance of an inorganic host, a mineral known as palygorskite, chemical formula $Si_8O_{20}Al_2Mg_2\left(OH\right)_2\left(H_2O\right)_4 \cdot 4H_2O$, allowing

the preservation of the paintings against the adversities of time and environment for centuries [2].

In the industrial era, hybrids started being successfully commercialized and became part of the manufacturing technology. It can be said that paints were the bridge between Mayas and modern applications of hybrids. However, it was only in the nineteen-eighties that the concept of "organic-inorganic hybrid" was developed with the expansion of soft (mild conditions) inorganic chemistry processes. Since then, the study of this type of materials at all scale ranges, lately with special interest in the nanoscale, became a growing field of research yielding innovative, advanced materials with high added value [2].

Scientists and engineers started combining materials, usually by incorporating a basic structural material in the form of particles, fibbers, or lamellae, into a matrix of a second substance, resulting in a novel material with improved mechanical properties. The structural building blocks that are incorporated into the second substance are predominantly inorganic in nature and, can assume different sizes. These early produced hybrid materials had heterogeneous composition, with inorganic units ranging from a few micrometers to millimeters, being often visible at naked eye. Soon it became evident that if the inorganic units are as small as the organic building blocks, more homogeneous materials could be obtained, allowing a further tuning of the properties at molecular and nanoscale levels. Such observation is now more tangible with today's technological breakthroughs, in particular the availability of physico-chemical characterization methods that have given a positive twist to the field of nanoscience, opening many perspectives for approaches to new materials [3].

1.1 Motivation and objectives

A great interest has been given to synthetic and stoichiometric hydroxyapatite (HAp) as a biomaterial due to its similarity with the mineral phase found in hard tissues [4]. It possesses exceptional biocompatibility [5] and bioactivity [6, 7] with respect to bone cells and surrounding tissues, which makes it a suitable material for the replacement of small parts of bone, filling of cavities in dentistry, and coating of metallic implants [8]. Additionally, this bioceramic has a high capacity of ad- and absorption, making it an excellent candidate for

drug delivery applications, such as long–acting drugs for anticancer treatment of bone tumours [9, 10].

Bones are not only the frame that supports human body, allowing its mobility and protecting it against injury, but also the storehouse for minerals that are essential for the functioning of other life-sustaining systems in the body. For these reasons, healthy bones are critically important for the overall health and quality of life. Unfortunately, bone is the second tissue most frequently transplanted, second only after blood transfusions. The clinical need to replace, restore, or regenerate bone tissue comprises the fields of dental, maxillofacial, orthopaetic, spinal, and cranial surgery, being osteoporosis the most important cause of fracture in the elderly [11-13]. The International Osteoporosis Foundation reported in 2010 an estimation of 3.5 million new fractures in the EU caused by osteoporosis, representing an economic burden of approximately 37 billion EUR [14].

Medical solutions for bone repair and regeneration are still a major challenge. Even though they present serious drawbacks, biologically derived bone grafts have been implanted for many years, as temporary or permanent prosthesis. Among the available possibilities, autologous grafts (*autografts*) are still considered the "golden standard" today. They are usually well accepted and integrate rapidly with the surrounding tissue; however, the number of donor sites is very limited, and additional traumas and scars are involved requiring further healing at the patient's donation site, long-term postoperative pain, with the risk of possible infections [12, 15]. Alternatively, the so-called *xenograft*, obtained from other animal species, is commercially available but it presents a high risk for viral infections, usually resorbs faster than autogenous bone, and has low osteogenicity and high immunogenicity. The use of *allografts*, obtained from another individual of the same species, present similar limitations, such as potential risks of transmitting bacterial and viral infections, as well as tumour cells. Moreover, there is a strong possibility of immunological and blood group incompatibility [16].

Given such scenario, the development of man-made materials appears as a promising option that, in comparison with orthodox treatments, have great potential to improve the regeneration of bone or its replacement when damaged, with the advantage that they are easily available and might be processed and modified to suit specific needs [11, 17]. They can be shaped to adapt to defects of different forms and sizes, and produced with particular properties such as antimicrobial capacity, or loaded with active ingredients such as anti-

inflammatory drugs [18]. Nevertheless, despite of the evident clinical need for this type of materials, the bone graft substitutes market is still relatively small. According to a review published in 2010 in Materials Today [18], the global annual production of bone graft substitutes is close to 10 tons with a price of about 100 USD per gram. Synthetic materials represent only about 15% of the global market, but with a promising growing rate of about 10% per year.

In this light, the development of hydroxyapatite-based hybrid materials is very promising not only in terms of market opportunities, but also due to the contribution it could impart to regenerative medicine, particularly for hard tissue regeneration. The incorporation of nano-hydroxyapatite (n-HAp) into polymeric materials, particularly natural polymers, is recognized as one of the most viable approaches to produce materials mimicking natural bone. Besides the expected biodegradability, natural polymers can be biologically active promoting better interactions with cells and, therefore, excellent cell adhesion and growth [19]. In particular, the combination of n-HAp with chitosan (CS) has been of great interest for the production of non-load bearing bone grafts, given the advantageous properties of chitosan that allows the manufacturing of n-HAp/CS materials with improved properties. Among other features, chitosan promotes osteoblasts adhesion and proliferation, possesses antimicrobial properties, can be processed using mild conditions and shaped into different forms [20].

The aim of this work is to develop high-added value hybrid materials based on highly pure, nanometric hydroxyapatite. For this purpose, chitosan has been selected as the organic component, and the production of three different forms of n-HAp/CS hybrid materials, having in view different potential applications, was studied: dispersions, powder (microparticles), and scaffolds. In order to obtain these different forms of the n-HAp/CS hybrids, the following main processing stages were considered (see Figure 1.1): (1) dispersion preparation in which n-HAp is incorporated into the chitosan solution; (2) phase separation/solvent elimination in which the fixation of structural forms as microparticles and scaffolds takes place; (3) purification and potential sterilization procedures. Different parameters and processing conditions were evaluated in order to define the best formulation to achieve adequate properties of the final products.

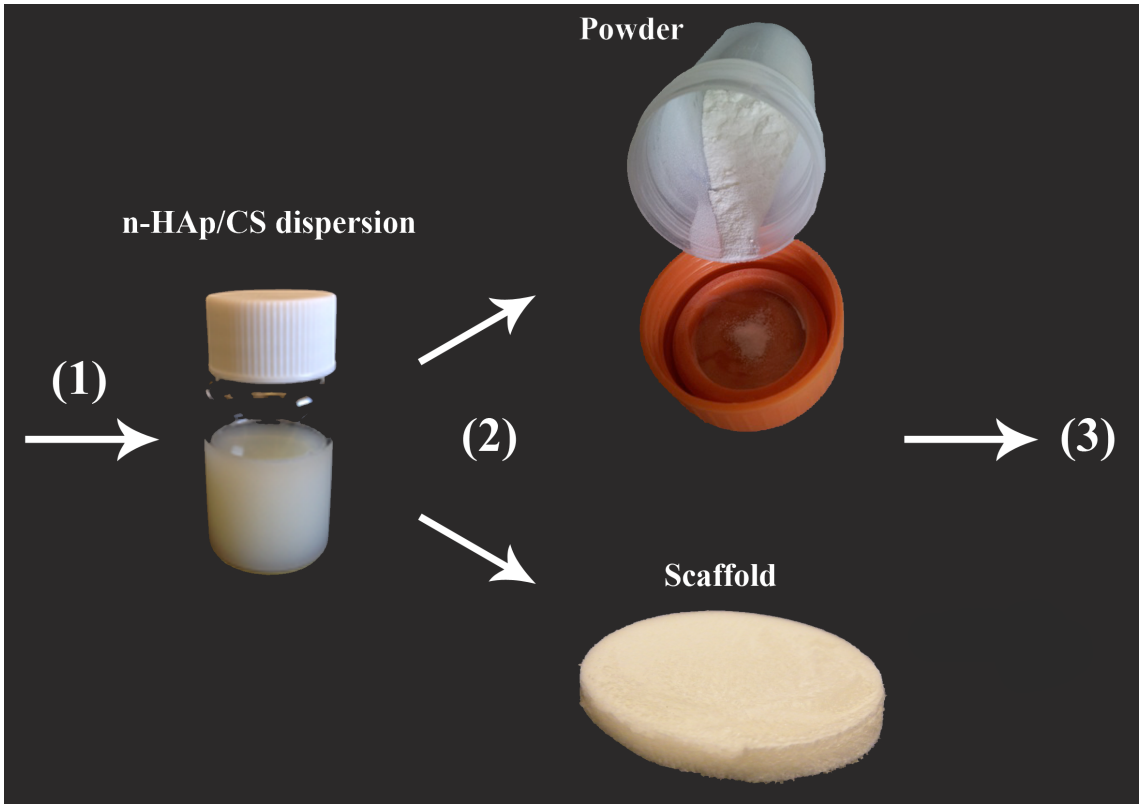

Figure 1.1. Schematic representation of the main processing stages considered in this thesis: (1) dispersion preparation; (2) phase separation/solvent elimination in which the fixation of structural forms as microparticles and scaffolds takes place; (3) purification and potential sterilization procedures

The work developed in this thesis is organized in the following chapters:

Chapter 2 consists of a compilation of the main achievements that have been published on hydroxyapatite-based hybrid materials, focusing on the combination of hydroxyapatite with chitosan. This chapter also includes fundamental definitions about hydroxyapatite and chitosan, their chemistry and structure-properties relationship. Methods for the preparation of n-HAp based hybrid materials with chitosan are introduced and further discussed in the remaining chapters.

Based on the method of physically mixing n-HAp particles with chitosan in solution, **Chapter 3** presents the preparation and characterization of aqueous dispersions of n-HAp, alone or in the presence of chitosan. This chapter includes an introduction focused on the basic principles of colloidal science and characterization techniques. Additionally, an experimental part in which the n-HAp dispersions were prepared by ultrasonication and characterized in terms of particle size and zeta potential is presented. Considering that the

incorporation of HAp nanoparticles into an acidic environment (chitosan solution) can influence HAp solubility, phase stability and surface chemistry, this chapter also discusses the effect of different parameters, such as pH, chitosan content and the presence of salts (KCl) on the resulting particle size and electrostatic stability of the dispersions.

Chapter 4 is dedicated to the production of n-HAp/CS hybrid microparticles. First, a method for the preparation of n-HAp/CS dispersions by fast stirring (ultraturrax) is presented. The produced nanodispersions were characterized in terms of particle size and zeta potential, and the results were analysed taking into account the study carried out in Chapter 3. Afterwards, the n-HAp/CS dispersions were used as base materials for the production of microparticles by spray drying. Given that the n-HAp paste used to prepare the n-HAp/CS dispersions contains KCl in its formulation, the effect of the presence of this salt on the final microparticles properties was analysed. Moreover, two different types of microparticles were prepared based on different pH values (5.5 and 7.0) of the original n-HAp/CS nanodispersions and a comparative study is presented. Finally, in order to infer if the spray-drying conditions have an effect on the degradation of chitosan, the n-HAp/CS microparticles were characterized in terms of thermal degradation, and results were compared with analogous samples prepared by freeze-drying.

The development of a 3-step process for producing n-HAp/CS hybrid scaffolds is presented in **Chapter 5**. The developed process comprises sequentially the following stages: dispersion preparation, freeze-drying, and supercritical CO_2 extraction. Supercritical CO_2 extraction is introduced as an innovative purification step with potential sterilization capacity. Different process parameters, as temperature (40 and 75 °C) and number of extraction cycles (1 and 2), were tested, while keeping the pressure constant at 8.0 MPa. The advantages of this method were studied over other currently used procedures, often based on neutralization with an alkaline solution. The produced scaffolds were evaluated based on key features required for bone regeneration, such as micro-architechture (interconnected pores and porosity), swelling capacity, and mechanical properties. Moreover, microbiological and cytotoxicity assays are carried out in order to assess the sterility of the produced scaffolds, and their ability to promote cell attachment and growth.

Finally, **Chapter 6** comprises the main conclusions of the thesis, as well as suggestions for future work.

1.2 References

[1] Park, J. and R.S. Lakes, *Biomaterials: an introduction*. 2007: Springer Science & Business Media.

[2] Sanchez, C., et al. *Applications of hybrid organic-inorganic nanocomposites.* Journal of Materials Chemistry, 15, 3559-3592 (2005).

[3] Kickelbick, G., *Introduction to Hybrid Materials*, in *Hybrid Materials*. 2007, Wiley-VCH Verlag GmbH & Co. KGaA. p. 1-48.

[4] Levengood, S.K.L. and M. Zhang. *Chitosan-based scaffolds for bone tissue engineering.* J. Mater. Chem. B, 2, 3161 (2014).

[5] Chen, F., et al. *Biocompatibility of electrophoretical deposition of nanostructured hydroxyapatite coating on roughen titanium surface: In vitro evaluation using mesenchymal stem cells.* Journal of Biomedical Materials Research Part B: Applied Biomaterials, 82B, 183-191 (2007).

[6] Hossein Fathi, M., V. Mortazavi, and S.I. Roohani Esfahani, *Bioactivity Evaluation of Synthetic Nanocrystalline Hydroxyapatite*. 2009. Vol. 5. 2009.

[7] Fathi, M., A. Hanifi, and V. Mortazavi. *Preparation and bioactivity evaluation of bone-like hydroxyapatite nanopowder.* Journal of materials processing technology, 202, 536-542 (2008).

[8] Ferraz, M., F. Monteiro, and C. Manuel. *Hydroxyapatite nanoparticles: a review of preparation methodologies.* Journal of Applied Biomaterials and Biomechanics, 2, 74-80 (2004).

[9] Itokazu, M., et al. *Development of porous apatite ceramic for local delivery of chemotherapeutic agents.* Journal of Biomedical Materials Research, 39, 536-538 (1998).

[10] Bose, S. and S. Tarafder. *Calcium phosphate ceramic systems in growth factor and drug delivery for bone tissue engineering: A review.* Acta Biomaterialia, 8, 1401-1421 (2012).

[11] Brydone, A., D. Meek, and S. Maclaine. *Bone grafting, orthopaedic biomaterials, and the clinical need for bone engineering.* Proceedings of the Institution of Mechanical Engineers, Part H: Journal of Engineering in Medicine, 224, 1329-1343 (2010).

[12] Campana, V., et al. *Bone substitutes in orthopaedic surgery: from basic science to clinical practice.* Journal of Materials Science: Materials in Medicine, 25, 2445-2461 (2014).

[13] Services, U.S.D.o.H.a.H., *The Frequency of Bone Disease*, in *Bone Health and Osteoporosis: A Report of the Surgeon General*. 2004, U.S. Department of Health and Human Services, Office of the Surgeon General.

[14] Svedbom, A., et al. *Osteoporosis in the European Union: a compendium of country-specific reports.* Archives of Osteoporosis, 8, 1-218 (2013).

[15] Kurien, T., R. Pearson, and B. Scammell. *Bone graft substitutes currently available in orthopaedic practice The evidence for their use.* Bone & Joint Journal, 95, 583-597 (2013).

[16] Dorozhkin, S.V. *Biocomposites and hybrid biomaterials based on calcium orthophosphates.* Biomatter, 1, 3-56 (2011).

[17] Bose, S., M. Roy, and A. Bandyopadhyay. *Recent advances in bone tissue engineering scaffolds.* Trends in Biotechnology, 30, 546-554 (2012).

[18] Bohner, M. *Resorbable biomaterials as bone graft substitutes.* Materials Today, 13, 24-30 (2010).

[19] O'Brien, F.J. *Biomaterials & scaffolds for tissue engineering.* Materials Today, 14, 88-95 (2011).

[20] Costa-Pinto, A.R., R.L. Reis, and N.M. Neves. *Scaffolds based bone tissue engineering: the role of chitosan.* Tissue Eng Part B Rev, 17, 331-47 (2011).

2 State of the art

Due to its excellent bioactivity [1, 2] and biocompatibility [3], hydroxyapatite (HAp) has been widely used for hard tissue regeneration, being incorporated in dental and orthopaedic implants mainly as powders, granules, and scaffolds. The chemical and structural similarity of synthetic HAp to minerals in natural bone makes it a great candidate as a bone substitute material. However, at the nanostructural level, natural bone is composed not only by a mineral but also by an organic component, collagen, that provides resilience and ductility to bone, complementing the stiffness provided by the mineral phase [4]. Therefore, with the aim of emulating natural bone, efforts have been focused in combining calcium phosphates (Ca-P), particularly HAp, with biodegradable and/or natural polymers.

The first attempt to produce an implantable polymer/Ca-P composite was carried out in 1981 and consisted in the development of HAp/polyethylene formulations by pioneer Prof. William Bonfield and his colleges [5]. Ever since, many studies have been conducted in this field, including the use of FDA-approved, synthetic-biodegradable polymers such as poly(L-lactic acid) (PLA) [6], poly(glycolic acid) (PGA) [7], and their copolymers (PLGA), with applications as drug carriers, bone fixation screws, plates, resorbable sutures, among others [8, 9].

More recently, the combination of nano-hydroxyapatite (n-HAp) with natural polymers became a new trend. Besides the expected biodegradability, natural polymers can be biologically active promoting better interactions with cells and, therefore, excellent cell adhesion and growth [10]. In this context, chitosan, the main derivative of natural polymer chitin, appears as a great candidate gathering a wide list of desirable properties for bone regeneration.

This chapter is a compilation of fundamentals in bone tissue engineering, focusing recent advances on the use of hydroxyapatite and chitosan as biomaterials for bone regeneration, and progresses in what concerns the fabrication of HAp/CS hybrid materials.

2.1 Overview of bone biology

Natural bone is a complex hybrid material which extracellular matrix composed of approximately 60-70% of an inorganic mineral, precipitated onto 20-30% of an organic matrix, and a small portion of water [11, 12]. Structurally, it is highly organized in a hierarchical manner, from the nano- to the macroscale, as shown in Figure 2.1. At the nanoscale, the mineral phase consists of calcium-phosphate, plate-like nanocrystals, with 2-6 nm thick, 30-50 nm width and 60-100 nm long, chemically and structurally very similar to synthetic nano hydroxyapatite [11, 12] (see Table 2.1).

At a microscale, bone can be divided in two categories based on density: cortical and cancellous bone. Cortical or compact tissue is very dense, with a porosity of 3-5%, and forms the outer layer of bone, providing support and protection. The less-dense inner part is constituted by cancellous bone, also known as trabecular or spongy bone; it is highly porous, with 30-90% porosity, and contains the bone marrow [4, 12-14]. Together, the cortical and trabecular tissues form the skeletal element of bone. However, bone is also a very dynamic tissue that constantly experiences modelling and remodelling processes as a consequence of mechanical and metabolic changes.

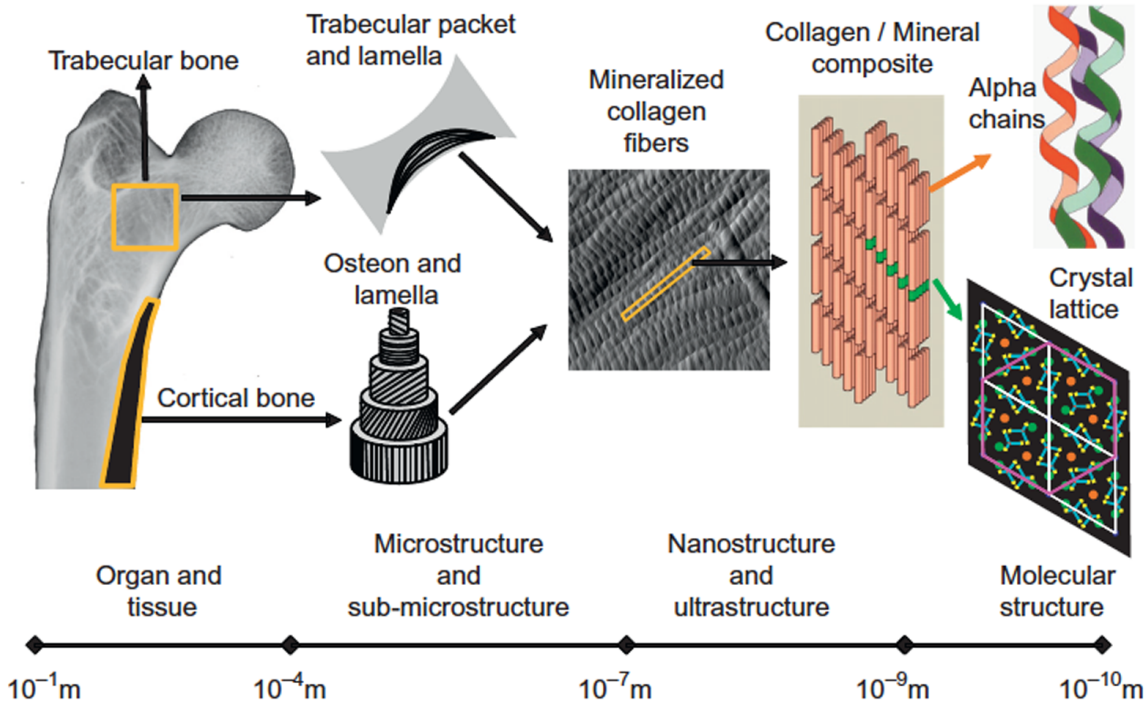

Figure 2.1. Hierarchical organization of bone
(Reproduced from Burr and Allen, 2013 [4])

Five primary cells dictate bone formation and remodelling: mesenchymal stem cells (MSCs), osteoblasts, osteocytes, osteoclasts and bone lining cells. MSCs are found in the bone marrow and in the periosteum, the fibrous layer on the outside surface of bone. They are multipotent stromal cells that can differentiate into osteoblasts, the single-nuclei cells in charge of bone matrix protein secretion and bone mineralization. After completing their main function of synthesizing bone matrix, osteoblasts undergo three different transformations: they remain entrapped in bone as osteocytes, they flatten into bone lining cells, and the remnants suffer apoptosis.

Osteocytes are the most abundant cells present in bone, representing more than 90% of cells within the bone matrix and surfaces, and their main function is the coordination of osteoblasts and osteoclasts functions in response to mechanical and hormonal signals. Bone lining cells are relatively inactive forms of osteoblasts which function is to cover inactive surface of bone; they may recover the ability to synthesize bone matrix and participate in the regulation of calcium exchanges. Finally, osteoclasts are the cells responsible for the resorption of mineralized bone. All these cells work together in a balanced way to maintain

the integrity of healthy bone, as well as to regenerate bone that has suffered trauma or disease. In the last case, when the size defect is critical, bone grafts are necessary to assist bone healing [4, 12, 14].

Table 2.1. Typical composition of the inorganic phase of adult human calcified tissues and hydroxyapatite (Adapted from Bose et al., 2012 [13])

Composition	**Enamel**	**Dentin**	**Bone**	**Hydroxyapatite**
Calcium [wt.%]	36.5	35.1	34.8	39.6
Phosphorus (as P) [wt.%]	17.7	16.9	15.2	18.5
Ca/P (molar ratio)	1.63	1.61	1.71	1.67
Sodium [wt.%]	0.5	0.6	0.9	-
Magnesium [wt.%]	0.44	1.23	0.72	-
Potassium [wt.%]	0.08	0.05	0.03	-
Carbonate (as CO_3^{2-}) [wt.%]	3.5	5.6	7.4	-
Fluoride [wt.%]	0.01	0.06	0.03	-
Chloride [wt.%]	0.30	0.01	0.13	-
Pyrophosphate (as $P_2O_7^{-4}$) [wt.%]	0.022	0.10	0.07	-
Total inorganic [wt.%]	97	70	65	-
Total organic [wt.%]	1.5	20	25	-
Water [wt.%]	1.5	10	10	-

2.2 The ideal bone graft

Considering the compositional, structural, mechanical and biological complexity of natural bone, the design of an ideal bone graft is not an easy task. The requirements for a graft intended to mimic all features of bone are numerous and diverse, however, there are a few key factors that must be fulfilled. Based on O'Brien (2011) [10], they can be summarized in terms of biocompatibility, biodegradability, mechanical properties, structural requirements and manufacturing technology.

2.2.1 Biocompatibility

An indispensible requirement of bone grafts is biocompatibility. This term can be defined as the ability of a material to support normal cellular activity, including molecular signalling systems, without causing any systematic or local effects to the host tissue [15]. Therefore, the graft should be *osteoconductive*, that is, it should promote cell adhesion on its surface and migration within its pores, cell proliferation and formation of ECM. In addition, *osteoinductive* property is necessary, that is, the bone substitute must induce the formation of new bone through the reclusion of progenitor cells and biomolecular signalling [15, 16]. Along with osteoconductive and osteoinductive properties, degradation products of the bone graft should be non-toxic and easily excreted by metabolic pathways [17].

2.2.2 Biodegradability

The main objective of a bone graft is to assist tissue regeneration by providing a bridge that will fill critical size bone defects in such a way that it allows the body's own cells to replace, over time, the implanted substitute. Therefore, grafts should not be permanent and they must degrade *in vivo* in a controlled manner, ideally at a rate that closely matches the rate of new tissue formation in the implantation site [10, 15, 18].

2.2.3 Mechanical properties

One of the main challenges in bone tissue engineering is, still today, to achieve an adequate balance between mechanical properties and structural requirements, such as high porosity. The bone substitute should be able to support mechanical stresses in the implantation site from the moment of grafting throughout the whole remodelling process, which leads to a

further challenge considering that healing times vary with age; tissue of a younger individual normally requires less time to heal than that of the elderly. In addition, the graft should be able to resist surgical handling during the implantation process [10].

2.2.4 Structural requirements

The structural features of the bone substitute are critical since they can affect both, its mechanical properties and its capacity to promote *osteogenesis*, the formation of bone tissue. Bone grafts can be cortical, cancellous, or a combination of both, each one with different mechanical and structural properties, which can be used in different applications depending on the surgical requirements. Cortical bone grafts are less frequently used and they are often applied onlay, i.e. it is applied or laid on the surface of the tissue, to provide structural support and strength. Cancellous bone grafts, on the other hand, lack of mechanical strength but are characterized for inducing osteogenesis. This type of bone substitute is commonly implanted in non-union fractures, maxillofacial and dental defects, spinal fusion, and other small defects [19].

Typically, cancellous bone grafts take the form of 3D-porous scaffolds, and the ability to promote adequate osteogenesis greatly depends on its architecture. Scaffolds should be highly porous, to guarantee cellular penetration, and their pores should be interconnected, both to allow the diffusion of nutrients to cells as well as the exit of waste and degradation products out of the scaffold [10].

2.2.5 Manufacturing technology

Last but not least, clinical and commercial viability are key factors to consider when engineering bone grafts. The manufacturing process should be cost effective and easily scalable from laboratorial to industrial production. Additionally, it is important to consider the clinician's point of view, since they are the ones ultimately using the product. For example, they typically prefer a bone graft that can be easily adapted into different shapes and an off-the shelf product ready to be implanted; the less extra surgical procedures prior implantation, the better [10].

2.3 Commercially available materials for bone grafts

Solutions for bone repair include the use of materials that, if not autologous, are either from natural origin or synthetic. Biological or natural bone grafts are those obtained from either human or animal origin; thus, autogenous, allogenous, and xenogenous grafts are all within this classification [20]. Synthetic grafts, also known as alloplastic grafts, include the use of polymers but mainly ceramic-based materials such as hydroxyapatite, calcium sulphate, and bioactive glass [20, 21]. There is also the alternative of using composite and hybrid materials, commonly consisting in the combination of ceramic-based materials with polymers.

Autogenous grafts are obtained from non-essential bones of the same individual receiving the graft. They fulfil all primordial properties for bone regeneration as they are osteoconductive, osteoinductive, and they carry osteogenic cells and growth factors without the risk of transmitting immune or infective diseases. Nevertheless, due to the requirement of a surgical donor site, this type of graft can lead to post-operative pain, blood loss or hematomas, possibility of infection and aesthetic deformity, among other complications [22].

Bone grafts obtained from another individual of the same species are called allogenic; they are harvested from cadavers, making them readily available in different shapes and sizes. Allografts are also osteoinductive and osteoconductive but not osteogenic, since they lack of viable cells. They can be acquired from bone banks unprocessed and frozen, thus including all growth factors and normal ultrastructure. Otherwise, their processing includes steps such as defatting, removing the bone marrow, and commonly freeze-drying, which changes the graft's mechanical properties making them less resistant. Finally, they have to be sterilized before use. This type of graft overcomes the limitations presented by autografts, but presents some limitations such as high cost, risk of rejection, and there are still concerns related to disease transmission in spite of undergoing sterilization [23].

The term xenograft refers to bone substitutes acquired from a species other than human, frequently bovine bone tissue. Usually, all organic material is removed from the animal tissue by a high temperature treatment, followed by a chemical procedure with a strong base, such as NaOH, to obtain a porous HAp material. Xenogenic materials are readily available and show adequate absorption characteristics; however, they exhibit the same disadvantages than allografts, with additional risk of transmission of zoonoses, allergenic response, and a more

likely rejection of the graft [19]. In addition to ceramic-based xenografts, another readily available biological graft is the so-called demineralized bone matrix (DBM). It is obtained mainly from human, bovine or equine bone tissue through decalcification and sterilization, resulting in a sponge-like collagen material [20, 23]. Some commercially natural bone substitute materials are listed in Table 2.2.

Table 2.2. List of some commercially available biological grafts

Company	**Product Name**	**Composition/source**	**Form**	**Ref**
Ace Surgical Supply Co., Inc.	Nu-Oss®	Both, mineral phase and DBM derived from bovine tissue	Granules and blocks	[24]
	AlloOss®	Both, mineral phase and DBM derived from human tissue	Particles, blocks and putty	
AlloSource™	AlloFuse®	Derived from DBM of human tissue	Gel, paste and putty	[25]
	AlloFuse® Plus	Derived from DBM and ground cancellous bone of human tissue	Paste and putty	
Biomet *3i*™	Endobon®	Derived from mineral phase of bovine bone	Granules	[26]
Botiss Dental GmbH	Cerabone®	Derived from mineral phase of bovine bone	Granules and blocks	[27]
	Maxgraft®	Derived from cancellous and cortical bone of human tissue	Granules and blocks	
D-bone®	D-bone®	Derived from mineral phase of bovine bone	Granules	[28]
DePuy Synthes™	Allograft Bone Chips and Blocks	Derived from cancellous and cortical bone of human tissue	Chips and blocks	[29]
	DBX™ Material	Derived from DBM of human tissue in sodium hyaluronate carrier	Putty and strip	

Table 2.2 (continuation). List of some commercially available biological grafts

Company	Product Name	Composition/source	Form	Ref
Exactech	Optecure®	Derived from DBM of human tissue and a hydrogel carrier provided separately	Dry mix kit (powder with hydrogel)	[30]
	Optecure® *+ccc*	Cortical cancellous chips derived from human tissue	Chips (1-3 mm)	
Geistlich Pharma	Geistlich Bio-Oss®	Derived from mineral phase of bovine bone	Granules	[31]
	Geistlich Bio-Oss Collagen®	90% Geistlich Bio-Oss (granules) and 10% Porcine collagen	Scaffold	
Ost-Developpement	Laddec	Derived from mineral phase of bovine bone	Chips and blocks	[32]
	Lubboc	Derived from mineral phase of bovine bone	Chips, grafts and blocks	
Osteohealth®	Equimatrix®	Derived from mineral phase of equine bone	Granules	[33]
	OSSIF-i sem™	Both, mineral phase and DBM derived from human tissue	Particles, sponge strip and filler	
	Optimatrix®	Derived from DBM of porcine tissue	Membrane	
SigmaGraft Biomaterials	InterOss®	Derived from mineral phase of bovine bone	Granules	[34]
Tecnoss®	Tecnoss® mp3 and Tecnoss® putty	Derived from mineral phase of equine bone and additional collagen gel	Pre-hydrated bone mix, putty	[35]
	Tecnoss® Gen-Oss and Tecnoss® Chips	Derived from mineral phase of equine bone	Granules and chips	

With regard to synthetic materials, ceramic-based grafts are the most commonly used, especially based on hydroxyapatite and β-tricalcium phosphate (β-TCP), due to the advantages they present in what concerns osteoconductivity, long shelf life, unlimited supply, and absence of risk of disease or virus infection. In addition, they can be produced with different shapes, porosity and composition; commercially they are usually sold as granules, injectable pastes, and cements, among other forms [23, 36]. As for the disadvantages of these alloplastic grafts, the synthesis of HAp and β-TCP with the desire characteristics (Ca/P ratio, crystallinity and morphology, etc.) can be challenging and, despite its hardness and porosity, they are brittle, limiting their applications [23].

In efforts to improve the overall properties of ceramic materials, they have been combined with other components, mainly polymers, to produce composite and hybrid materials. Many scientists use these terms interchangeably and there is still no clear borderline between them. For the purposes of this work, the terms are used according to IUPAC definitions [37]; therefore, a composite is a material constituted by two or more components comprising multiple, different non-gaseous phases such that at least one of which is a continuous phase. The term hybrid refers to a material composed by an intimate mixture of organic or inorganic components, or both, in which normally the components interpenetrate on scales of less than 1 μm.

A number of biodegradable polymers, both synthetic and natural, have been used in combination with ceramic materials, including PLA, PGA, PLGA, collagen, alginate, and chitosan, among others. In this context, the combination with collagen has been widely studied and currently the market offers a variety of ceramic/collagen products. Chitosan-based products on the other hand, besides the many studies proving its suitability for tissue regeneration, have not yet reached the market at great scale. A list of some commercially available calcium phosphate-based alloplastic, composites and hybrid grafts is shown in Table 2.3.

Table 2.3. List of some commercially available alloplastic and composites grafts

Company	Product Name	Composition	Form	Ref
Artoss GmbH	NanoBone®	HAp (76% for granules, 61% for blocks and putty) and silicon dioxide (24% granules and 39% blocks and putty)	Granules, blocks and putty	[38]
Baxter	Actifuse	Silicate substituted calcium phosphate	Granules and scaffolds	[39]
Berkeley Advanced Biomaterials Inc	Bi-Ostetic	Tricalcium phoshpate and HAp	Granules, blocks and cylinders	[40]
	Bi-Ostetic Foam	Type I bovine collagen, tri-calcium phosphate and HAp	Foam	
Biocomposites® Ltd.	geneX®	β-TCP and calcium sulphate	Putty	[41]
	Allogran-R™	β-TCP	Granules	
Ceramed	NeoBone®	75% HAp and 25% tricalcium phosphate	Granules, blocks and wedges	[42]
	NeoCement®	Solid phase: tetracalcium phosphate and tricalcium phosphate. Liquid phase: citric acid, chitosan and apyrogenic water.	Cement (to be mixed before use)	
	k-IBS®	Calcium phosphate granules and chitosan	Injectable gel	
	n-IBS®	100% HAp nanoparticles	Injectable	
Curasan	Cerasorb M®	>99% β-TCP	Granules	[43]
Sunstar Degradable Solutions AG	Guidor® *easy-graft*®	β-tricalcium phosphate (β-TCP) granules coated with PLGA, mixed with BioLinker® (N-methyl-2-pyrrolidone (NMP) liquid activator)	Granules	[44]
DePuy Synthes™	chronOS™	100% β-TCP	Granules and scaffolds	[29]
	Norian®	Carbonated apatite and polylactide/glycolide copolymer fibers	Injectable and fast-set putty	

Table 2.3 (continuation). List of some commercially available synthetic and composites grafts

Company	Product Name	Composition	Form	Ref
Exactech	OpteMx™	60% HAp and 40% β-TCP	Granules and scaffolds	[30]
Fluidinova	nanoXIM-HAp100	100% HAp nanoparticles in pure water at concentrations 15.0 wt.% and 30.0 wt.%	Paste	[45]
	nanoXIM-HAp200	100% HAp nanoparticles agglomerates	Powder	
	nanoXIM-TCP200	100% Ca-deficient HAp nanoparticles agglomerates with 90% β-TCP phase purity	Powder	
Heraeus Kulzer GmbH	Ostim®	100% HAp nanoparticles suspended aqueous phase at concentrations 35.0 wt.%	Paste	[46]
Hoya Technosurgical Corporation	Apaceram	HAp	Particles and scaffolds	[47]
Implandent Ltd.	Osteogen®	Calcium apatite (non specified)	Powder	[48]
Kerr™	Bioplant®	Calcium hydroxide and Biodegradable polymer (non-specified)	Spherical beads	[49]
Stryker GmbH & Co.	HydroSet® Injectable	*Powder:* Di-, tri- and tetra-calcium phosphate. *Liquid:* Sodium phosphate, polyvinyl-pyrrolidone and water	Paste (to be mixed before use)	[50]
	BoneSave®	80% tricalcium phosphate and 20% HAp	Granules	
	BoneSource®	HAp	Cement	
	Vitoss® BBTrauma	β-tricalcium phosphate and bioactive glass (non-specified)	Scaffold	
Teknimed S.A.S	Cementek®	Calcium apatite (non specified) powder plus separate aqueous solution.	Injectable (to be mixed before use)	[51]
Zimmer Biomet™	Calcitite	100% HAp	Granules	[52]
	IngeniOs™	100% HAp or 100% β-TCP	Particles	

2.4 Hydroxyapatite as biomaterial for bone regeneration

Hydroxyapatite (HAp) is a member of a large isomorphous series of minerals called *apatites* that means *deceivers* in Greek, name given due to the diversity of form and colour. Apatites can be found in nature mainly in mineral deposits and in mammalians bones and teeth [53]. The apatite profusely found in sedimentary rocks is essentially carbonate fluoroapatite, whereas the one found in bones and teeth is very similar, in terms of crystallography and chemical composition, to HAp [53, 54].

The stoichiometry of HAp is represented by the formula $Ca_{10}(PO_4)_6(OH)_2$; it is a double salt of tricalcium phosphate and calcium hydroxide with a Ca/P ratio of 1.67. Deviations from Ca/P stoichiometric ratio can lead to phase impurities in HAp, such as tricalcium phosphate or CaO, that may affect biological responses [55]. At physiological temperature and pH ranging from 4 to 12, it is considered the most stable and less soluble calcium phosphate of all [55, 56]. However, the solubility of HAp, which is partly responsible for vital properties such as biocompatibility and bioactivity, depends on several factors; thus, the study of its dissolution mechanisms and rate is a subject of great interest.

The solubility rate of HAp depends on differences in shape, crystal size, porosity, crystallinity and crystallite size. In general, it is soluble in acidic solutions, insoluble in alkaline ones and slightly soluble in distilled water, which increases with addition of electrolytes. Therefore, solubility varies depending on the surrounding environment; for example, in physiological environments it is affected by the presence of amino acids, proteins, enzymes, and other organic compounds.

Barbucci (2002) [57] explains the solubility equilibrium dynamics of calcium phosphates in wet and biological environments, starting from the influence of their chemical nature on the solubility product value. Phosphate-containing compounds in solution are ruled by the following equilibria:

$$H_3PO_4 \leftrightarrow H_2PO_4^- + H^+ \quad \text{pKa} = 2.1192 \tag{2.1}$$

$$H_2PO_4^- \leftrightarrow HPO_4^{2-} + H^+ \quad \text{pKa} = 7.2076 \tag{2.2}$$

$$HPO_4^{2-} \leftrightarrow PO_4^{3-} + H^+ \quad \text{pKa} = 12.0000 \tag{2.3}$$

These equations show that in a very acidic solution, $H_2PO_4^-$ species are predominant, near neutrality HPO_4^{2-} is favoured, and PO_4^{3-} species are dominant in basic solutions. Consequently, in the presence of Ca^{2+} the precipitation of HAp is favoured in a basic environment; thus, with the contribution of the OH^- groups, its solubility product (K_{SP}) is:

$$K_{SP} = \left[Ca^{2+}\right]^5 \left[PO_4^{3-}\right]^3 \left[OH^-\right] \tag{2.4}$$

Then, in acidic conditions, below pH values of 4.3 – 4.8, HAp becomes very slowly soluble and undergoes the following transformation as a result of the decrease in OH^- concentration and the presence of H^+:

$$Ca_5\left(PO_4\right)_3 OH + 4H^+ \rightarrow 3CaHPO_4 + 2Ca^{2+} + H_2O \tag{2.5}$$

2.4.1 Structure-properties relationship

Chemical composition and crystallinity of HAp are two of the main factors that directly influence biological responses. Hydroxyapatite can be found in two different crystal forms, hexagonal and monoclinic. The hexagonal structure is most frequently found, with $P6_3/m$ space group and lattice parameters of $a=b=9.432$, $c=6.881$, and $\gamma=120^o$. In this structure, tetrahedral PO_4 groups are held together by interspersed Ca ions. The Ca ions are arranged in two distinct sites, the so-called Ca(I) are accurately aligned in columns, and the Ca(II) are organised in equilateral triangles centered on the screw axis. Finally, the hydroxide groups (OH) are found on the screw axes arranged in a column (see Figure 2.2) [58].

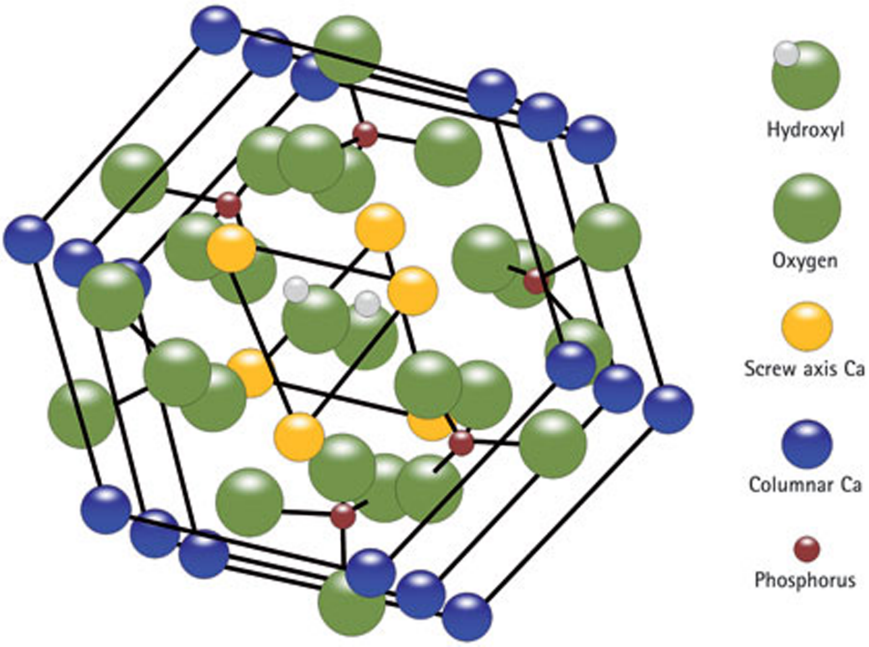

Figure 2.2. Schematic representation of hexagonal HAp
(Reproduced from Brunton et al., 2013 [59])

The atomic arrangement in HAp structure is directly related to its properties and potential biomedical applications. In aqueous media, HAp presents different net charges in its crystal planes; *a* and *b* planes are positively charged, while charges in *c* plane, are negative. Therefore, it is expected that *a* and *b* planes tend to attract acidic groups of proteins, whereas the *c* planes attract basic groups of proteins [55, 60, 61]. Moreover, morphology of HAp particles has an effect on their net charge; due to the elongation of HAp particles along the *c*-axis in their typical rod-like morphology, it is believed that the net charge of the particles would be shifted positive, giving a higher specificity of adsorption onto negatively charged proteins [61]; nevertheless, this is influenced by the pH of the aqueous medium which, at the same time, influences the dissolution mechanism and rate of HAp, as previously explained.

Dissolution mechanism and rate of HAp are, to a great extent, responsible for HAp's well known osseointegration and bioactivity properties, where *osseointegration* refers to the ability to bind to the bone, whereas *bioactivity* is the ability of a material to induce a specific biological activity such as forming Ca-containing minerals. It has been proposed that these two remarkable properties are due to a mechanism that happens at the HAp-tissue interface after implantation, starting by the dissolution of HAp [55, 62, 63]. Following dissolution, the

super-saturated solution at the interface causes the re-precipitation of calcium and phosphate ions, with the formation of carbonate apatite [64]. At this point, an exchange of ions between the HAp implant and the host bone starts, promoting both, bone bonding through the deposition of the ions on the collagenous matrix, and the adsorption of the host bone proteins to HAp surface [55, 62, 63]. Finally, attracted by the high concentration of phosphate and calcium ions, MSCs migrate to the implant surface, differentiate into osteoblasts, and start producing new bone [63]. An illustration of this mechanism is shown in Figure 2.3.

Besides chemical composition, crystallinity and morphology, particle size is another key property that affects biological responses to HAp-containing grafts and, thus, its performance throughout the mechanism described above. In its nanometric form, nano-hydroxyatatite has been proven to be more advantageous to the conventional micrometric sized HAp in what concerns the promotion of osteoblast adhesion, differentiation and proliferation, osseointegration, and deposition of Ca-containing minerals on its surface [65, 66].

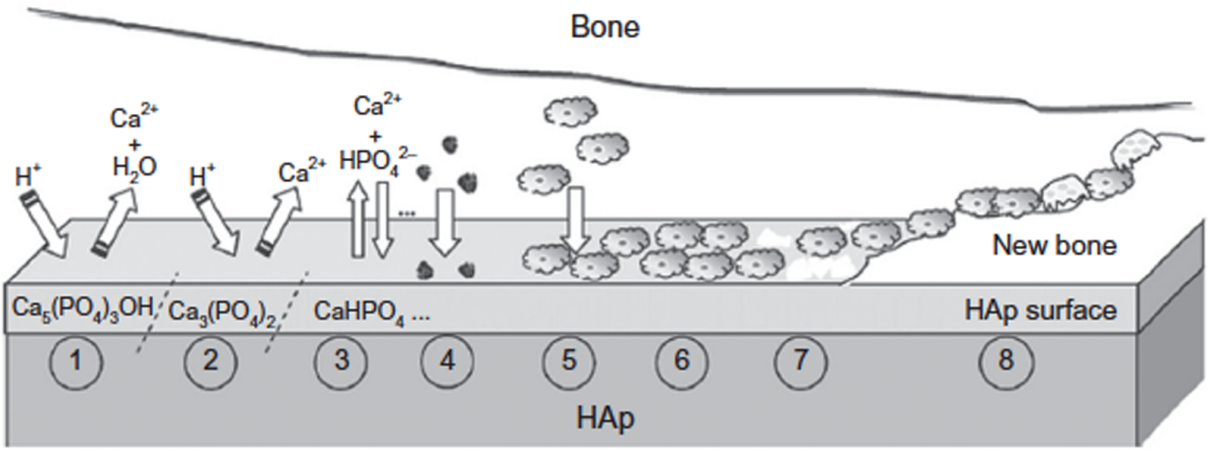

Figure 2.3. Schematic diagram representing the proposed mechanism that occurs at the surface of hydroxyapatite after implantation. (1) Dissolution of HAp after implantation; (2) Continuation of solubilisation of HAp; (3) Ionic exchange between the HAp implant and host bone; (4) Adsorption of proteins and organic material; (5) Cell adhesion; (6) Cell proliferation; (7) New bone formation; (8) New bone formed and natural bone metabolism. (Reproduced from Bertazzo et al., 2010 [62])

Cells are sensitive to the topography of an implant, both at micro- and nanoscale, since it influences factors affecting protein adsorption; among them, surface chemistry, roughness, and surface-free energy [67, 68]. Thanks to their increased surface area and higher percentages of atoms at the surface, nanoscale materials have higher surface energy, wettability and surface reactivity when compared to conventional sized materials [69, 70], which is translated into increased numbers of grain boundaries, to which proteins preferentially adsorb. As a result, grafts containing HAp in its nanometric form have shown enhanced osteoblast adhesion and function, decrease fibroblast adhesion, and enhance bone remodelling [71, 72].

Finally, when it comes to biomedical applications, biodegradation of materials into non-toxic products is highly desirable. In this sense, HAp is an appropriate ceramic material, not only for bone regeneration applications but also as a drug delivery system. Its degradation products are Ca^{2+} and PO_4^{3+} ions that already naturally occur in the body, since they are found in the bloodstream at relatively high concentrations (1-5 mM) [13].

2.5 Chitosan as biomaterial for bone regeneration

Chitosan (CS) is the main derivative of natural polymer chitin, the second most abundant natural polysaccharide on earth, estimated to be produced almost as much as cellulose, with an annual production assessed in over 10^5 tons worldwide [73, 74]. Chitin is a white, inelastic, hard, nitrogenous polysaccharide found in the exoskeleton and in the internal structure of invertebrates, mainly in crustacean shells but also in some microorganisms, yeast and fungi [75]. The use of chitin-based and chitin-derived biomaterials is growing particularly for applications that require the biodegradability property.

The high percentage of nitrogen give unique properties to chitin and chitosan, making them of commercial interest [76]. Chitosan is obtained from the partial deacetylation of chitin, typically by chemical hydrolysis under strong alkaline conditions or by enzymatic hydrolysis under the action of particular enzymes such as chitin deacetylase [77]. Therefore, chitosan is characterized mainly by its degree of deacetylation (DD); to be considered chitosan DD should be at least 50% [14]. Structures of both natural polymers are shown in Figure 2.4.

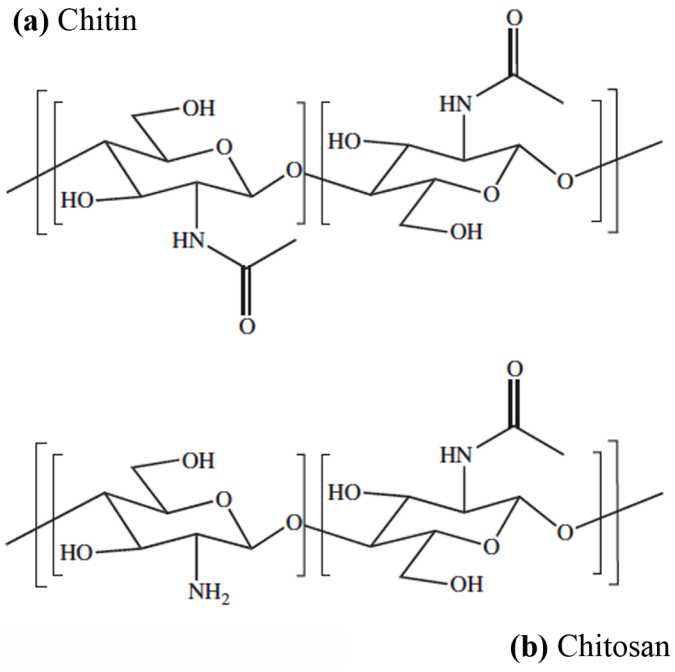

Figure 2.4. Structure of (a) chitin and; (b) chitosan.
(Reproduced from Croisier & Jérôme, 2013 [77])

Most synthetic polymers commonly used for biomedical applications present more limitations in terms of their biocompatibility and biodegradability than natural polymers such as cellulose, alginate, collagen, chitin, chitosan and their derivatives. On the other hand, some of these natural polymers may exhibit limitations in their processability [74]. In this respect, the presence of the free amino and *N*-acetyl groups in chitosan's structure, allows its solubility in aqueous, slightly acidic solutions, and therefore, allowing its processability under mild conditions.

2.5.1 Structure-properties relationship

Chitosan is a linear polymer of $(1 \rightarrow 4)$- linked 2 - amino - 2 - deoxy - β - D - glucopyranose characterized mainly by its degree of deacetylation (DD), usually ranging from 50-95%, and molecular weight, which can vary from 50 to more than 1000 kDa depending on its source and preparation method [14, 78, 79]. It is semi-crystalline, where its crystallinity is dependent on its DD, and soluble in aqueous acidic solutions, where its solubility is mostly dependent on the protonation of amino groups [14].

Chitosan presents a wide list of desirable properties for bone regeneration and controlled drug delivery, namely: biocompatibility [80, 81]; mucoadhesiveness [82, 83]; hydrophilic character which promotes osteoblast adhesion and proliferation [84]; wound healing properties [85, 86]; and non-toxic biodegradation products [77, 78]. Most of these properties are caused mainly by its cationic nature. This polymer contains in its main backbone primary amino groups that become positively charged in acidic medium, as shown in Figure 2.5 [87].

With a pKa around 6.0 – 6.5 [87, 88], it is both reactive and soluble as a function of pH, presenting solubility in the majority of organic acidic solutions including formic, acetic, tartaric, and citric acid [89]. Thus, at low pH, the amines are protonated so chitosan becomes a cationic polyelectrolyte. This polyelectrolyte property has been employed to generate multilayer films or capsules using layer-by-layer assembly [90, 91]. Otherwise, at high pH the amines are deprotonated and chitosan changes from a soluble cationic polyelectrolyte to an insoluble polymer.

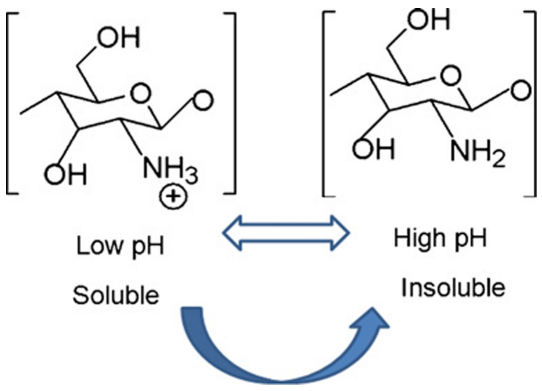

Figure 2.5. Cationic nature of chitosan
(Reproduced from Dash et al. 2012 [88])

A notable effect of chitosan's polyelectrolyte behaviour is the improved adhesion and proliferation of cells in the surface of chitosan-containing materials, caused by the electrostatic interaction of positively charged chitosan with negatively charged glycosaminoglycans (GAG), proteoglycans and other negatively charged molecules. GAG and proteoglycans are non-collagenous extracellular matrix proteins that regulate and direct the

construction and maintenance of the ECM [4]. Given that both cytokines and growth factors bond to GAG, the formation of chitosan-GAG complexes in a bone graft is beneficial because they can promote the retention and concentration of these desirable substances on its surface [78, 92].

In swollen state, chitosan acts as a natural bioadhesive polymer, ability that has been of special interest for drug delivery applications [14, 93, 94]. The mucoadhesive property of chitosan is caused by its electrostatic interaction between positively charged chitosan and negatively charged residues, namely sialic acid, on mucosal surfaces [77]. Another feature of chitosan attributed to electrostatic interactions is its capacity to induce haemostasis, which has been related to interactions of positive charges of chitosan with negatively charged red blood cell membranes [77, 95, 96].

The antimicrobial activity of chitosan, a fundamental property in wound healing processes, has been widely studied [96-99]. In what regards orthopaedic implants, bacterial infection is a major concern due to the severe consequences it can lead to, such as implant failure, hospitalization and sometimes even mortality of the patient [98]. Mechanisms explaining antibacterial and antifungal activity of chitosan are more complex. The first mechanism proposes that the high affinity of cationic groups of chitosan towards the anionic components in microorganisms' cell wall, such as Gram-negative lipopolysaccharide and cell surface proteins, alters the cells permeability preventing the mass transport of essential materials across the cell wall. The second mechanism proposes the inhibition of the microbial RNA synthesis due to the bonding of protonated amino groups of chitosan with the cell DNA [77, 79, 100].

Another important property of chitosan is its biodegradability. A wide range of biomedical applications, including matrices for controlled drug release, resorbable devices such as bone cements, and scaffolds for tissue engineering, require the controlled degradation of the biomaterials over time in order to let the natural tissue develop and completely replace the foreign element [101]. Chitosan's biodegradability takes place by lysozyme action, an abundant enzyme found in the human body, through the degradation into small glycomino chains, with degradation rate being inversely related to the degree of deacetylation. Regarding the biocompatibility of the degradation products, it has been reported that these

products undergo a quick elimination by the kidney, thus avoiding accumulation in the body [14, 101].

In addition to all the above-mentioned desirable properties, the solubility of chitosan in aqueous acidic medium allows its processing under mild conditions [12, 77] that, together with chitosan's ability to be shaped into different forms such as porous scaffolds [102-104], fibers [105, 106], sponges [84] and microparticles [107-109], are advantageous features for tissue engineering applications [14]. Another advantage is its availability in large quantities and at adequate commercial grades [110].

2.6 HAp/CS hybrid materials

The combination of nano-hydroxyapatite (n-HAp) with chitosan (CS) has been of special interest for biomedical applications, particularly for bone regeneration. Hydroxyapatite by itself is highly brittle, whereas chitosan, despite its capacity to promote osteogenic cells attachment and proliferation, it does not induce the deposition of bone minerals on its own. Therefore, when combining both components, HAp provides the required bioactivity while chitosan adds elasticity to the final material, resulting in a great candidate for non-load-bearing bone graft applications [9, 12]. However, even though combining HAp and chitosan can be advantageous, the production of such hybrid system still faces several challenges.

The final properties of any hybrid inorganic–organic system are affected by several important aspects that must be considered. A hybrid material consists of at least two phases separated by an interface, in which one of the phases is usually inorganic, consisting of filler particles, dispersed in the second phase, a polymeric matrix. The filler's shape and size, properties and volume percentage, the matrix properties such as molecular weight, the dispersion stability of the filler in the polymeric matrix, and the interactions in the filler/matrix interface are some of the main factors influencing the properties of the hybrid [65]. Furthermore, in the case of hybrid materials for biomedical applications, biocompatibility, degradation rate and non-toxicity must be considered as previously discussed.

From a chemical point of view, there are several ways to incorporate inorganic particles (fillers) into organic polymers, depending on the interactions between the constituents, either

strong, weak, or without any chemical interactions between them. Strong interactions can be covalent, coordination type, and ionic bonds, whereas van-der-Waals, hydrogen bonds, and hydrophilic–hydrophobic are considered weak interactions. Inorganic–organic hybrid materials can be classified based on such interactions and the different arrangements of the polymer chains relative to the inorganic nanoparticles. In this regard, Kickelbick (2003) proposed four different types of arrangements, as shown in Figure 2.6**.**

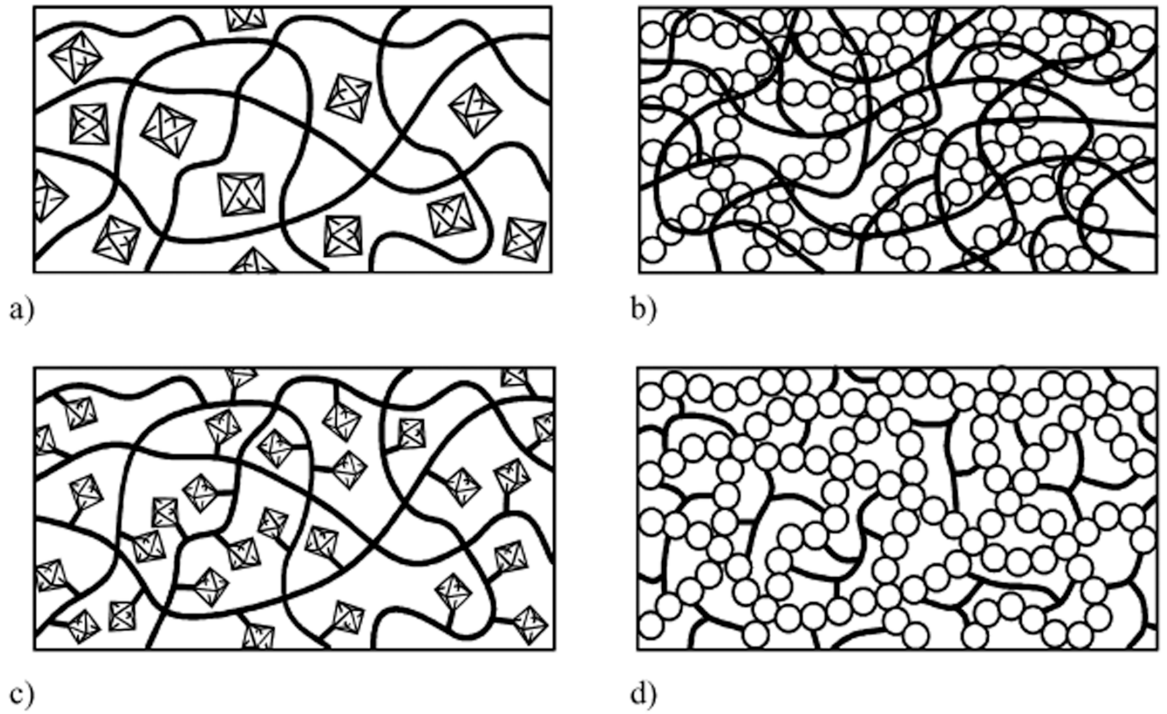

Figure 2.6. Schematic representation of different types of inorganic-organic hybrid materials based on polymeric chain arrangements relative to the inorganic particles: (a) inorganic particles embedded into the organic polymer; (b) interpenetrating polymer networks (IPNs); (c) inorganic particles chemically bound to the polymer backbone and; (d) dual inorganic-organic hybrid polymer.
(Reproduced from Kickelbick, 2003 [111])

The first arrangement (Figure 2.6a) takes place when, in the absence of strong interactions, the inorganic particles are dispersed in the organic matrix such that, depending on the functionalities of the components, the inorganic units undergo weak crosslinking through physical interactions with the polymer or, the inorganic particles are entrapped in a crosslinked polymeric matrix [112]. Interpenetrating polymer networks (IPNs) consist of a polymer comprising two or more networks that are, on a molecular scale, partially or totally

interlaced but not covalently bound (Figure 2.6b). In the case of inorganic–organic IPNs, formed for example by sol-gel reactions, one of the networks is formed by the inorganic component, and they can be processed either simultaneously or sequentially [113]. Finally, the hybrids can be produced by discrete (Figure 2.6c) or interconnected (Figure 2.6d) inorganic particles attached to the polymer backbone by covalent bonds [111, 112].

The chemical nature of chitosan makes it a versatile polymer as it can be either chemically or physically crosslinked. Chemical crosslinking is irreversible since a polymeric network is formed by covalent bonds, requiring the assistance of a crosslinking agent such as glutaraldehyde or genipin. Physical crosslinking, on the other hand, is reversible since linkage occurs through van der Waals forces, ionic attractions, hydrogen bonding, or hydrophobic interactions [101, 114]. Considering this, the incorporation of HAp nanoparticles into a chitosan solution can be done following several techniques as described in the next section.

2.7 Overview of HAp/CS materials preparation, purification and sterilization methods

With advances in technology, various methods for producing HAp/CS hybrid materials have been reported, following both, chemical and physical paths. In general, the production of HAp/CS materials requires a first stage of dispersion preparation, in which HAp and chitosan are combined to produce the base material that, in a second stage, is shaped into the final form. Thus, the second stage consists in the fixation of the structure – into microparticles, granules, scaffolds, cements, etc. – carried out by inducing phase separation and the elimination of the solvent. Afterwards, the produced hybrids usually have to be subjected to purification and sterilization processes, since their potential applications are within the biomedical field. One of the key issues in these sequential procedures is to guarantee that none of the stages compromises, among other desirable properties, the morphological and architectural features of the final envisaged forms (scaffolds, powders etc.) in order to ensure a suitable environment for cell attachment and proliferation.

2.7.1 Dispersion preparation

This is the first and key stage since here is when HAp is incorporated into the chitosan solution. The dispersion preparation step can be done in a number of ways; among all the methods reported, *in situ* co-precipitation and simple mixing are the most popular [12, 115].

One of the methods preferred by some authors is the so-called *in situ* co-precipitation [116-118]. In this method, the synthesis of HAp is carried out in the presence of chitosan in a neutral or basic environment (pH $\geq$ 7), therefore, causing the precipitation of chitosan along with HAp simultaneously. Yamaguchi et al. (2001) [116] developed a methodology that consisted in dripping chitosan in H_3PO_4 solution on a calcium hydroxide suspension. Homogeneous incorporation of HAp into the chitosan solution has been reported using this process, however, the fact that the formation of HAp occurs in the presence of chitosan can hinder the synthesis of HAp particles with high purity and desired morphology.

An alternative attractive method consists in physically mixing previously synthesized HAp particles, usually in powder form or ultrasonically dispersed in water, into a chitosan solution. Typically, this technique, also called simple mixing method, is carried out at lab-scale, by mixing both components in a vessel using a magnetic stirrer, resulting in final hybrid materials with quite favourable physicochemical and biological properties [119-121]. This is a simple and straightforward technique, that can also be advantageous in terms of reproducibility relative to the co-precipitation method; nevertheless it can lead to non-homogenous dispersions at a microscopic level due to the difficulty in controlling the mixing between the two dissimilar phases that can undergo phase separation [65, 122] and, therefore, originate final materials with weaker mechanical properties when compared to other methods [123, 124].

Another important parameter to consider when preparing n-HAp/CS hybrid dispersions is the pH, especially if HAp has to be introduced into an acidic environment that can influence its solubility, chemistry and phase stability [125]. When the method of physically mixing both components is used, HAp is often introduced in an acidic chitosan solution, resulting in dispersions with pH typically around 4, potentially causing the dissolution of HAp [126].

2.7.2 Phase separation/Solvent elimination

This stage involves the structural fixation of the n-HAp/CS hybrid material in its final form, such as microparticles, granules, pastes, scaffolds, cements, etc. The most typical structure produced for bone regeneration is 3D scaffolds, which are frequently produced from the previously prepared n-HAp/CS dispersion by thermally induced phase separation (TIPS). This is a simple procedure usually carried out by freeze-drying, in which phase separation is induced by the formation of ice crystals upon freezing, followed by the elimination of the solvent by the sublimation of the ice crystals, producing the final hybrid 3D porous structure [12, 14, 127]. Many authors using this technique obtained n-HAp/CS based hybrid scaffolds with desirable high porosity and interconnected pores [6, 120, 121, 127-131]. Other popular phase separation/solvent elimination techniques to produce n-HAp/CS scaffolds are particulate leaching [132, 133], gas foaming [134], and freeze-gelation [135].

Another attractive n-HAp/CS structure to be produced for biomedical applications is in the form of microparticles. The use of microparticles in tissue engineering and regenerative medicine can be very beneficial from a functional point of view; these are very versatile structures that, thanks to their reduced size, can be used as injectable systems, shaped into a solid substrate with increased surface area capable to promote chemical and biological reactions, or even be embedded into hybrid scaffolds for controlled release of bio-active substances [136-138]. Among the methods that have been exploited to produce n-HAp/CS microparticles are: water-in-oil (W/O) emulsion [139]; supercritical assisted atomization [140], spray-coagulation [141], electro-spray coagulation [142], dispersion polymerization [143], and spray-drying [144, 145].

2.7.3 Purification/Neutralization

In most cases the obtained n-HAp/CS hybrid material still contains residual substances left from the process. The residual substances are commonly reagents in excess, e.g. a base when the synthesis of HAp is carried out during co-precipitation method, or acetic acid used to solubilize the chitosan in the case of simple mixing method. Thus, a purification/neutralization step is usually necessary to eliminate the residual substances that can affect the final properties of the material, cause structure disruption, or even inhibit cell growth and proliferation. The presence, for example, of residual acid can potentially cause

structure disruption due to dissolution of chitosan in aqueous medium [14]. Whereas, in order to promote cell survival and proliferation, the culture environment must fulfil some fundamental physiological requirements, such as composition and pH [146], that may be affected due to the presence of acid and/or alkaline impurities.

2.7.4 Sterilization

As any medical device that is implanted in the human body, n-HAp/CS hybrid materials produced for biomedical applications must be subjected to sterilization. The term *sterilization* refers to a procedure, either chemical or physical, which purpose is to destroy all microbial life, including highly resistant bacterial endospores [147]. Typical sterilization techniques include saturated water steam (autoclave), dry heat, ethylene oxide (EtO), and *gamma*-irradiation. These techniques have proven to be effective eliminating microorganisms, however, they can induce changes in the macromolecular structure of polymeric materials by chain scission, oxidation, hydrolysis, and depolymerisation, depending on the polymer's nature and the used sterilization technique [148].

Therefore, when designing n-HAp/CS hybrid materials, sterilization is an important procedure to consider. Given that chitosan is a thermo-sensitive material, common sterilization techniques, such as dry heat and steam, are not appropriate since they can cause thermal degradation of the material. Ethylene oxide and *gamma* irradiation, on the other hand, can affect its chemical properties; the use of ethylene oxide risks the deposition of toxic residues on the materials surfaces and high-energy *gamma* irradiation can cause material degradation as well [149]. In such a scenario, the use $scCO_2$ as an innovative sterilization technique has recently emerged [149-156] and it appears as a promising technique to sterilize n-HAp/CS hybrid materials.

2.8 Conclusions

Hydroxyapatite is an outstanding material that has been proven to exhibit highly desirable properties for biomedical applications, mostly for bone regeneration due to its similarity with the mineral phase of bone. It has been combined with several polymers as an effort to produce materials with improved properties. Particularly, its combination with chitosan has

been of great interest for the production of non-load bearing bone grafts, given the possibility to generate materials mimicking bone composition and with improved properties, namely in what concerns elasticity. In addition, chitosan provides a wide list of desirable properties: it promotes osteoblasts adhesion and proliferation, possesses antimicrobial properties, it can be processed using mild conditions and can be shaped into different forms, to name some.

Commercially available products for bone regeneration still consist, in a great extent, of biological grafts, either from human or animal sources. However, these grafts exhibit a list of concerning drawbacks, namely, high cost, risk of rejection, risk of diseases and zoonoses transmission, allergenic responses, etc. In what concerns synthetic materials, currently the market offers a variety of calcium phosphate-based products, alone or in combination with other components, mainly collagen. In this work, only one company commercialising calcium phosphate-based products containing chitosan was found, showing that, besides the many studies proving its suitability for tissue regeneration, HAp/CS hybrid materials have not yet made the leap from the laboratory to the market.

Relative to the production of n-HAp/CS hybrid materials suitable for biomedical applications, a sequence of productive steps must be followed without neglecting purification and sterilization. Generally, a key first stage of dispersion preparation is required, in which n-HAp is incorporated into the chitosan solution. A second stage consists in a phase separation/solvent elimination process in which the fixation of the final structural form takes place, to produce n-HAp/CS hybrid microparticles, pastes, scaffolds, cements, etc. Finally, as their potential applications are within the biomedical field, the produced hybrid materials have to be subjected to purification and sterilization processes.

However, each of the above-mentioned stages faces challenges. The preparation of n-HAp/CS hybrid dispersions requires the introduction of HAp into an aqueous environment that can influence its solubility, surface chemistry and phase stability, affecting, at the same time, the HAp-nanoparticles/CS-matrix interface interactions and, therefore, the final properties of the material. The phase separation/solvent elimination stage determines important structural features of the final product, such as pore size and interconnectivity, particle size and morphology, and it can dictate the need for subsequent purification processes. Purification is a fundamental procedure that can be time consuming, ineffective and potentially alter the properties of the obtained n-HAp/CS hybrid materials. Sterilization is as well a key step, but

most common methods available today can cause thermal degradation or risks concerning the deposition of toxic residues on the materials surfaces. Finally, the overall process will have an important influence in the final product in terms of efficiency, costs, reproducibility, properties and versatility. It is of utmost importance from a clinical point of view to have ready-to-use products without requiring extra steps prior use, and materials that can be easily adapted into different shapes.

2.9 References

[1] Fathi, M., A. Hanifi, and V. Mortazavi. *Preparation and bioactivity evaluation of bone-like hydroxyapatite nanopowder.* Journal of materials processing technology, 202, 536-542 (2008).

[2] Hossein Fathi, M., V. Mortazavi, and S.I. Roohani Esfahani, *Bioactivity Evaluation of Synthetic Nanocrystalline Hydroxyapatite*. 2009. Vol. 5. 2009.

[3] Teixeira, S., M. Ferraz, and F. Monteiro. *Biocompatibility of highly macroporous ceramic scaffolds: cell adhesion and morphology studies.* Journal of Materials Science: Materials in Medicine, 19, 855-859 (2008).

[4] Burr, D.B. and M.R. Allen, *Basic and Applied Bone Biology*. 2013: Elsevier Science.

[5] Bonfield, W., et al. *Hydroxyapatite reinforced polyethylene — a mechanically compatible implant material for bone replacement.* Biomaterials, 2, 185-186 (1981).

[6] Wei, G. and P.X. Ma. *Structure and properties of nano-hydroxyapatite/polymer composite scaffolds for bone tissue engineering.* Biomaterials, 25, 4749-57 (2004).

[7] Agrawal, C.M., G.G. Niederauer, and K.A. Athanasiou. *Fabrication and characterization of PLA-PGA orthopedic implants.* Tissue engineering, 1, 241-252 (1995).

[8] Agrawal, C. and R.B. Ray. *Biodegradable polymeric scaffolds for musculoskeletal tissue engineering.* Journal of biomedical materials research, 55, 141-150 (2001).

[9] Dorozhkin, S.V. *Biocomposites and hybrid biomaterials based on calcium orthophosphates.* Biomatter, 1, 3-56 (2011).

[10] O'Brien, F.J. *Biomaterials & scaffolds for tissue engineering.* Materials Today, 14, 88-95 (2011).

[11] Amit, S.M., S. Xinfeng, and G.M. Antonios, *Nanocomposite Scaffolds for Tissue Engineering*, in *Tissue Engineering and Artificial Organs*, J.D. Bronzino, Editor. 2006, CRC Press. p. 40-1-40-11.

[12] Levengood, S.K.L. and M. Zhang. *Chitosan-based scaffolds for bone tissue engineering.* J. Mater. Chem. B, 2, 3161 (2014).

[13] Bose, S. and S. Tarafder. *Calcium phosphate ceramic systems in growth factor and drug delivery for bone tissue engineering: A review.* Acta Biomaterialia, 8, 1401-1421 (2012).

[14] Costa-Pinto, A.R., R.L. Reis, and N.M. Neves. *Scaffolds based bone tissue engineering: the role of chitosan.* Tissue Eng Part B Rev, 17, 331-47 (2011).

[15] Bose, S., M. Roy, and A. Bandyopadhyay. *Recent advances in bone tissue engineering scaffolds.* Trends in Biotechnology, 30, 546-554 (2012).

[16] Ricciardi, B.F. and M.P. Bostrom. *Bone graft substitutes: Claims and credibility.* Seminars in Arthroplasty, 24, 119-123 (2013).

[17] Liu, X. and P.X. Ma. *Polymeric scaffolds for bone tissue engineering.* Annals of biomedical engineering, 32, 477-486 (2004).

[18] Rodrigues, S.C., et al. *Preparation and characterization of collagen-nanohydroxyapatite biocomposite scaffolds by cryogelation method for bone tissue engineering applications.* Journal of Biomedical Materials Research Part A, 101A, 1080-1094 (2013).

[19] Oryan, A., et al. *Bone regenerative medicine: classic options, novel strategies, and future directions.* Journal of Orthopaedic Surgery and Research, 9, 1-27 (2014).

[20] Kolk, A., et al. *Current trends and future perspectives of bone substitute materials – From space holders to innovative biomaterials.* Journal of Cranio-Maxillofacial Surgery, 40, 706-718 (2012).

[21] Kumar, P., B. Vinitha, and G. Fathima. *Bone grafts in dentistry.* Journal of Pharmacy & Bioallied Sciences, 5, S125-S127 (2013).

[22] Campana, V., et al. *Bone substitutes in orthopaedic surgery: from basic science to clinical practice.* Journal of Materials Science. Materials in Medicine, 25, 2445-2461 (2014).

[23] Zimmermann, G. and A. Moghaddam. *Allograft bone matrix versus synthetic bone graft substitutes.* Injury, 42, Supplement 2, S16-S21 (2011).

[24] *Ace Surgical Supply Co., Inc.* [cited 2016 March 24th]; Available from: http://www.acesurgical.com/bone-grafting.html.

[25] *AlloSource TM.* [cited 2016 March 24th]; Available from: http://www.allosource.org.

[26] *Biomet3i TM.* [cited 2016 March 24th]; Available from: http://www.biomet3i.com/index.cfm?cty=US&lang=EN.

[27] *Botiss Dental GmbH.* [cited 2016 March 24th]; Available from: https://www.botiss.com/en/.

[28] *D-bone®.* [cited 2016 March 24th]; Available from: http://dbonegraft.com.

[29] *DePuy Synthes TM.* [cited 2016 March 24th]; Available from: http://emea.depuysynthes.com/hcp/biomaterials.

[30] *Exactech.* [cited 2016 March 24th]; Available from: https://www.exac.com/products/biologics/.

[31] *Geistlich Pharma.* [cited 2016 March 24th]; Available from: http://www.geistlich-pharma.com/en/.

[32] *Ost-Developpement.* [cited 2016 March 24th]; Available from: http://www.ost-developpement.com.

[33] *Osteohealth®.* [cited 2016 March 24th]; Available from: http://www.osteohealth.com/Products.aspx.

[34] *SigmaGraft Biomaterials.* [cited 2016 March 24th]; Available from: http://sigmagraft.com/inteross.

[35] *Tecnoss®*. [cited 2016 March 24th]; Available from: http://www.tecnoss.com/product.html.

[36] Dorozhkin, S.V. *Calcium Orthophosphates as Bioceramics: State of the Art.* Journal of Functional Biomaterials, 1, 22 (2010).

[37] McNaught, A.D. and A.D. McNaught, *Compendium of chemical terminology (Gold Book, version 2.3.3)*. 2014: Blackwell Science Oxford.

[38] *Artoss GmbH.* [cited 2016 March 28th]; Available from: http://www.artoss.com/dental/produkte.html?L=1.

[39] *Baxter.* [cited 2016 March 28th]; Available from: http://www.baxterbiosurgery.com/us/products/actifuse//formulations/actifuse_mis.html.

[40] *Berkeley Advanced Biomaterials Inc.* [cited 2016 March 28th]; Available from: http://www.ostetic.com/products.html.

[41] *Biocomposites® Ltd.* [cited 2016 March 28th]; Available from: http://www.biocomposites.com/our-products/.

[42] *Ceramed.* [cited 2016 March 28th]; Available from: http://www.ceramed.pt.

[43] *Curasan.* [cited 2016 March 28th]; Available from: http://www.curasan.de/en/portfolio-item/cerasorb-m-granulate-dental/ - toggle-id-2.

[44] *Sunstar Degradable Solutions AG.* [cited 2016 March 28th]; Available from: http://us.guidor.com.

[45] *Fluidinova.* [cited 2016 March 28th]; Available from: http://www.fluidinova.com.

[46] *Heraeus Kulzer GmbH.* [cited 2016 March 28th]; Available from: http://heraeus-kulzer.com/en/int/dentist/products_from_a_to_z/ostim_1/ostim.aspx.

[47] *Hoya Technosurgical Corporation.* [cited 2016 March 28th]; Available from: http://www.hoyatechnosurgical.co.jp/pentax/newceramics_e.php.

[48] *Implandent Ltd.* [cited 2016 March 28th]; Available from: http://www.impladentltd.com/OsteoGen-p/200.htm.

[49] *Kerr TM.* [cited 2016 March 28th]; Available from: https://www.kerrdental.com/kerr-restoratives/bioplant-dental-bone-grafting-material.

[50] *Stryker GmbH & Co.* [cited 2016 March 28th]; Available from: http://www.stryker.com/emea/Products/Orthopaedics/BoneSubstitutes/index.htm.

[51] *Teknimed S.A.S.* [cited 2016 March 28th]; Available from: http://www.teknimed.com/products-portfolio/products/orthopaedic-trauma-cmf/bone-substitutes/cementek/.

[52] *Zimmer Biomet TM.* [cited 2016 March 28th]; Available from: http://www.zimmerdental.com/Products/Regenerative/rg_BoneGraftOverview.aspx.

[53] Park, J., *Bioceramics: Properties, Characterizations, and Applications*. 2009: Springer New York.

[54] Kantharia, N., et al. *Nano-hydroxyapatite and its contemporary applications.* Bone, 34, 1.71 (2014).

[55] Mucalo, M., *Hydroxyapatite (HAp) for Biomedical Applications*. 2015: Elsevier Science.

[56] Koutsopoulos, S. *Kinetic Study on the Crystal Growth of Hydroxyapatite.* Langmuir, 17, 8092-8097 (2001).

[57] Barbucci, R., *Integrated biomaterials science*. 2002: Springer Science & Business Media.

[58] Ma, G. and X.Y. Liu. *Hydroxyapatite: hexagonal or monoclinic?* Crystal Growth and Design, 9, 2991-2994 (2009).

[59] Brunton, P.A., et al. *Treatment of early caries lesions using biomimetic self-assembling peptides - a clinical safety trial.* Br Dent J, 215, E6-E6 (2013).

[60] Kandori, K., et al. *Synthesis of positively charged calcium hydroxyapatite nano-crystals and their adsorption behavior of proteins.* Colloids and Surfaces B: Biointerfaces, 73, 140-145 (2009).

[61] Uskoković, V. and D.P. Uskoković. *Nanosized hydroxyapatite and other calcium phosphates: Chemistry of formation and application as drug and gene delivery agents.* Journal of Biomedical Materials Research Part B: Applied Biomaterials, 96B, 152-191 (2011).

[62] Bertazzo, S., et al. *Hydroxyapatite surface solubility and effect on cell adhesion.* Colloids and Surfaces B: Biointerfaces, 78, 177-184 (2010).

[63] Ducheyne, P. and Q. Qiu. *Bioactive ceramics: the effect of surface reactivity on bone formation and bone cell function.* Biomaterials, 20, 2287-2303 (1999).

[64] Ducheyne, P., S. Radin, and L. King. *The effect of calcium phosphate ceramic composition and structure on in vitro behavior. I. Dissolution.* Journal of Biomedical Materials Research, 27, 25-34 (1993).

[65] Supova, M. *Problem of hydroxyapatite dispersion in polymer matrices: a review.* J Mater Sci Mater Med, 20, 1201-13 (2009).

[66] Webster, T.J., et al. *Enhanced functions of osteoblasts on nanophase ceramics.* Biomaterials, 21, 1803-1810 (2000).

[67] Rouahi, M., et al. *Physico-chemical characteristics and protein adsorption potential of hydroxyapatite particles: Influence on in vitro biocompatibility of ceramics after sintering.* Colloids and Surfaces B: Biointerfaces, 47, 10-19 (2006).

[68] dos Santos, E.A., et al. *Chemical and topographical influence of hydroxyapatite and β -tricalcium phosphate surfaces on human osteoblastic cell behavior.* Journal of Biomedical Materials Research Part A, 89A, 510-520 (2009).

[69] Gleiter, H. *Nanostructured materials: state of the art and perspectives.* Nanostructured Materials, 6, 3-14 (1995).

[70] Sato, M. and T.J. Webster. *Nanobiotechnology: implications for the future of nanotechnology in orthopedic applications.* Expert review of medical devices, 1, 105-114 (2004).

[71] Tran, N. and T.J. Webster. *Nanotechnology for bone materials.* Wiley Interdisciplinary Reviews: Nanomedicine and Nanobiotechnology, 1, 336-351 (2009).

[72] Yang, L., L. Zhang, and T.J. Webster. *Nanobiomaterials: State of the Art and Future Trends.* Advanced Engineering Materials, 13, B197-B217 (2011).

[73] Zikakis, J., *Chitin, Chitosan, and Related Enzymes*. 2012: Elsevier Science.

[74] Ravi Kumar, M.N.V. *A review of chitin and chitosan applications.* Reactive and Functional Polymers, 46, 1-27 (2000).

[75] Hamid, R., et al. *Chitinases: An update.* Journal of Pharmacy & Bioallied Sciences, 5, 21-29 (2013).

[76] Georgieva, V., D. Zvezdova, and L. Vlaev. *Non-isothermal kinetics of thermal degradation of chitosan.* Chemistry Central Journal, 6, 81-81 (2012).

[77] Croisier, F. and C. Jérôme. *Chitosan-based biomaterials for tissue engineering.* European Polymer Journal, 49, 780-792 (2013).

[78] Di Martino, A., M. Sittinger, and M.V. Risbud. *Chitosan: A versatile biopolymer for orthopaedic tissue-engineering.* Biomaterials, 26, 5983-5990 (2005).

[79] Domb, A.J. and N. Kumar, *Biodegradable polymers in clinical use and clinical development*. 2011: John Wiley & Sons.

[80] Bavariya, A.J., et al. *Evaluation of biocompatibility and degradation of chitosan nanofiber membrane crosslinked with genipin.* Journal of Biomedical Materials Research Part B: Applied Biomaterials, 102, 1084-1092 (2014).

[81] Shin, S.-Y., et al. *Biological evaluation of chitosan nanofiber membrane for guided bone regeneration.* Journal of periodontology, 76, 1778-1784 (2005).

[82] He, P., S.S. Davis, and L. Illum. *In vitro evaluation of the mucoadhesive properties of chitosan microspheres.* International Journal of Pharmaceutics, 166, 75-88 (1998).

[83] Lehr, C.-M., et al. *In vitro evaluation of mucoadhesive properties of chitosan and some other natural polymers.* International Journal of Pharmaceutics, 78, 43-48 (1992).

[84] Seol, Y.-J., et al. *Chitosan sponges as tissue engineering scaffolds for bone formation.* Biotechnology letters, 26, 1037-1041 (2004).

[85] Azad, A.K., et al. *Chitosan membrane as a wound-healing dressing: Characterization and clinical application.* Journal of Biomedical Materials Research Part B: Applied Biomaterials, 69B, 216-222 (2004).

[86] Ueno, H., et al. *Accelerating effects of chitosan for healing at early phase of experimental open wound in dogs.* Biomaterials, 20, 1407-1414 (1999).

[87] Samal, S.K., et al. *Cationic polymers and their therapeutic potential.* Chemical Society Reviews, 41, 7147-7194 (2012).

[88] Dash, M., et al. *Chitosan—A versatile semi-synthetic polymer in biomedical applications.* Progress in Polymer Science, 36, 981-1014 (2011).

[89] Nagpal, K., S.K. Singh, and D.N. Mishra. *Chitosan nanoparticles: a promising system in novel drug delivery.* Chemical and Pharmaceutical Bulletin, 58, 1423-1430 (2010).

[90] Berth, G., et al. *Polyelectrolyte Complexes and Layer-by-Layer Capsules from Chitosan/Chitosan Sulfate.* Biomacromolecules, 3, 579-590 (2002).

[91] Picart, C., et al. *Controlled degradability of polysaccharide multilayer films in vitro and in vivo.* Advanced Functional Materials, 15, 1771-1780 (2005).

[92] Kim, I.-Y., et al. *Chitosan and its derivatives for tissue engineering applications.* Biotechnology Advances, 26, 1-21 (2008).

[93] Şenel, S. and S.J. McClure. *Potential applications of chitosan in veterinary medicine.* Advanced Drug Delivery Reviews, 56, 1467-1480 (2004).

[94] Bertram, U. and R. Bodmeier. *In situ gelling, bioadhesive nasal inserts for extended drug delivery: In vitro characterization of a new nasal dosage form.* European Journal of Pharmaceutical Sciences, 27, 62-71 (2006).

[95] Rao, S.B. and C.P. Sharma. *Use of chitosan as a biomaterial: studies on its safety and hemostatic potential.* Journal of biomedical materials research, 34, 21-28 (1997).

[96] Ong, S.-Y., et al. *Development of a chitosan-based wound dressing with improved hemostatic and antimicrobial properties.* Biomaterials, 29, 4323-4332 (2008).

[97] Altiok, D., E. Altiok, and F. Tihminlioglu. *Physical, antibacterial and antioxidant properties of chitosan films incorporated with thyme oil for potential wound healing applications.* Journal of Materials Science: Materials in Medicine, 21, 2227-2236 (2010).

[98] Saravanan, S., et al. *Preparation, characterization and antimicrobial activity of a bio-composite scaffold containing chitosan/nano-hydroxyapatite/nano-silver for bone tissue engineering.* International Journal of Biological Macromolecules, 49, 188-193 (2011).

[99] Shi, Z., et al. *Antibacterial and mechanical properties of bone cement impregnated with chitosan nanoparticles.* Biomaterials, 27, 2440-2449 (2006).

[100] Kong, M., et al. *Antimicrobial properties of chitosan and mode of action: A state of the art review.* International Journal of Food Microbiology, 144, 51-63 (2010).

[101] Reis, R.L., et al., *Natural-based polymers for biomedical applications*. 2008: Elsevier.

[102] Araujo, J.V., et al. *Novel porous scaffolds of pH responsive chitosan/carrageenan-based polyelectrolyte complexes for tissue engineering.* Journal of Biomedical Materials Research Part A, 102, 4415-4426 (2014).

[103] Ji, C., et al. *Fabrication of porous chitosan scaffolds for soft tissue engineering using dense gas CO2.* Acta Biomaterialia, 7, 1653-1664 (2011).

[104] Siddiqui, N., K. Pramanik, and E. Jabbari. *Osteogenic differentiation of human mesenchymal stem cells in freeze-gelled chitosan/nano β-tricalcium phosphate porous scaffolds crosslinked with genipin.* Materials Science and Engineering: C, 54, 76-83 (2015).

[105] Aklog, Y.F., et al. *Preparation of chitosan nanofibers from completely deacetylated chitosan powder by a downsizing process.* International Journal of Biological Macromolecules, 72, 1191-1195 (2015).

[106] Albanna, M.Z., et al. *Chitosan fibers with improved biological and mechanical properties for tissue engineering applications.* Journal of the Mechanical Behavior of Biomedical Materials, 20, 217-226 (2013).

[107] Custódio, C.A., et al. *Cell selective chitosan microparticles as injectable cell carriers for tissue regeneration.* Biomaterials, 43, 23-31 (2015).

[108] Obaidat, R., et al. *Drying Using Supercritical Fluid Technology as a Potential Method for Preparation of Chitosan Aerogel Microparticles.* AAPS PharmSciTech, 1-10 (2015).

[109] Shen, Y.-B., et al. *Preparation of chitosan microparticles with diverse molecular weights using supercritical fluid assisted atomization introduced by hydrodynamic cavitation mixer.* Powder Technology, 254, 416-424 (2014).

[110] Bansal, V., et al. *Applications of chitosan and chitosan derivatives in drug delivery.* Advances in Biological Research, 5, 28-37 (2011).

[111] Kickelbick, G. *Concepts for the incorporation of inorganic building blocks into organic polymers on a nanoscale.* Progress in Polymer Science, 28, 83-114 (2003).

[112] Kickelbick, G., *Introduction to Hybrid Materials*, in *Hybrid Materials*. 2007, Wiley-VCH Verlag GmbH & Co. KGaA. p. 1-48.

[113] Alemán, J., et al. *Definitions of terms relating to the structure and processing of sols, gels, networks, and inorganic-organic hybrid materials (IUPAC Recommendations 2007).* Pure and Applied Chemistry, 79, 1801-1829 (2007).

[114] Berger, J., et al. *Structure and interactions in covalently and ionically crosslinked chitosan hydrogels for biomedical applications.* European Journal of Pharmaceutics and Biopharmaceutics, 57, 19-34 (2004).

[115] Venkatesan, J. and S.-K. Kim. *Nano-hydroxyapatite composite biomaterials for bone tissue engineering—A review.* Journal of biomedical nanotechnology, 10, 3124-3140 (2014).

[116] Yamaguchi, I., et al. *Preparation and microstructure analysis of chitosan/hydroxyapatite nanocomposites.* Journal of biomedical materials research, 55, 20-27 (2001).

[117] Chen, F., Z.-C. Wang, and C.-J. Lin. *Preparation and characterization of nano-sized hydroxyapatite particles and hydroxyapatite/chitosan nano-composite for use in biomedical materials.* Materials Letters, 57, 858-861 (2002).

[118] Danilchenko, S.N., et al. *Characterization and in vivo evaluation of chitosan-hydroxyapatite bone scaffolds made by one step coprecipitation method.* Journal of Biomedical Materials Research Part A, 96A, 639-647 (2011).

[119] Kim, S.-H., et al. *Preparation of high flexible composite film of hydroxyapatite and chitosan.* Polymer Bulletin, 62, 111-118 (2009).

[120] Thein-Han, W.W. and R.D.K. Misra. *Biomimetic chitosan–nanohydroxyapatite composite scaffolds for bone tissue engineering.* Acta Biomaterialia, 5, 1182-1197 (2009).

[121] Zhao, F., et al. *Preparation and histological evaluation of biomimetic three-dimensional hydroxyapatite/chitosan-gelatin network composite scaffolds.* Biomaterials, 23, 3227-3234 (2002).

[122] Peniche, C., et al. *Chitosan/hydroxyapatite-based composites.* Biotecnología Aplicada, 27, 202-210 (2010).

[123] Hu, Q., et al. *Preparation and characterization of biodegradable chitosan/hydroxyapatite nanocomposite rods via in situ hybridization: a potential material as internal fixation of bone fracture.* Biomaterials, 25, 779-785 (2004).

[124] Chen, J., et al. *Effects of in situ and physical mixing on mechanical and bioactive behaviors of nano hydroxyapatite–chitosan scaffolds.* Journal of Biomaterials Science, Polymer Edition, 22, 2097-2106 (2011).

[125] Ito, M., et al. *In vitro properties of a chitosan-bonded bone-filling paste: Studies on solubility of calcium phosphate compounds.* Journal of Biomedical Materials Research, 32, 95-98 (1996).

[126] Wilson, O.C. and J.R. Hull. *Surface modification of nanophase hydroxyapatite with chitosan.* Materials Science & Engineering C-Biomimetic and Supramolecular Systems, 28, 434-437 (2008).

[127] Sultana, N., et al. *Chitosan-based nanocomposite scaffolds for tissue engineering applications.* Materials and Manufacturing Processes, 30, 273-278 (2015).

[128] Jiang, L., et al. *Preparation and properties of nano-hydroxyapatite/chitosan/carboxymethyl cellulose composite scaffold.* Carbohydrate Polymers, 74, 680-684 (2008).

[129] Kong, L., et al. *Preparation and characterization of nano-hydroxyapatite/chitosan composite scaffolds.* Journal of Biomedical Materials Research Part A, 75A, 275-282 (2005).

[130] Kong, L., et al. *A study on the bioactivity of chitosan/nano-hydroxyapatite composite scaffolds for bone tissue engineering.* European Polymer Journal, 42, 3171-3179 (2006).

[131] Oliveira, J.M., et al. *Novel hydroxyapatite/chitosan bilayered scaffold for osteochondral tissue-engineering applications: Scaffold design and its performance when seeded with goat bone marrow stromal cells.* Biomaterials, 27, 6123-6137 (2006).

[132] Lim, J.I., et al. *Preparation of interconnected porous chitosan scaffolds by sodium acetate particulate leaching.* Journal of Biomaterials Science, Polymer Edition, 22, 1319-1329 (2011).

[133] Tsioptsias, C., et al. *A novel method for producing tissue engineering scaffolds from chitin, chitin–hydroxyapatite, and cellulose.* Materials Science and Engineering: C, 29, 159-164 (2009).

[134] Kim, H.J., et al. *Gas foaming fabrication of porous biphasic calcium phosphate for bone regeneration.* Tissue Engineering and Regenerative Medicine, 9, 63-68 (2012).

[135] García Cruz, D.M., et al. *Differentiation of mesenchymal stem cells in chitosan scaffolds with double micro and macroporosity.* Journal of Biomedical Materials Research Part A, 95A, 1182-1193 (2010).

[136] Oliveira, M.B. and J.F. Mano. *Polymer-based microparticles in tissue engineering and regenerative medicine.* Biotechnology Progress, 27, 897-912 (2011).

[137] Silva, G., et al. *Materials in particulate form for tissue engineering. 2. Applications in bone.* Journal of tissue engineering and regenerative medicine, 1, 97-109 (2007).

[138] Silva, G., P. Ducheyne, and R. Reis. *Materials in particulate form for tissue engineering. 1. Basic concepts.* Journal of Tissue Engineering and Regenerative Medicine, 1, 4-24 (2007).

[139] Ding, C.-C., S.-H. Teng, and H. Pan. *In-situ generation of chitosan/hydroxyapatite composite microspheres for biomedical application.* Materials Letters, 79, 72-74 (2012).

[140] Reverchon, E. and R. Adami. *Supercritical assisted atomization to produce nanostructured chitosan-hydroxyapatite microparticles for biomedical application.* Powder Technology, 246, 441-447 (2013).

[141] Granja, P., et al. *Preparation and characterization of injectable chitosan-hydroxyapatite microspheres*. Book of 573-576 Key Engineering Materials, 2004.

[142] Chen, J., et al. *Preparation of chitosan/nano hydroxyapatite organic–inorganic hybrid microspheres for bone repair.* Colloids and Surfaces B: Biointerfaces, 134, 401-407 (2015).

[143] Sivakumar, M., I. Manjubala, and K. Panduranga Rao. *Preparation, characterization and in-vitro release of gentamicin from coralline hydroxyapatite–chitosan composite microspheres.* Carbohydrate Polymers, 49, 281-288 (2002).

[144] Başargan, T. and G. Nasün-Saygılı. *Spray Dried Mesoporous Hydroxyapatite-Chitosan Biocomposites.* Polymer-Plastics Technology and Engineering, null-null (2015).

[145] Ruphuy, G., et al. *Spray drying as a viable process to produce nano-hydroxyapatite/chitosan (n-HAp/CS) hybrid microparticles mimicking bone composition.* Advanced Powder Technology,

[146] Davis, J.M., *Animal Cell Culture: Essential Methods*. 2011: Wiley.

[147] Rao, S.B. and C.P. Sharma. *Sterilization of chitosan: implications.* Journal of biomaterials applications, 10, 136-143 (1995).

[148] Juan, A.S., et al. *Degradation of chitosan-based materials after different sterilization treatments.* IOP Conference Series: Materials Science and Engineering, 31, 012007 (2012).

[149] Checinska, A., et al. *Sterilization of biological pathogens using supercritical fluid carbon dioxide containing water and hydrogen peroxide.* Journal of Microbiological Methods, 87, 70-75 (2011).

[150] Dillow, A.K., et al., *Supercritical fluid sterilization method.* 2000, Google Patents.

[151] Hemmer, J.D., et al. *Sterilization of bacterial spores by using supercritical carbon dioxide and hydrogen peroxide.* Journal of Biomedical Materials Research Part B: Applied Biomaterials, 80B, 511-518 (2007).

[152] Kamihira, M., M. Taniguchi, and T. Kobayashi. *Sterilization of microorganisms with supercritical carbon dioxide.* Agricultural and Biological Chemistry, 51, 407-412 (1987).

[153] White, A., D. Burns, and T.W. Christensen. *Effective terminal sterilization using supercritical carbon dioxide.* Journal of Biotechnology, 123, 504-515 (2006).

[154] Zani, F., et al. *Sterilization of corticosteroids for ocular and pulmonary delivery with supercritical carbon dioxide.* International Journal of Pharmaceutics, 450, 218-224 (2013).

[155] Zhang, J., et al. *Sterilizing Bacillus pumilus spores using supercritical carbon dioxide.* Journal of Microbiological Methods, 66, 479-485 (2006).

[156] Zhang, J., et al. *Sterilization using high-pressure carbon dioxide.* The Journal of Supercritical Fluids, 38, 354-372 (2006).

3 HAp and HAp/CS aqueous dispersions

Nanoparticles are extraordinary systems that, due to their high surface area-to-volume ratio, exhibit unique properties. Their incorporation into polymeric matrices, yet challenging, has been of great interest aiming to produce final materials with enhanced properties relative to the individual components. It is expected that the large surface to volume ratio results in increased interfacial particle-matrix interactions, which can improve the overall properties of the hybrid material [1]. However, the physical mixture of inorganic particles and organic polymers leading to homogeneous dispersions can be a complex task. Intermolecular van der Waals forces between particles dominate when their sizes are below 100 nm, causing their agglomeration or clustering. In addition, the difficulty in controlling the mixing between two dissimilar phases can lead to separation in discrete phases, resulting in a product with poor properties [1, 2].

The mineral phase of natural bone consists of blade-like crystals of nanometric size, very similar to stoichiometric hydroxyapatite nanoparticles, well distributed throughout collagen fibres. In order to be able to mimic nature, it is desirable to produce highly homogeneous and stable n-HAp dispersions as base materials, with an intimate interaction between the nanoparticles and the organic component, to be further shaped into final structures that will serve as bone substitutes. Many methods have been used to prepare n-HAp dispersions using chitosan solutions as the organic component, since this combination is an interesting

approach for non-load-bearing bone graft applications, however, not many studies are found regarding the influence of chitosan on the stability of HAp nanoparticles.

The objective of this chapter is to analyse the effects on particle size and zeta potential of n-HAp aqueous dispersions, alone or in the presence of chitosan. Diluted nanodispersions are prepared by ultrasonication and the influence of different parameters, such as the presence of salts, n-HAp/CS weight ratio, pH, and storage time, is studied.

3.1 Introduction

Some studies [3, 4] have revealed that HAp nanoparticles, with sizes <100 nm, exhibit an improved performance in what concerns osteointegration, osteoblast adhesion and proliferation, synthesis of alkaline phosphatase and deposition of calcium containing minerals, when compared to HAp particles with larger sizes. Furthermore, nanoparticles are beneficial as drug delivery systems; particles with sizes from 10 to 100 nm are considered satisfactory to allow adequate blood circulation, and facilitate nanoparticles penetration through cell membranes, among other advantages [5]. For these reasons, the use of nano-sized HAp has been of great interest for biomedical applications.

Dispersions of HAp nanoparticles, within the abovementioned size range, in an aqueous continuous medium, can be considered as colloidal systems; therefore, understanding the basic principles of colloidal science is important in order to be able to produce dispersions with the desired characteristics, mainly in what concerns homogeneity and stability. A colloidal system, by definition, comprises two or more phases, one of which, the *dispersed phase*, consists of sub-microscopic particles typically smaller than 1 μm but larger than 1 nm, that are suspended in a medium called the *continuous phase*. Colloids are commonly referred to as *dispersions* or *suspensions* because the particles are dispersed or suspended in the continuous phase [6, 7].

Particles in a colloidal system have a particular behaviour; they move randomly throughout the fluid, the continuous phase, in which they are suspended. Collisions of the particles with other particles, and with atoms or molecules of the fluid are the cause of such random movement known as *Brownian motion* [6, 8]. Usually, if the particle size is small enough,

Brownian motion dominates other surrounding effects such as gravity; however, under certain circumstances, the particles may stick to one another following collision, thus forming aggregates of growing size, and undergoing flocculation or coagulation processes that can lead to phase separation [9]. This event may be desirable for certain applications, namely water treatment, and can be induced by addition of a clarifying agent. On the contrary, as desired for the biomedical applications pretended in the present study, stability of the dispersion can be improved commonly by addition of surface-active agents, i.e. *surfactants*, but also by the presence of macromolecules or polymers [6].

In nature, biological colloids often exhibit good stability due to the presence of proteins, e.g. casein acts as a stabilizer of the fatty acid droplets in milk. Such stabilization is attained by different mechanisms; mainly, the macromolecule is adsorbed on the nanoparticles surface, surrounding it and avoiding the near approach from other particles. Furthermore, if charged, the adsorbed macromolecules layer enhances stability by repelling the other particles. This is common when polyelectrolytes are incorporated in the dispersions, either to provoke aggregation or as stabilizing agents [6].

The production of n-HAp based hybrid materials involves the dispersion of the nanoparticles in an organic component (chitosan for this particular study), which properties are strongly influenced by the shape, size and size distribution of the nanoparticles, the organic component properties, and the nanoparticle/organic matrix interface, among others [4]. Chitosan is a polyelectrolyte that can either cause aggregation or improve stability of the n-HAp dispersions. In order to assess this and the other mentioned factors, two of the most important physical properties of colloidal systems to evaluate are the particle size and the zeta potential. These properties can be measured and analysed using different techniques such as dynamic light scattering (DLS) and laser diffraction spectroscopy (LD) for particle size, and electrophoretic light scattering (ELS) for zeta potential.

3.1.1 Particle size

Among the various available techniques to analyse particle size, choosing the right technique depends on a number of criteria, but most importantly, it depends on the size range of the sample. Table 3.1 presents the approximate working size ranges for commonly used characterization techniques; limits can slightly vary depending on the particular equipment.

Table 3.1. Typical working size ranges for commonly used characterization techniques (Adapted from Malvern® Instruments Ltd [10])

Technique	Particle size range
Dynamic Light Scattering	0.1 nm – 10 μm
Laser Diffraction	10 nm – 10 mm
Electrophoretic Light Scattering	1 nm – 10 μm

3.1.1.1 Dynamic light scattering (DLS)

When a particle is illuminated by a source of light, such as a laser, it scatters light in all directions. If a screen is held close to such particle, the scattered light will be reflected in the screen. In the case of many stationary particles being illuminated, the screen will then show a speckle pattern with dark and bright areas, as shown in Figure 3.1a, in which the bright areas correspond to the light scattered by the particles [8].

When particles are dispersed in a liquid, they are not stationary; instead, they experience Brownian motion. Thus, the resulting speckle pattern produced appears to move; the bright and dark areas grow and diminish (fluctuate) in intensity due to the constructive and destructive phase addition of the scattered light. Considering that small particles move quicker than larger ones, intensity fluctuations that happen along time in a particular point of the speckle pattern are directly related with particle size. Dynamic light scattering (DLS), also known as Photo correlation spectroscopy (PCS), is based on the measurement of the rate of such fluctuations and the calculation of particle size using *Stokes-Einstein* equation, which describes the relationship between particle size and its speed due to Brownian motion [8].

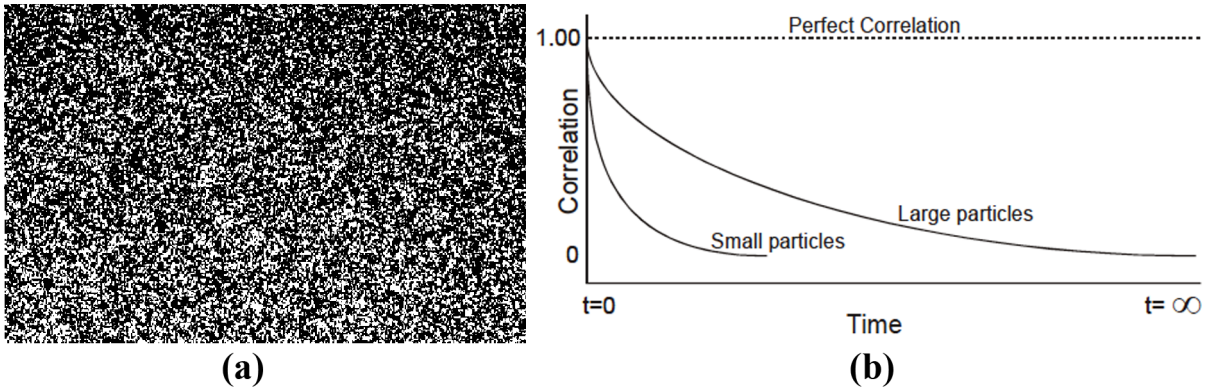

Figure 3.1. DLS measurements: a) characteristic speckle pattern; (b) correlation function of small and large particles. (Reproduced from Malvern® Instruments Ltd 10] and Briers (2001) [11])

The rate of the fluctuations is determined using a digital correlator that measures the degree of similarity between speckle patterns at different instants over a period of time. The resulting correlation decreases with time as shown in Figure 3.1b; the intensity of the speckle pattern changes slowly for large particles that move slow, whereas it changes faster for small particles that move quickly [12]. This correlation function is used to produce a size distribution based on intensity, i.e. particle size is plotted as a function of the intensity of the scattered light. However, this intensity distribution can be converted to a size distribution in volume or in number. The difference between the three cases is shown in Figure 3.2.

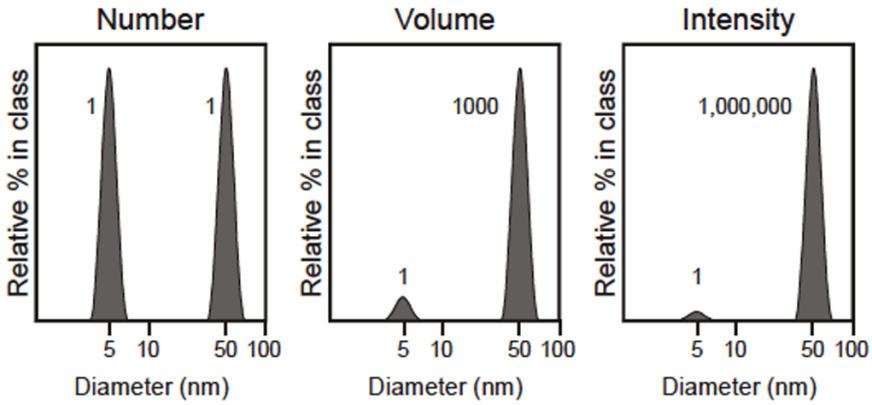

Figure 3.2. Comparison between DLS size distributions in number, in volume and in intensity (Reproduced from Malvern® Instruments Ltd 10])

For a sample with the same amount of 5 nm-particles and 50 nm-particles, the ratio of relative percentage is 1:1 in the size distribution in number, but it increases to 1:1000 for the distribution in volume, since the volume occupied by the 50 nm-particles is 1000 larger than the one occupied by the same amount of particles with size of 5 nm. The ratio is even larger (1:1000000) for intensity distributions; using Rayleigh approximation, the intensity of scattering is proportional to the sixth power of the particle diameter [8].

Frequently, DLS results are stated in terms of *Z-average*, also known as cumulants mean since it is calculated by the method of cumulants. This value is often preferred because it is a mathematically stable value and insensitive to experimental noise. Cumulants analysis consists on a fit of a polynomial to the log of the correlation function, $G1$ [8, 13]:

$$\ln(G1) = a + bt + ct^2 + dt^3 + et^4 + \ldots \tag{3.1}$$

where the second order cumulant, b, is the Z-average diffusion coefficient that, together with dispersant viscosity and other known parameters, is used to compute Z-average using Stokes-Einstein equation. Thus, Z-average along the so-called *Polydispersity Index* (PdI), a width parameter also provided by cumulants analysis, are reliable values to describe particle size. However, it must be used with caution; the Z-average is only comparable with other techniques for monomodal, spherical and monodispersed samples, otherwise, it can only be used to compare results obtained using the same technique, as long as samples are measured in the same dispersant and PdI values obtained are below 0.5 [8, 13].

Finally, for optimal DLS measurements, two important physical properties must be considered: particle size and sample concentration. Typical working size ranges for DLS are shown in Table 3.1. The adequate sample concentration, on the other hand, varies depending on the sample material. If concentration is too low not enough light is scattered to allow a measurement, whereas if the sample is too concentrated, measurement can be affected by multiple scattering, i.e. the light scattered by one particle is then scattered by another particle nearby. Furthermore, it is also important to keep in mind that concentrated dispersions may form a colloidal gel, since a gel is unsuitable for DLS measurements [8].

3.1.1.2 Laser diffraction spectroscopy (LD)

When a stone is thrown vertically into static water, waves in the form of rings of different sizes are formed in the water around the stone. Large stones create stronger waves with shorter distance between the lobes than small ones. This is a simple analogy to describe what happens when a particle is hit by light; it creates a pattern of rings that are proportional to the size of the particle, a phenomenon called *diffraction*. Laser diffraction spectroscopy (LD) measures the intensities and distance among the rings, and relates them with particle size. Thus, unlike DLS, the motion of the particles is not relevant [14].

However, this measurement is not as simple as it seems because when light hits a particle it is not only diffracted, it undergoes absorption, diffraction, refraction and reflection, as shown in Figure 3.3. Therefore, the pattern created, named *scattering pattern*, is actually a result of the sum of all these phenomena, and its shape depends on the ratio particle size/incident wavelength. Depending on such ratio, the scattering pattern can adopt one of three shapes: *Fraunhofer* scattering, when the particles are much larger than the wavelength; *Mie* scattering, for particle sizes about the same as the wavelength size; and *Rayleigh* scattering, when particles are much smaller than the wavelength. This is mathematically described by the so-called *Mie* formula [14, 15].

Considering the above, LD uses a laser of known wavelength, as light source, that passes through an optical system, to widen the laser so it hits the whole sample; next, the scattered light is focused through a Fourier lens into a detector. The shape and intensity of scattering pattern are then detected and particle size is computed through software using the *Mie* formula. The lower limit of detection using this technique is about 400 nm, depending on the wavelength of the laser. Therefore, for samples with smaller particles, the use of Polarisation Intensity Differential Scattering (PIDS) technology is required. PIDS is based on the fact that the shape of the scattering pattern changes if the wavelength also changes; thus, the same sample is analysed using three different wavelengths (450 nm, 600 nm and 900 nm) to obtain different scattering patterns that are compared to each other. Since the scattering pattern also depends on light polarization, the measurement is made twice for each wavelength, once using vertically polarized light, and the second one using horizontally polarized light. The intensities of the scattered light are detected at six different angles, and the information gathered is related to particle size. By using different wavelengths, the

particle size/incident wavelength ratio changes for a specific particle size; consequently, differences in scattering patterns due to variations in wavelengths enables conclusions on particle size [14, 15].

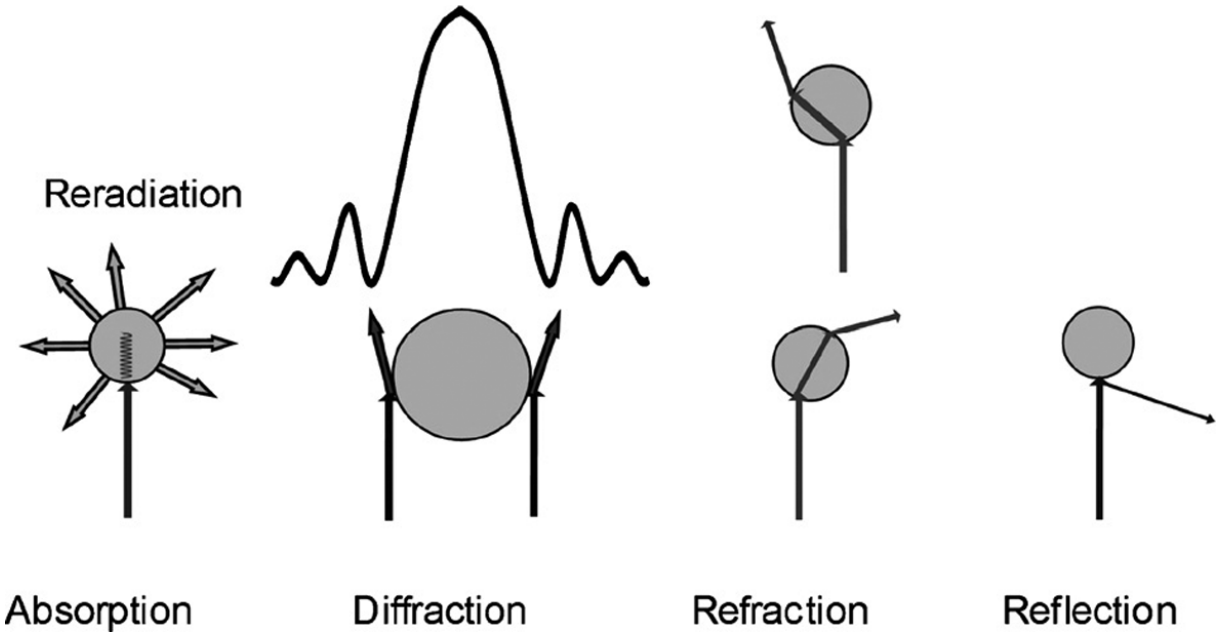

Figure 3.3. Schematic representation of scattering phenomena that occurs when a particle is hit by light; from left to right: absorption, diffraction, refraction and reflection. (Reproduced from Keck (2008) [14])

3.1.2 Colloidal stability

Colloidal stability was explained in the 1940s through a theory developed by scientists Derjaguin, Verwey, Landau and Overbeek (DVLO theory), which establishes that the stability of a particle in solution is determined by the total potential energy function, V_T, which is a balance of the potential energy due to the solvent, V_S, and the attractive, V_A, and repulsive, V_R, contributions [9]:

$$V_T = V_A + V_R + V_S \tag{3.2}$$

The contribution of V_S is usually negligible compared to the influence of V_A and V_R; hence, V_T is generally considered only as the sum of attractive Van der Waals forces and electrical repulsion caused by the net surface charge that particles undergo as they approach each other due to Brownian motion. Therefore, a colloidal system is stable when the particles have enough high repulsion to resist flocculation [9, 16].

Two primary mechanisms can affect the stability of dispersions: steric and electrostatic stabilization. In the first case, polymers are added to the colloidal system to adsorb onto the particles surface and form a coating that, when thick enough, causes particles separation by steric repulsions between polymer layers, thus weakening van der Waals forces and avoiding particles to adhere to each other. Whereas electrostatic or charge stabilization originates from the interaction of particles with charged species in the colloidal system [9].

One way of determining the stability of a colloidal system is by analysing the particles surface charge. Nowadays, one of the preferred techniques to characterize particles surface charge in colloidal systems is by measuring zeta potential. It is a simple and straightforward method, based on electrophoretic mobility, referred as *Electrophoretic Light Scattering* and explained next.

Particles dispersed in an aqueous medium usually carry an electric charge. The net charge at the surface of the particle has an effect on the distribution of ions of the surrounding interfacial region, so that the concentration of ions of opposite charge to that of the particle increases close to the surface. Thereby, two distinctive parts can be identified in the surrounding interfacial region, as shown in Figure 3.4. The *Stern layer* comprises the ions closer to the particle surface that are strongly attached to it. An outer layer, called the *diffuse layer*, consists of ions whose bonding to the particle is weaker. Together, the Stern and diffuse layers, form the *electrical double layer*. A notional boundary located within the diffusion layer, known as *slipping plane*, delimits a region within which the ions form a stable entity with the particle. Thus, only the ions within this boundary travel with the particle when it moves due to external forces, namely gravity. Finally, the potential that exists in the slipping plane is called the *zeta potential* [8, 17].

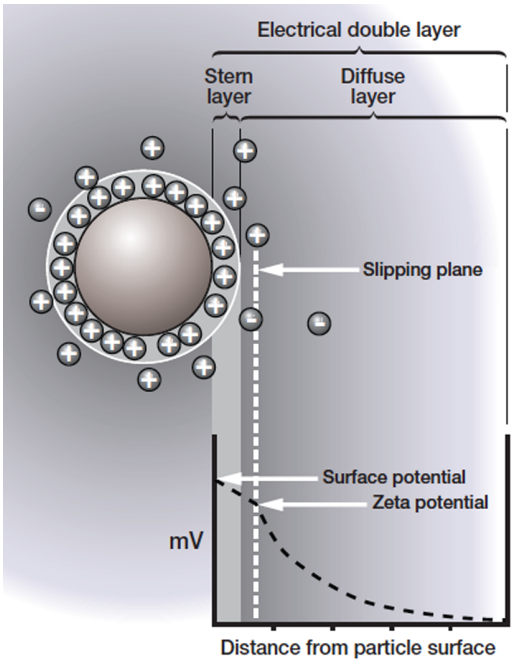

Figure 3.4. Electrical double layer
(Reproduced from Malvern® Instruments Ltd [8])

Colloidal stability can be evaluated by measuring the zeta potential, which can be carried out by electrophoretic light scattering (ELS). This technique is based on electrophoresis, the phenomenon of the movement of charged particles relative to the suspending medium, induced by the application of an electric field. Viscous forces resist to the electrically induced movement of the particles; when equilibrium between these forces is reached, the particles then move at a constant velocity, known as mobility. The zeta potential is proportional to this electrophoretic mobility and thus can be computed using Henry's equation [8, 9]. In general, it is considered that dispersions with absolute zeta potential values around 20 mV exhibit short-term stability, above 30 mV dispersions have good stability, and above 60 mV stability is excellent. Furthermore, for dispersions with combined steric and electrostatic stabilization, a minimum of absolute zeta potential of 20 mV is considered appropriate [16].

Several factors can affect the zeta potential, and the pH is the most critical. Negatively charged particles tend to acquire more negative charge with the addition of alkali (increase of pH). On the contrary, with the addition of acid (decrease of pH), particles become less negative until a point in which charge is neutralized, corresponding to a zeta potential of 0 mV. This point in a plot of zeta potential versus pH is called the *isoelectric point*. If more acid is further added, particles can acquire a positive charge (see Figure 3.5) [8, 9].

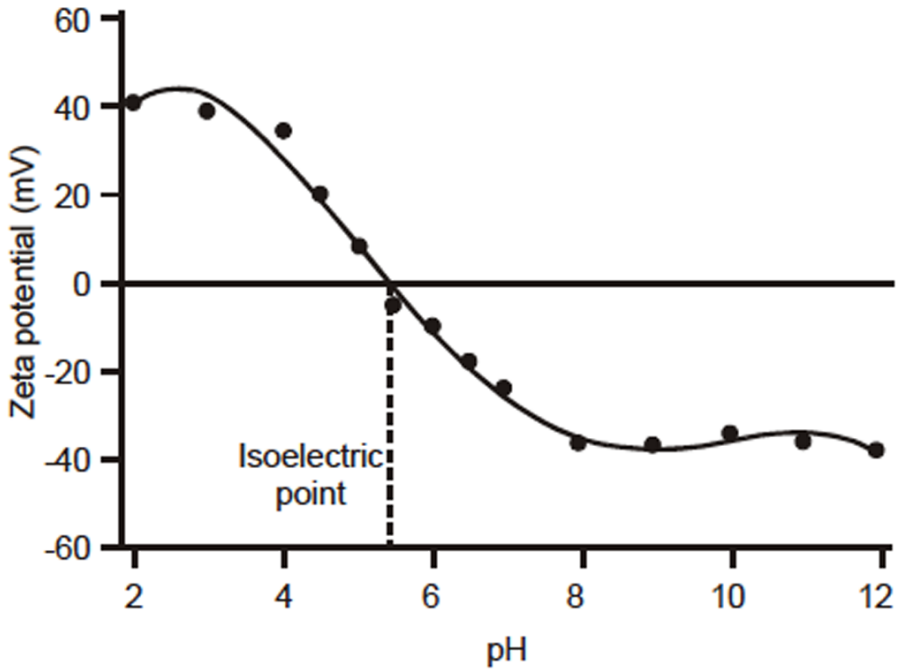

Figure 3.5. Typical plot of zeta potential versus pH showing isoelectric point (Reproduced from Malvern® Instruments Ltd [8])

3.1.3 Context and objectives of the present chapter

The mixing method described in Chapter 2, is a simple and straightforward method, and thus very convenient. However, it implies the incorporation of HAp nanoparticles into an acidic environment that can influence HAp solubility, phase stability and surface chemistry [18]. Despite the numerous publications on the preparation of HAp and HAp/CS hybrid materials, studies regarding the influence of chitosan on HAp surface properties are insufficient. Wilson et al. (2007) [18] was the only report found in which HAp surface chemistry was studied after aging nanophase HAp particles in 0-2.5 wt.% chitosan acetate solutions for 30 days. After incorporation of HAp into chitosan solution, the HAp/CS mixtures had a pH around 4-5. The authors reported that HAp suffered changes in surface chemistry, colloid stability and chemical composition after long-term aging of HAp in chitosan acetate gel solutions. Such changes were attributed to solubility effects, since HAp becomes slowly soluble at pH values lower than 5. It was also found that chitosan strongly adsorbs to HAp particles and improves colloid stability.

No studies were found analysing the effects of important parameters, such as pH, on particle size and zeta potential of n-HAp/CS dispersions. In this work, aqueous dispersions of nano hydroxyapatite (n-HAp), alone or in the presence of chitosan (CS), were prepared by ultrasonication. The produced dispersions were analysed in what concerns particle size and zeta potential, then related with parameters such as pH, chitosan content, the presence of salts, and storage time. Particle size was determined by dynamic light scattering, for diluted dispersions, and by laser diffraction, for high concentration dispersions. Zeta potential was determined by electrophoretic light scattering.

3.2 Materials and methods

3.2.1 Materials

The nanodispersions were prepared using chitosan 90/200/A1, acquired from Biolog-Biotechnologie GmbH (Germany), corresponding to flakes with size <200 μm, deacetylation degree of 91.9%, and dynamic viscosity of 128 mPa·s (1% at 20 C in 1% acetic acid solution); and hydroxyapatite aqueous paste, *nanoXIM-CarePaste* (15% wt., $Ca_{10}(PO_4)_6(OH)_2$) provided by Fluidinova S.A. Glacial acetic acid, sodium acetate tri-hydrate, and sodium hydroxide, all of analytical grade, from Sigma Aldrich were used to prepare the solutions.

3.2.2 Dispersions preparation by ultrasonication

Aqueous dispersions of nano-hydroxyapatite (n-HAp), alone or in the presence of chitosan (CS), were prepared at concentrations 1.6 g/l, 6.4 g/l and 20 g/l, corresponding to mean free paths of 3.0, 1.5 and 0.70 respectively. Calculations of these concentrations are shown in Appendix A.

Samples were subjected to different ultrasonication time periods at 50% amplitude, using an Ultrasonic Processor (Sonicator) QSonica Q700, with a maximum power output of 700 W, frequency output of 20 kHz and 12.5 mm diameter horn with replaceable tip (**Figure 3.6**). Special care was taken to assure that both, the geometry of the vessel and the position of the probe's tip, were fixed. Geometric factors affect the amount of energy absorbed by the particles due to their relative position. Special emphasis was given to the production of n-

HAp/CS dispersions with a weight ratio of 70/30 since it represents the typical bone composition. Finally, the pH of all prepared n-HAp/CS samples was checked to be of approximately 5.5 at room temperature.

Figure 3.6. Ultrasonic Processor QSonica Q700 used in the preparation of the HAp nanodispersions (Reproduced from QSonica, LLC. [19])

3.2.3 Characterization

Particle size and zeta potential of the prepared nanodispersions were determined by dynamic and electrophoretic light scattering respectively, using a Zetasizer Nano ZS from Malvern Instruments; model ZEN 3600 with a 633 nm red laser. Temperature and pH were also monitored during each preparation process.

Samples subjected to ultrasonication were analysed in what concerns the influence of the presence of salts (particularly KCl), n-HAp/CS mass ratio, pH, and storage time on particle size and zeta potential. The effect of pH on the zeta potential was studied by performing titrations using the MPT-2 Autotitrator, an external device connected to the Zetasizer Nano

ZS from Malvern Instruments. Moreover, dispersions with higher n-HAp concentration, alone and in the presence of chitosan, were characterized by laser diffraction spectroscopy using a Coulter LS-230.

3.3 Results and discussion

3.3.1 Dispersions preparation by ultrasonication

When particles adhere to each other to form large clusters it becomes difficult to separate them back into primary particles. Frequently, high-energy inputs are required to break the clusters. In this context, ultrasonication has become a common laboratory method, used either for reduction of particle size or agglomeration disruption. This is achieved by transferring sound energy that stirs the particles; ultrasonic frequencies (>20 kHz) are converted to a mechanical rapid vibration that, when applied into a dispersion, causes cavitation, the formation and collapse of bubbles, in the liquid. A great amount of energy is released due to the collapse of thousands of microscopic bubbles, causing clusters disruption [19].

Energy efficiency was firstly considered in the present study. The optimal process parameters were determined by running experiments at fixed amplitude (50%) and varying ultrasonication time. Particle size was measured along pre-defined time intervals, and its variation with energy input is presented in Figure 3.7 and Figure 3.8. Dispersions of HAp alone (Figure 3.7) subjected to ultrasonication show that, for relatively low energy input (processing times of 10 to 30 s), large agglomerates were completely broken down into smaller ones. Zeta potential data exhibited low variability for all the examined samples, with values comprised between +27 and +30 mV ($9.0 < pH < 10.0$).

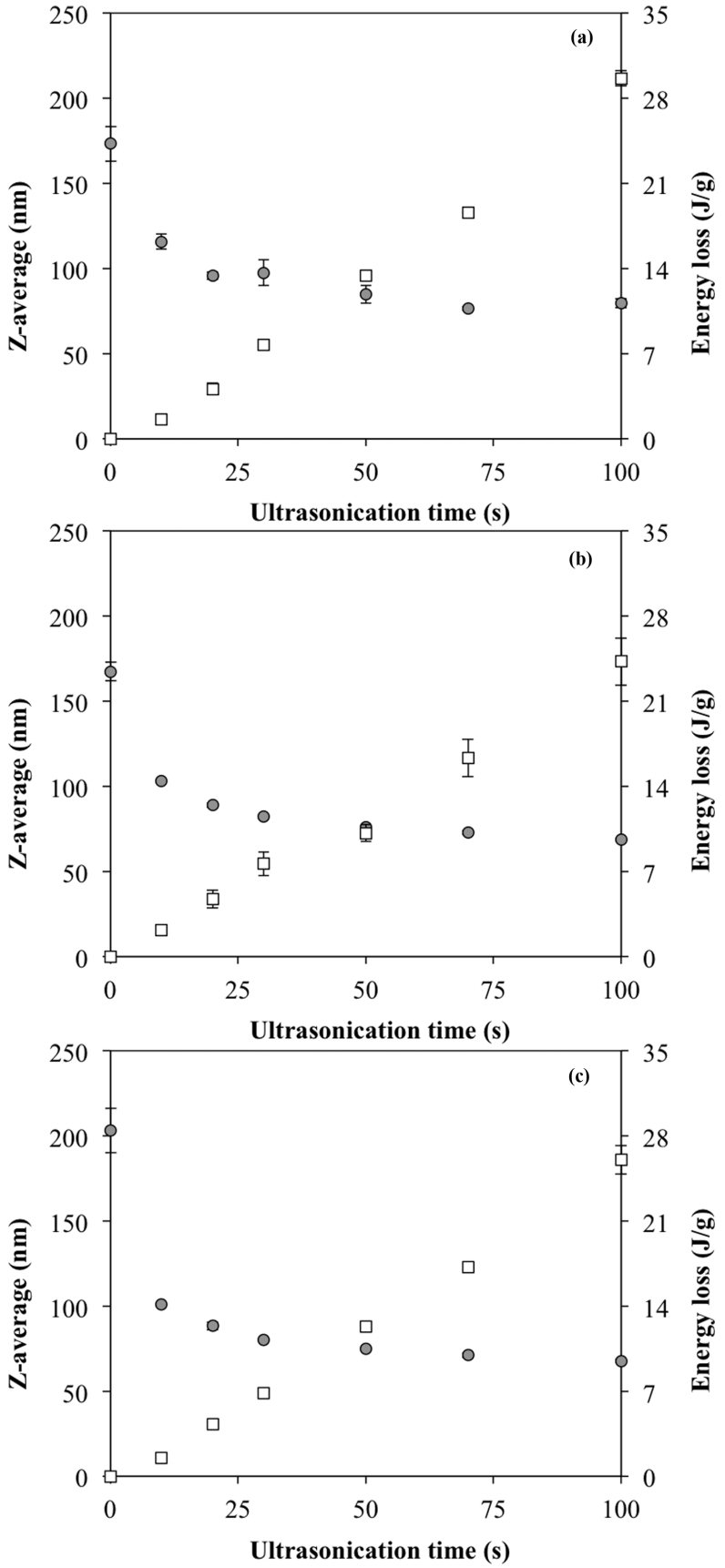

Figure 3.7. Z-average (filled circle) and energy loss (white square) versus ultrasonication time of nanodispersions of HAp alone of concentrations: (a) 1.6 g/l; (b) 6.4 g/l; (c) 20 g/l. All measurements show standard deviation (SD) based on 3 replicas

A logarithmic tendency of the z-average to decrease with ultrasonication time was also observed for the n-HAp/CS dispersions (Figure 3.8). However, larger particle sizes were detected, suggesting that HAp nanoparticles remain as clusters when dispersed in chitosan solutions, but with increased zeta potential that remained nearly constant at values comprised between +32 to +34 mV (pH 5.5). Generally, if a dispersion is not stabilized, by electrostatic, steric, or electrosteric effects, nanoparticles tend to cluster again shortly after ultrasonication. Stabilization through electrosteric effects can be achieved by addition of a polyelectrolyte [20]. Therefore, the observed increase of zeta potential observed in the n-HAp/CS dispersions, relative to dispersions of n-HAp alone, may be due to electrosteric effects imparted by chitosan. It was also observed that the z-average of the agglomerates increases as the n-HAp concentration increases. Measurements of n-HAp/CS dispersions with a concentration of 20 g/l were unsuitable for DLS.

Furthermore, the results obtained from the energy balance for both, n-HAp alone and n-HAp/CS samples, within the studied range of concentrations, point out that energy loss as heat form increases linearly with ultrasonication time, reaching values around 25 to 30 J/g at 100 s of ultrasonication, the higher time tested. Considering this and the tendency of particle size to decrease with increasing ultrasonication times, an energy input of approximately 50 J/g (approximately 30% of energy loss), corresponding to 50 s of ultrasonication time at 50% amplitude, is considered optimal since higher ultrasonication times do not significantly affect HAp particle size.

Dispersions with the lowest concentration ($C_{HAp} = 1.6$ g/l) are considered more suitable for DLS measurements. Therefore, the study of the effects of the presence of salts (particularly KCl), n-HAp/CS mass ratio, pH, and storage time were carried out for nanodispersions with $C_{HAp} = 1.6$ g/l , and subjected to ultrasonication time of 50 s (50% amplitude), corresponding to the optimal energy input.

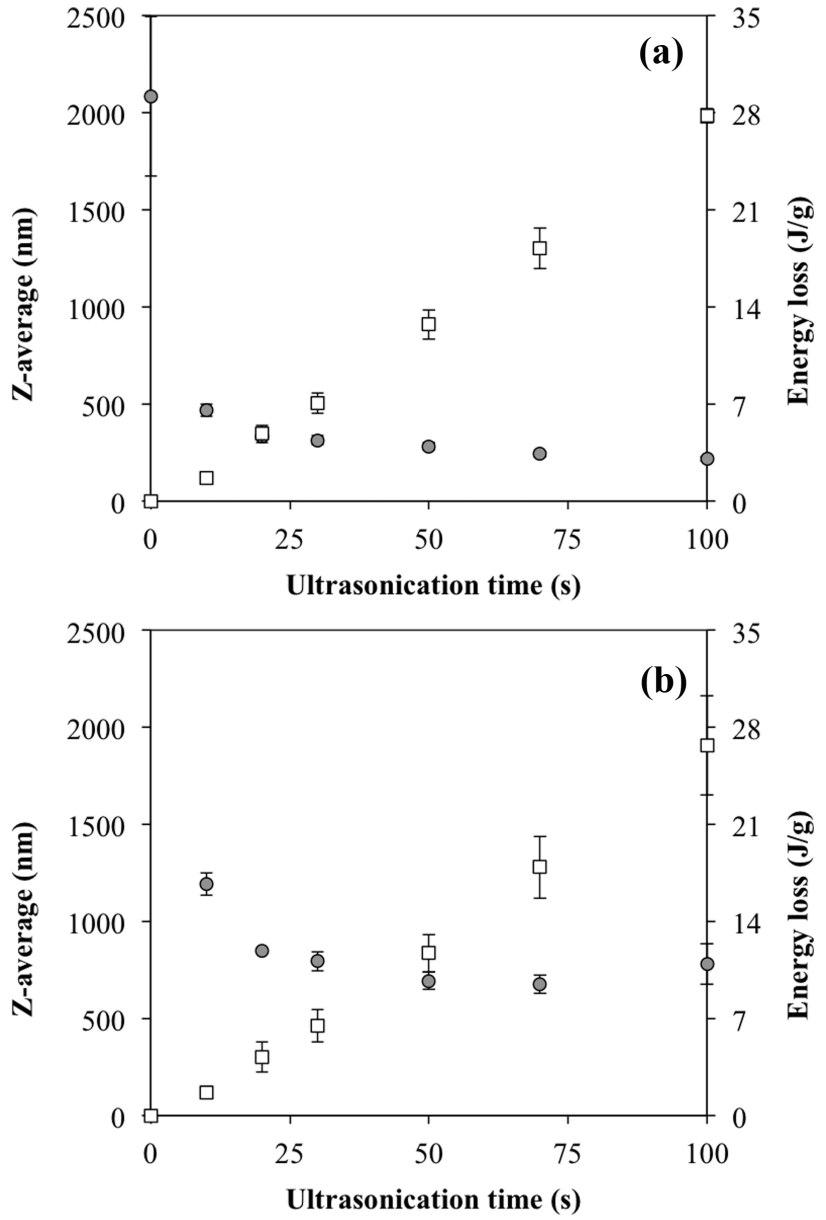

Figure 3.8. Z-average (filled circle) and energy loss (white square) versus ultrasonication time of n-HAp/CS dispersions of concentrations: (a) 1.6 g/l; (b) 6.4 g/l.
All measurements show SD based on 3 replicas

3.3.2 Effect of KCl on particle size and zeta potential

Surface charge of particles is strongly influenced by the presence of ions in the surrounding medium. Particularly, in aqueous medium there is a large content of ions usually resulting from the addition of ionic surfactants and electrolytes, namely acids, bases or salts [6]. Consequently, the ionic content of the aqueous medium strongly influences the surface charge

of particles that affects the electrostatic stability of the dispersion. Moreover, the presence of salts has an effect on the ionic strength of the medium, influencing the charge of certain polysaccharides, and consequently the polymer chain conformation [21] and, subsequently, the interfacial interactions with the particles that influences particle size and zeta potential, and the overall properties of the final hybrid material.

Given that the hydroxyapatite paste used for the preparation of the nanodispersions, nanoXIM-CarePaste, contains KCl in its formulation, the influence of this salt on particle size and zeta potential was evaluated. For that, n-HAp dispersions, both alone and in the presence of chitosan, were prepared using the nanoXIM-CarePaste after being washed three times with deionized water. In parallel, dispersions containing nanoXIM-CarePaste with KCl, as originally provided, were also prepared and characterized. Particle size distributions (PDS) in number obtained for n-HAp dispersions alone and in the presence of chitosan, with and without KCl, are shown in Figure 3.9. Monodispersed distributions were obtained in all cases, and no considerable differences were observed in terms of size due to the existence of KCl. Therefore, particle size increase is caused by the presence of chitosan and no evidence was found that KCl has an effect on the particle size of n-HAp dispersions.

While no important effect was observed in particle size due to the presence of KCl, its presence appears to influence the electrostatic stability of the dispersions. Zeta potential values of n-HAp alone and n-HAp/CS dispersions are shown in Table 3.2. HAp nanoparticles dispersed in water present higher zeta potential values (>+30 mV) in the presence of KCl, which indicates that this salt alone improves the stability of the n-HAp dispersions. However, the behaviour appears to be different for the hybrid dispersions, the higher zeta potential values obtained corresponded to the n-HAp/CS dispersions without KCl, which indicates that the stabilizing effect of chitosan is better without the interference of salts. In the case of n-HAp/CS dispersions with KCl, a good zeta potential value (+32,8 mV) was obtained as well, but smaller compared with n-HAp/CS without KCl (+33,7 mV). The differences observed could be attributed to different interactions between salt ions with the n-HAp particles surface and with chitosan chains, which carry a positive charge in solution.

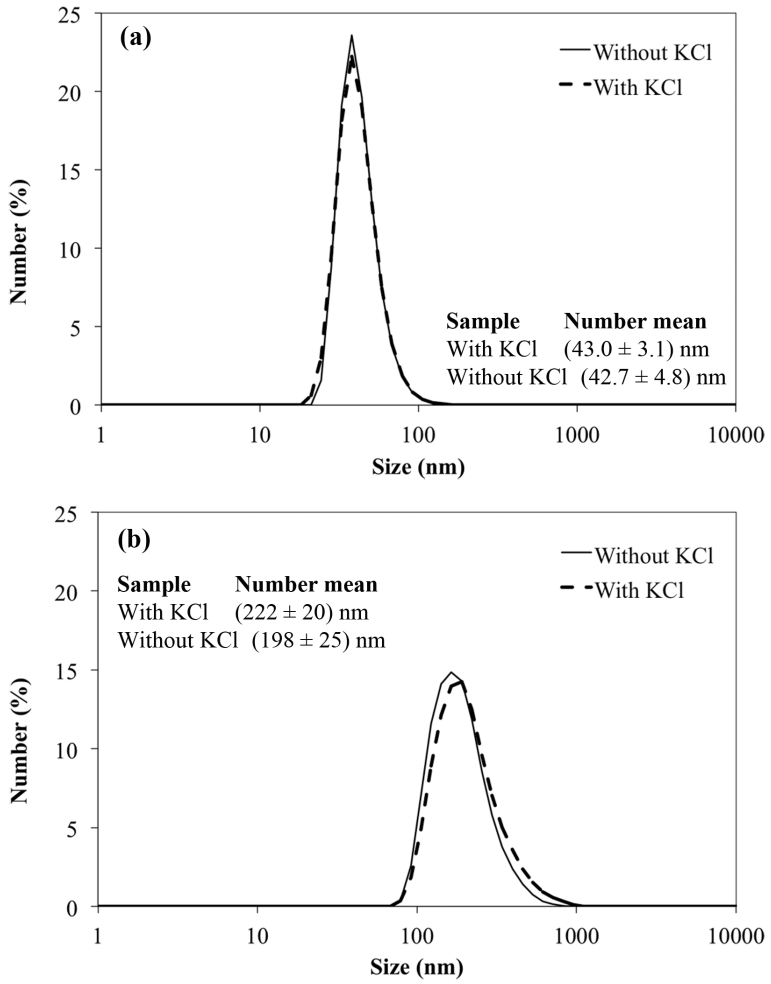

Figure 3.9. Particle size distributions in number for dispersions prepared with washed nanoXIM-CarePaste (without KCl) and with nanoXIM-CarePaste as originally provided (with KCl): (a) n-HAp alone and (b) n-HAp/CS

Table 3.2. Zeta potential values of dispersions of n-HAp prepared with washed nanoXIM-CarePaste (without KCl); and with nanoXIM-CarePaste as originally provided (with KCl)

Sample	Zeta potential (mV)	SD
HAp without KCl	+24,1	0,6
HAp with KCl	+31,2	0,3
HAp/CS without KCl	+33,7	0,2
HAp/CS with KCl	+32,8	0,2

3.3.3 Effect of chitosan concentration on particle size and zeta potential

As discussed before, larger particle sizes are obtained when HAp nanoparticles are dispersed in the presence of chitosan and, as observed in Figure 3.10, a linear tendency of particle size to increase with chitosan content was obtained. In terms of zeta potential, as soon as chitosan is incorporated into the n-HAp dispersions, the zeta potential increases to values above +30 mV, showing a linear tendency to increase with chitosan content as well.

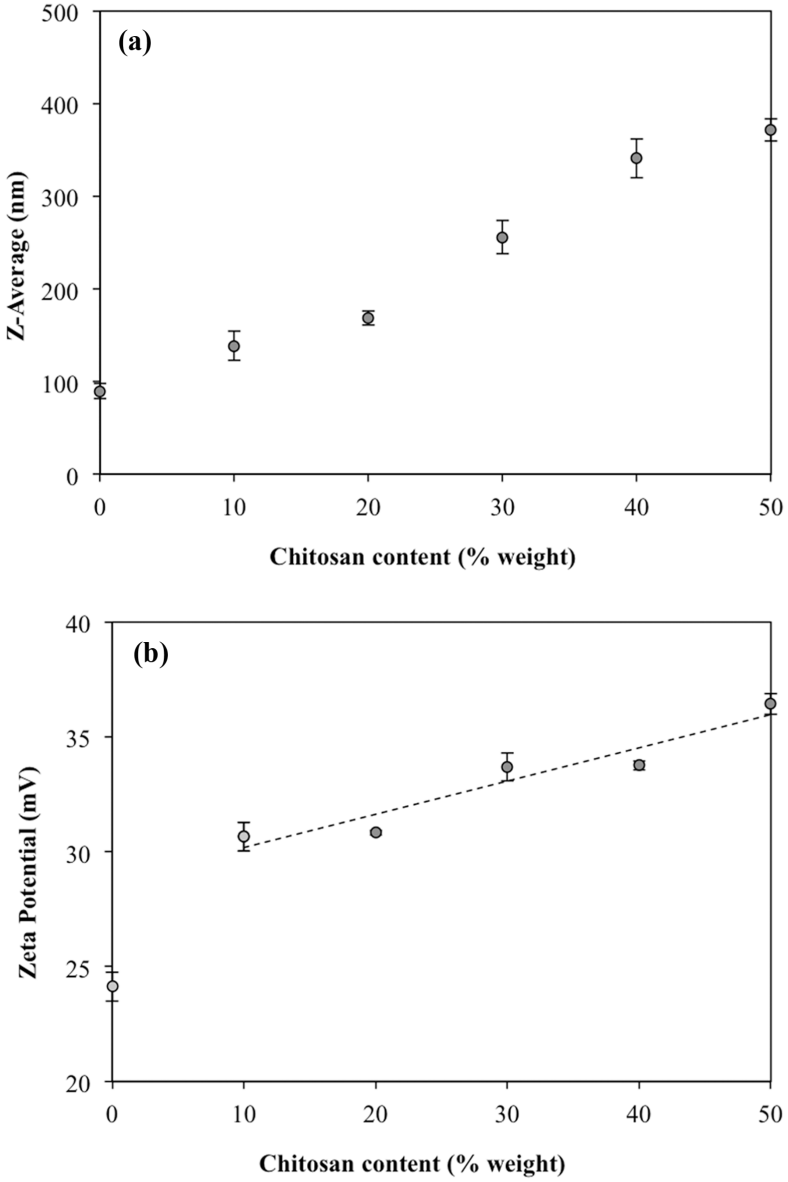

Figure 3.10 Effect of chitosan content on n-HAp dispersions on:
(a) Particle size; (b) Zeta Potential

Being a polyelectrolyte, chitosan can cause an electrosteric stabilizing effect in the nanodispersions. Consequently, the stabilization is probably caused by both, steric and electrostatic mechanisms. Thus, the incorporation of chitosan onto n-HAp particles forms a coating that causes stabilization by steric repulsions; with the increase in chitosan content the coating gets thicker, which may also influence the observed increase in particle size. At the same time, charge stabilization also takes place due to the positive charges in chitosan, which cause a linear increase in zeta potential with chitosan content. Therefore, even when the presence of chitosan in n-HAp dispersions causes the increase in particle size by particle aggregation, it improves the stability of the dispersions, which is a desirable characteristic.

3.3.4 Effect of pH on zeta potential

The surface charge of particles dispersed in aqueous media depends upon the nature of the particle and the surrounding medium. In this context, ionization of surface groups and adsorption of charged particles are the two most important mechanisms defining surface charge of colloidal particles. In the first case, a surface with alkaline groups, for instance, will give rise to a positive charge, as shown in Figure 3.11a, which magnitude depends on the alkaline strength of the surface groups and on the pH of the liquid medium. Typically, by increasing the pH, surface ionization of positively charged particles is suppressed until the surface charge is reduced to zero. The opposite behaviour takes place in the case of particles with acid groups in the surface. In the second mechanism, shown in Figure 3.11b, charged species, namely ions and ionic surfactants, specifically adsorb on the particle surface leading to a positively charged surface in the case of cationic species, or negatively charged if adsorption of anionic species occurs [9].

In the case of ionic solids, such as hydroxyapatite, the origin of surface charge is somewhat more complex. The mechanism involved consists in differential ion dissolution from a crystal lattice, i.e. the net charge of n-HAp particles in aqueous medium arises from the unequal dissolution of surface ions and may result in either a net positive or a net negative surface charge [22]. This mechanism is, as one would expect, highly dependent on the medium pH. The development of the particle surface net charge affects the ions distribution in the surrounding interfacial region and, consequently, the zeta potential [9].

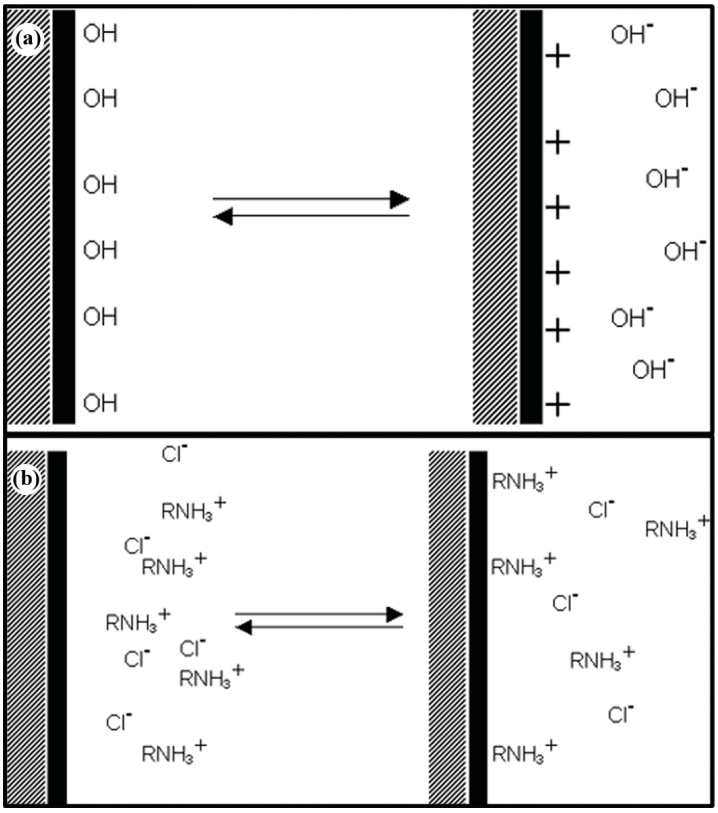

Figure 3.11. Origin of surface charge by: (a) ionization of alkaline groups; and (b) adsorption of cationic species
(Reproduced from Malvern® Instruments Ltda [9])

Figure 3.12 shows the results obtained from the autotitrations of dispersions of n-HAp alone (in water) and in the presence of chitosan. In alkaline medium (pH 9.0) dispersions of n-HAp alone exhibit good electrostatic stability, with a zeta potential value of around +29 mV. However, as the pH decreases, a tendency of zeta potential to decrease is observed, as shown in Figure 3.12a. With the incorporation of chitosan in the nanodispersions, on the other hand, a high zeta potential (>+30 mV) is obtained at low pH values (pH 5.5) and, oppose to what happens with dispersions of n-HAp alone, a linear tendency of zeta potential to decrease with the increase of pH is observed, as shown in Figure 3.12b.

The zeta potential tendency obtained for dispersions of n-HAp alone are attributed mainly to variations on pH that causes changes on surface charge by differential ion dissolution mechanism. Whereas for the n-HAp/CS dispersions, the mechanism of charged species also takes place, since chitosan acquires positive charges at pH<6.5. Thus, in slightly acidic environment (pH 5.5) the electrostatic stability of n-HAp particles dispersed in water is poor, with zeta potential between +10 and +15 mV, but with the incorporation of chitosan it improves considerably reaching zeta potential values >+30 mV.

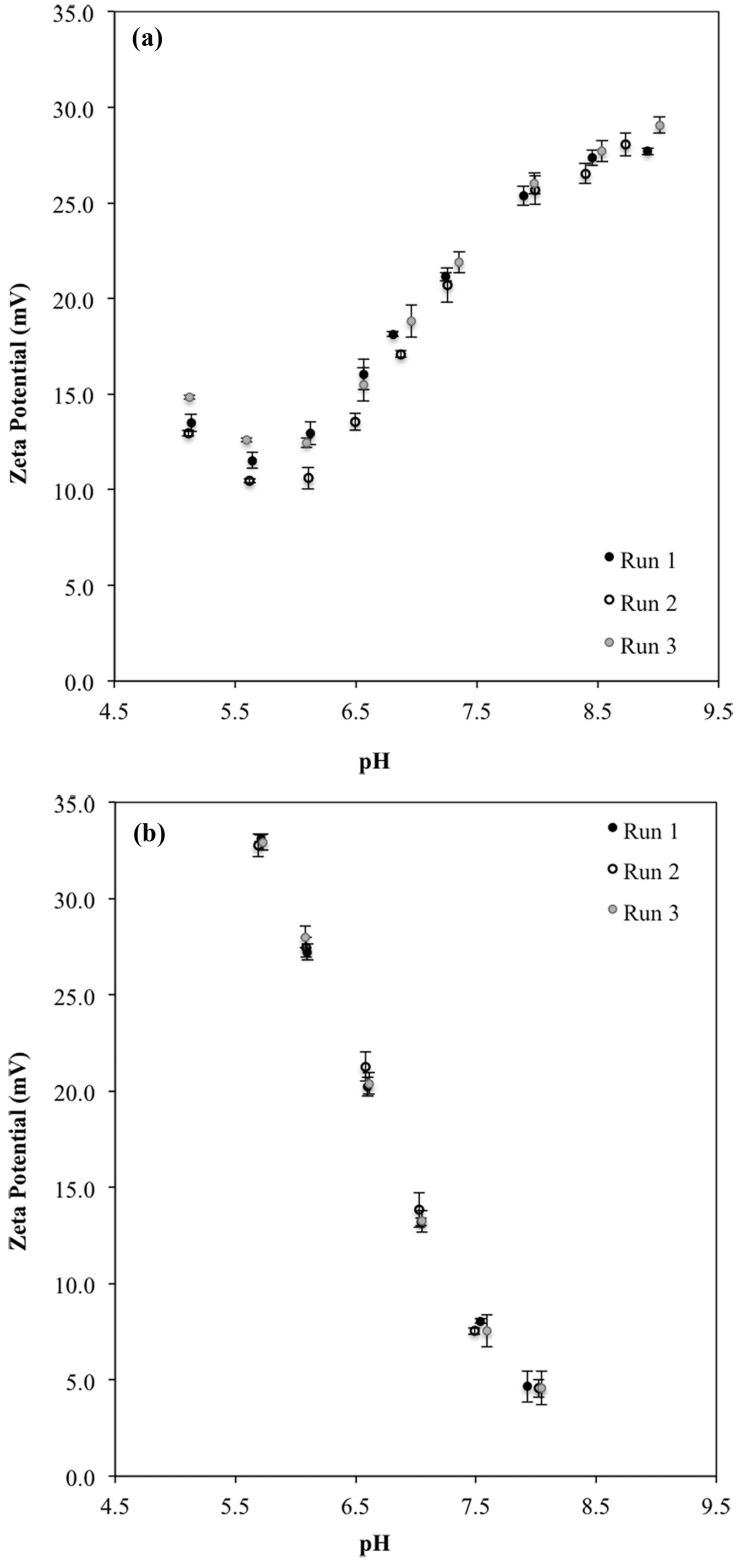

Figure 3.12. Zeta potential dependency on pH for aqueous nanodispersions of: (a) n-HAp dispersions alone using CH_3COOH 0.20 M (1 wt.%) as titrant; and (b) n-HAp/CS dispersions using NaOH 0.25 M as titrant

3.3.5 Effect of storage time

The electrostatic stability of n-HAp/CS dispersions was further studied by measuring zeta potential along time. The analysed dispersion, with C_{HAp}= 1.6 g/l and pH ~5.5, was prepared using the optimized process conditions, ultrasonication time of 50 s (50% amplitude), and store in a refrigerator at 4 °C. The zeta potential was measured at times ranging from 0, right after ultrasonication, to 30 days. Results in Figure 3.13 show that the zeta potential values were fairly constant along the time period analysed, ranging between +36 and +42 mV. This suggests that the prepared n-HAp/CS dispersions exhibit good electrostatic stability and that this behaviour is kept along time.

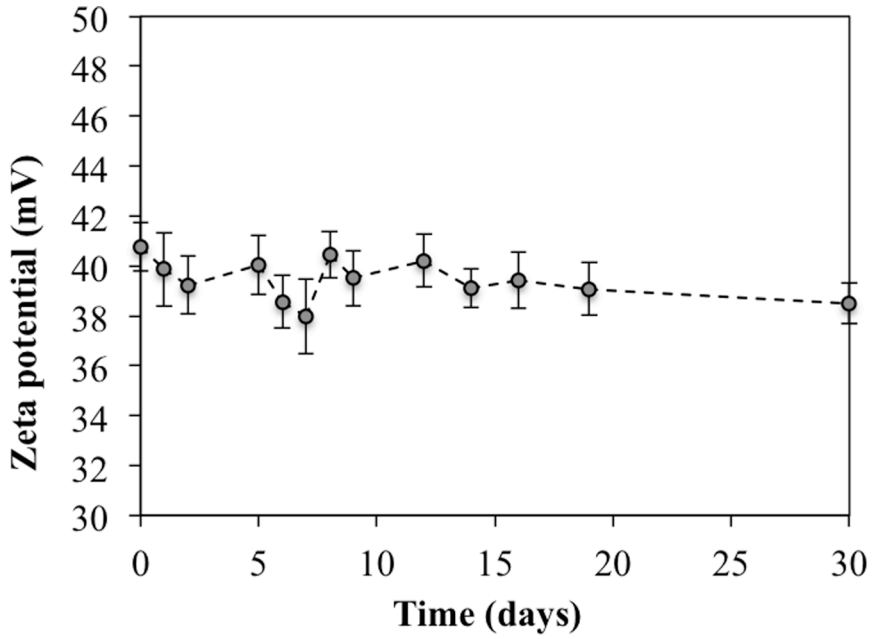

Figure 3.13. Effect of storage time on zeta potential

3.3.6 Characterization of n-HAp aqueous dispersions with higher concentration

Previously, diluted dispersions of n-HAp, with C_{HAp}= 1.6 g/l, were prepared and characterised to study the influence of different parameters on particle size and zeta potential. However, properties of colloidal systems may change as a function of concentration. Having in view the potential commercialization of n-HAp/CS products, the

production of hybrid dispersions with concentrations higher than $C_{HAp} = 1.6$ g/l is desirable. Therefore, n-HAp/CS dispersions with concentration $C_{HAp} = 20$ g/l were prepared and, since it was determined that such dispersions were unsuitable for DLS, particle size distributions (PDS) in volume were obtained by laser diffraction, both for n-HAp dispersions alone and in the presence of chitosan. Results obtained are shown in Figure 3.14. It is important to highlight that the obtained results in this section are not intended for comparison with previous results obtained by DLS, but only to evaluate particle size of n-HAp dispersions at higher concentrations.

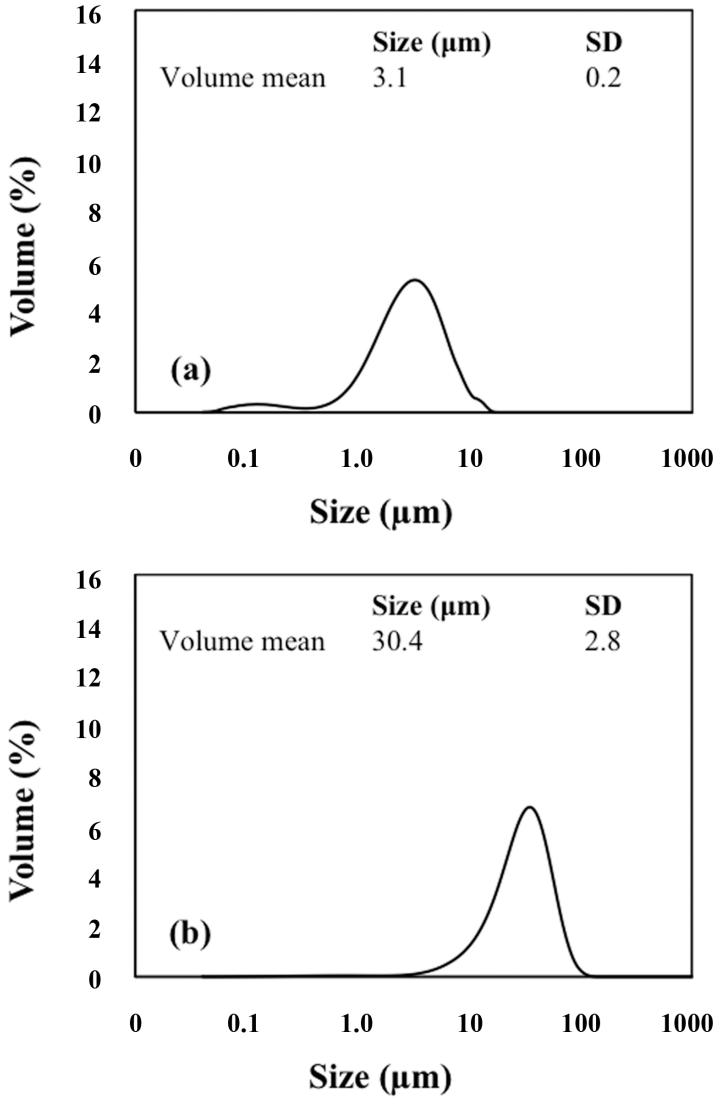

Figure 3.14. Particle size distributions in volume by laser diffraction for n-HAp dispersions with concentrations of 20 g/l: (a) n-HAp alone; (b) n-HAp/CS dispersions

It is observed that HAp nanoparticles form aggregates at this concentration level, $C_{HAp} = 20$ g/l, both for n-HAp dispersions alone and in the presence of chitosan. Furthermore, the agglomerates formed are larger in the presence of chitosan, in accordance with results previously discussed. Aggregation is caused by the collision and subsequent adhesion of particles. Collision of particles is mainly due to their Brownian motion, thus, the flow regime and the effects of external fields predominantly govern it. In addition, particle collisions are affected by the double layer interactions, which determine the repulsive forces. Finally, particle concentration is the third factor affecting particle aggregation since collisions frequency increases with particle concentration [23]. Therefore, the increase in particle size obtained for both types of n-HAp dispersions can be attributed to the increase in particles collision frequency, and the differences observed due to the incorporation of chitosan are probably related mainly to differences in the flow regime. However, even at high concentrations, n-HAp dispersions in the presence of chitosan showed improved electrostatic stability with zeta potential values >+30 mV (pH ~5.5).

3.4 Conclusions

Aqueous dispersions of n-HAp alone and in the presence of chitosan were prepared by ultrasonication and new insights on charge stability and particle size were explored. The study was carried out by preparing the dispersions using an optimum energy input of approximately 50 J/g of sample, corresponding to 50 % amplitude and 50 s of ultrasonication time. The Z-average presented low variability for ultrasonication times of 50 s and higher, showing that the breakup of agglomerates does not improve with longer processing times, and even there was a risk of re-agglomeration if long ultrasonication (processing times >100 s) are used. This was confirmed by the energy balance study.

The presence of KCl was analysed and, although no considerable influence on particle size was observed, it appears to improve the zeta potential of n-HAp dispersed in water, whereas in the presence of chitosan, the higher zeta potential values were obtained for the n-HAp/CS dispersions without KCl, indicating that the stabilizing effect of chitosan is better without the interference of salts. Furthermore, measurements carried out at different n-HAp/CS

weight ratios indicated that the zeta potential increases linearly with the increase of chitosan content.

It was also found that pH greatly influences the zeta potential of n-HAp dispersions. Zeta potential decreases with the increase of acidity in the dispersions of n-HAp alone, whereas the opposite behaviour is observed in the presence of chitosan. Thus, in slightly acidic environment (pH~5.5), the presence of chitosan greatly improves the electrostatic stability of n-HAp dispersions, exhibiting zeta potential values >+30 mV. Such zeta potential values remain nearly constant along time.

Finally, higher concentrations of n-HAp particles result in the formation of aggregates, as expected. However, it has been proven that chitosan acts as a stabilizer in aqueous dispersions of HAp nanoparticles, even when its presence promotes particle agglomeration (higher particle sizes were observed).

3.5 References

[1] Šupová, M., G.S. Martynková, and K. Barabaszová. *Effect of nanofillers dispersion in polymer matrices: a review.* Science of Advanced Materials, 3, 1-25 (2011).

[2] Kickelbick, G., *Introduction to Hybrid Materials*, in *Hybrid Materials*. 2007, Wiley-VCH Verlag GmbH & Co. KGaA. p. 1-48.

[3] Webster, T.J., et al. *Enhanced functions of osteoblasts on nanophase ceramics.* Biomaterials, 21, 1803-1810 (2000).

[4] Supova, M. *Problem of hydroxyapatite dispersion in polymer matrices: a review.* J Mater Sci Mater Med, 20, 1201-13 (2009).

[5] Goldberg, M., R. Langer, and X. Jia. *Nanostructured materials for applications in drug delivery and tissue engineering.* Journal of Biomaterials Science, Polymer Edition, 18, 241-268 (2007).

[6] Goodwin, J., *Colloids and Interfaces with Surfactants and Polymers*. 2009: Wiley.

[7] Pujala, R.K., *Dispersion Stability, Microstructure and Phase Transition of Anisotropic Nanodiscs*. 2014: Springer International Publishing.

[8] *Zetasizer Nano User Manual. Man0317 - Issue 5.0*. 2009, Malvern® Instruments Ltd.: England.

[9] *Zeta Potential - An introduction in 30 minutes. Technical Note*. 2015, Malvern® Instruments Ltd.

[10] *A basic guide to particle characterization. Whitepaper*. 2015, Malvern® Instruments Ldta.

[11] Briers, J.D. *Laser Doppler, speckle and related techniques for blood perfusion mapping and imaging.* Physiological Measurement, 22, R35 (2001).

[12] Goldburg, W. *Dynamic light scattering.* American Journal of Physics, 67, 1152-1160 (1999).

[13] *What is the Z-Average Size Determined by DLS? Technical Note*. 2012, Horiba Instruments, Inc.

[14] Keck, C.M. and R.H. Müller. *Size analysis of submicron particles by laser diffractometry—90% of the published measurements are false.* International Journal of Pharmaceutics, 355, 150-163 (2008).

[15] *Coulter LS Series. Product Manual*. 2011, Beckman Coulter, Inc.

[16] Honary, S. and F. Zahir. *Effect of zeta potential on the properties of nano-drug delivery systems-a review (Part 2).* Tropical Journal of Pharmaceutical Research, 12, 265-273 (2013).

[17] Honary, S. and F. Zahir. *Effect of zeta potential on the properties of nano-drug delivery systems-a review (Part 1).* Tropical Journal of Pharmaceutical Research, 12, 255-264 (2013).

[18] Wilson, O.C. and J.R. Hull. *Surface modification of nanophase hydroxyapatite with chitosan.* Materials Science & Engineering C-Biomimetic and Supramolecular Systems, 28, 434-437 (2008).

[19] *Sonicator Ultrasonic Processor: Operation Manual. Part No. Q700.* QSonica, LLC.

[20] Nguyen, V.S., et al. *Effect of ultrasonication and dispersion stability on the cluster size of alumina nanoscale particles in aqueous solutions.* Ultrasonics Sonochemistry, 18, 382-388 (2011).

[21] Carneiro-da-Cunha, M.G., et al. *Influence of concentration, ionic strength and pH on zeta potential and mean hydrodynamic diameter of edible polysaccharide solutions envisaged for multinanolayered films production.* Carbohydrate Polymers, 85, 522-528 (2011).

[22] *An Overview of the Zeta Potential: Technical Brief.* 2012, Particle Sciences, Inc.

[23] Babick, F., *Suspensions of Colloidal Particles and Aggregates.* 2016: Springer International Publishing.

4 Production of nano-hydroxyapatite/chitosan (n-HAp/CS) hybrid microparticles

This chapter is based on the published scientific article:

Ruphuy, G. et al. Spray drying as a viable process to produce nano-hydroxyapatite/chitosan (n-HAp/CS) hybrid microparticles mimicking bone composition, Advanced Powder Technology 27, 575-583 (2016). Doi:10.1016/j.apt.2016.02.010 [1]

In this work nano-hydroxyapatite/chitosan (n-HAp/CS) hybrid microparticles were prepared by spray drying following a methodology where, in a first step, aqueous nanodispersions of n-HAp in the presence of chitosan were produced by fast stirring at pH values below and above chitosan pKa (5.5 and 7.0, respectively). The mixing system used allowed the production of homogeneous and stable nanodispersions, and the subsequent spray-dried microparticles, incorporating highly pure HAp nanoparticles of approximately 50 nm, were successfully produced without degrading the organic component, chitosan. Comparatively with the n-HAp/CS-7.0, the n-HAp/CS-5.5 dispersions were characterized by a lower particle size and a higher zeta potential, being then more stable. Differences in the spray-dried microparticles were also evident from a morphological point of view. The n-HApCS-5.5 microparticles, which present an average size in volume of 15.8 μm and n-HAp crystals homogenously distributed, were found to be preferred over the n-HApCS-7.0 counterparts, which require an

extra step in the productive process and presented a tendency to form large agglomerates. Both prepared hybrid particles presented similar composition to that one of natural bone (HAp/CS of 70/30) and no traces of KCl salts were observed if a washed n-HAp paste was used.

4.1 Introduction

The combination of HAp with chitosan for bone tissue engineering applications is typically based in the production of porous scaffolds [2-4]; nonetheless, advances in science and technology have led to the development of particulate materials that, thanks to their reduced size, can be suitable as injectable systems or shaped into a solid substrate with increased surface area that will promote chemical and biological reactions [5-7]. In this context, the development of a particulate system containing n-HAp in a micrometer-sized matrix is advantageous; this approach allows HAp's superior properties at the nanoscale to be preserved in the form of microparticles that are easier to handle [8].

Among the existing techniques, spray drying appears as a promising technology for the manufacturing of microparticles with controllable size and morphology [9]. It is a process widely used as a microencapsulation/stabilization technique in the food [10, 11] and pharmaceutical [12, 13] industries. Easy industrialization, cost-effectiveness and continuous production are attractive features of this technique; however, special care must be taken with heat-sensitive materials, since prolonged contact with high temperatures can cause product degradation [14]. This method is based in the drying of atomized droplets of a previously prepared solution or emulsion/dispersion using a co-current stream of hot gas (see Figure 4.1). In the case of the process developed here, the first step comprises the preparation of HAp/CS nanodispersions.

One of the most common established methods used to prepare HAp/CS hybrid dispersions consists in simply mixing previously prepared HAp microparticles, usually as a powder, into a chitosan solution. This technique can lead to non-homogenous dispersions at a microscopic level, due to the difficulty in controlling the mixing between two dissimilar phases that can lead to phase separation. In efforts to overcome such problem, an adequate incorporation of HAp into the chitosan solution has been reported [15, 16] by using the so-called co-

precipitation method; nevertheless, this method implies the synthesis of HAp in the presence of chitosan, which hinders the formation of HAp particles with high purity and desired morphology.

Another important parameter to consider when preparing n-HAp/CS hybrid dispersions is pH, especially if HAp has to be introduced into an acidic environment that can influence its solubility, chemistry and phase stability [17]. Due to the amino-groups protonation character $\left(NH_2 \rightarrow NH_3^+\right)$, chitosan net charge can change with pH thus influencing solubility and reactivity. With a pKa value around 6.5, chitosan is insoluble in neutral and alkaline pH solutions, but it is soluble in aqueous acidic medium, allowing it to be processed under mild conditions [18, 19]. In the simple mixing method, HAp is often introduced in an acidic chitosan solution, resulting in dispersions with pH typically around 4-5. In the case of the co-precipitation method, the combination of both components is carried out in a neutral or basic environment (pH $\geq$ 7), causing the precipitation of chitosan along with HAp simultaneously.

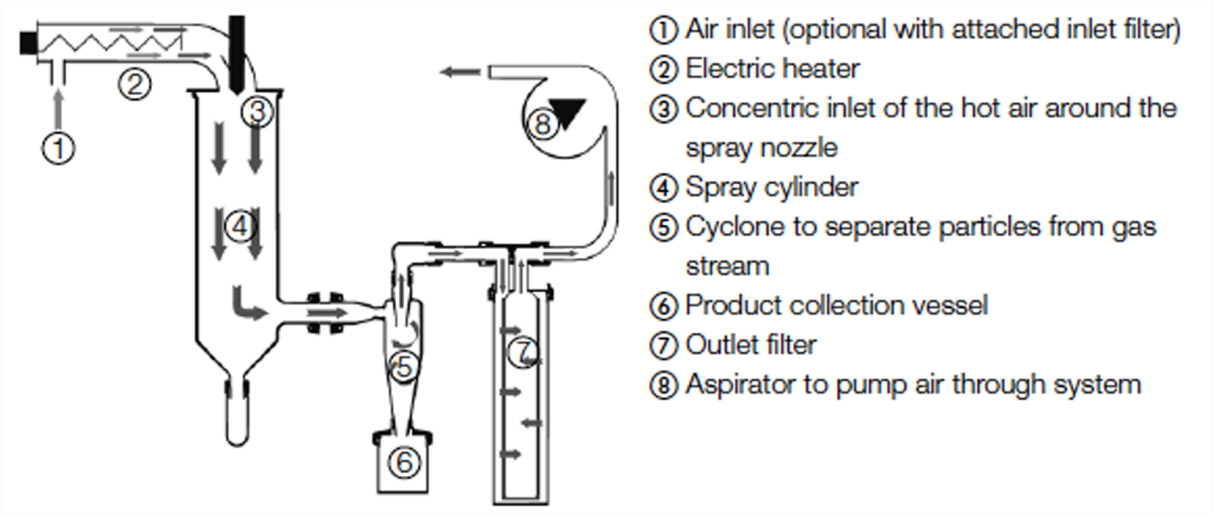

Figure 4.1. Schematic representation of the spray-drying process
(Reproduced from BÜCHI Labortechnik AG [20])

To the best of our knowledge, before this work, the only one reporting the production of HAp/CS microparticles by spray drying was the one of Başargan et al. (2015) [21]. In the approach used by the authors, a HAp/CS-slurry using the co-precipitation method (pH $\geq$ 9.0) was prepared, followed by spray drying. The effect of inlet temperatures (120 °C and 160

ºC) and different HAp/CS weight ratios was studied. Spherical microparticles of mean size 4-6 μm were produced, and an increase in the surface area with the addition of chitosan, as well as with the highest inlet temperature, were observed. However, the FTIR analysis suggested the substitution of carbonate in the apatite structures, compromising the purity of HAp. Thermal degradation studies were not reported. Other methods that have been explored to produce HAp/CS microparticles are: water-in-oil (W/O) emulsion [22]; supercritical assisted atomization [23], spray-coagulation [24], electro-spray coagulation [25], and dispersion polymerization [26].

In this work, n-HAp/CS microparticles mimicking bone composition, and containing highly pure HAp nanoparticles, were produced in a two-stage process. First, homogeneous and stable n-HAp/CS dispersions were produced using an innovative fast stirring set-up. With the aim of analysing the effect of pH on the final products, the dispersions were produced at two different pH values, right above and below the chitosan pKa. For the case of pH below chitosan pKa, special care was taken to assure pH values higher than 5.0 to avoid solubilisation of HAp. In a second step, hybrid microparticles were produced from the n-HAp/CS dispersions by spray drying. The effect of KCl content was also studied, since this salt is present in the original HAp paste used.

The n-HAp/CS nanodispersions were characterized by measuring particle size and zeta potential by static and electrophoretic light scattering methods, respectively. The produced microparticles were characterized by scanning electron microscopy (SEM) coupled with energy-dispersive X-ray spectroscopy (EDS), thermogravimetry (TG/DTG) and differential scanning calorimetry (DSC). In order to infer the effect of spray-drying conditions on material degradation, freeze-dried samples were also produced and characterized.

4.2 Materials and methods

4.2.1 Materials

The n-HAp/CS dispersions were prepared by using the chitosan brand 90/200/A1 from Biolog-Biotechnologie GmbH (Germany), composed of flakes with size <200 μm, with a deacetylation degree of 91.9%, and dynamic viscosity of 128 mPa·s (1% at 20ºC in 1% acetic acid solution). The hydroxyapatite aqueous paste used, *nanoXIM-CarePaste,* was supplied by Fluidinova S.A. It is composed of 15.5 ± 0.5 wt%. of HAp nanoparticles with particle size

<50 nm, 4.5 ± 0.5 wt%. KCl and a water content ≤ 81.0 wt%. Acetic acid, sodium hydroxide and sodium acetate tri-hydrate of analytical grade from Sigma Aldrich were used to prepare the solutions.

4.2.2 Dispersions preparation

Aqueous nanodispersions of HAp in the presence of chitosan, with a HAp concentration of 20 g/l, were prepared by using a high speed dispersing and homogenizing device Miccra D-9 at speed rate of 11 000 rpm. The mixing system was designed such that the HAp paste was injected into the chitosan solution inside the vessel right below the dispersing tip, as shown in Figure 4.2. The mixing time using a pump rate of 240 rpm (32 ml/min) was estimated to be less than 100 ms. A detailed description of the mixing time estimation is presented in Appendix B. All n-HAp/CS nanodispersions were prepared with a HAp-to-chitosan weight ratio of 70/30, since this ratio represents the typical bone composition in terms of inorganic/organic balance.

Two different pH values were considered, one lower and one higher than the chitosan pKa (5.5 and 7.0, respectively). For the preparation of the nanodispersion with lower pH, labelled as "n-HApCS-5.5", a pre-mixed solution prepared by adding a chitosan solution (3.0%, w/v) with an acetate buffer of pH = 5.5 was added to the reactor vessel, followed by the injection of the HAp paste (15%, w/w) continuously at a pump rate of 240 rpm into the chitosan solution. The sample with higher pH, labelled "n-HApCS-7.0", was prepared following the same procedure but with an extra final step consisting in the dropwise addition of NaOH 1M under fast stirring until neutralization.

For comparative purposes, analogous n-HAp/CS dispersions, with HAp concentration of 20 g/l and final pH 5.5 (room temperature), were prepared by ultrasonication using the optimum energy input determined in Chapter 3. Briefly, the sample was subjected to an energy input of 50 J/g of sample, using an Ultrasonic Processor (Sonicator) QSonica Q700 at 50% amplitude, with a maximum power output of 700 W, frequency output of 20 kHz and 12.5 mm diameter horn with replaceable tip. The produced nanodispersion, labelled "n-HApCS-5.5-ultrasonication", was characterized in terms of particle size and zeta potential, and a comparative analysis was carried out relative to the analogous n-HApCS-5.5 sample obtained by fast stirring as previously described.

The *nanoXIM-CarePaste* used in this work contains 4.5 wt%. KCl. In order to study the effect of KCl presence on the stability of the produced nanodispersions and morphology of the final microparticles, samples were obtained both with the original, unwashed paste and with a paste that was subjected to a washing process with water 3 times to remove the salt. The potassium content of the washed paste was found to be 15.0 ± 0.9 ppm, determined by Atomic Absorption Spectroscopy (AAS).

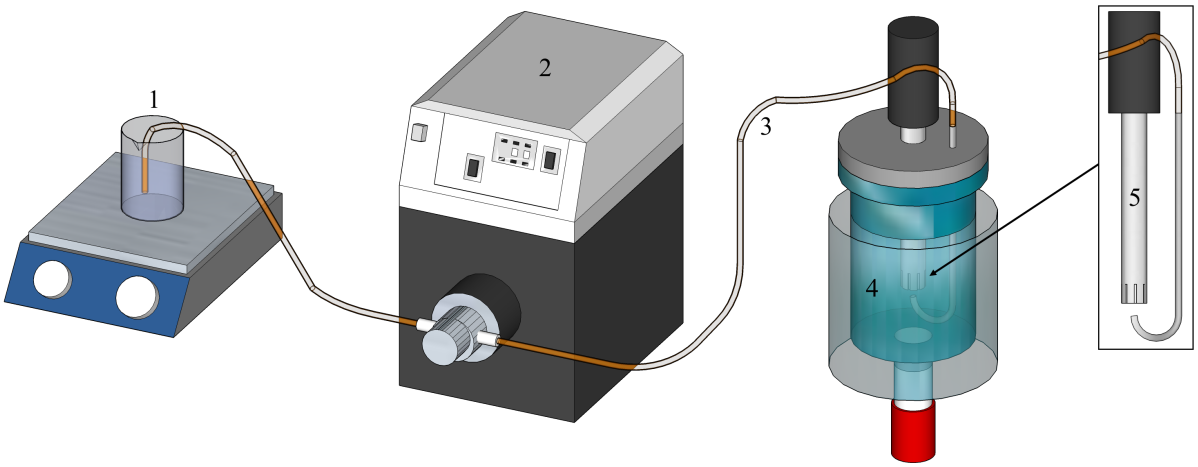

Figure 4.2. Experimental setup used to prepare the n-HAp/CS nanodispersions: (1) Beaker containing the n-HAp, *nanoXIM-CarePaste,* under stirring; (2) peristaltic pump; (3) tubing; (4) vessel containing the chitosan solution and buffer; (5) ultraturrax.

4.2.3 Microparticles preparation

The n-HAp/CS hybrid microparticles were prepared by spray-drying a volume of 150 ml of the prepared dispersions. The used apparatus was a Mini Spray Dryer B-290 from Büchi equipped with a nozzle of 0.7 mm of diameter and the operating conditions were: inlet temperature of 170°C; aspiration at 100%; spray gas flow at 30% (approximately 6 L/min); and pump rate at 15% (4.5 ml/min). The spray-drying yield was estimated as the ratio between the weight of the recovered powder and the initially used weight of solids of the atomized nanodispersions.

4.2.4 Preparation of freeze-dried samples

In order to infer the effect of spray-drying conditions on the micro particles' thermal degradation, samples prepared by direct freeze-drying of the obtained dispersions were produced. For that, 10 ml of each sample were firstly congealed by storing in a freezer for about 24 h followed by freeze-drying in a VirTis BenchTop 6K Freeze Dryer (model n°6KBTEL) during 48 h.

4.2.5 Characterization of dispersions

Particle size of the obtained dispersions, n-HApCS-5.5 and n-HApCS-7.0, was determined by using a Mastersizer 3000 laser diffraction analyser from Malvern Instruments. Dispersions stability was studied by electrophoretic light scattering using the Zetasizer Nano ZS from Malvern Instrument. The effect of pH on zeta potential was studied using the same equipment, Zetasizer Nano ZS, coupled with a MPT-2 Autotitrator using NaOH (0.25 M) as the titrant solution.

4.2.6 Characterization of microparticles

Morphology of the spray-dried microparticles was inspected by scanning electron microscopy (SEM) coupled with Energy-dispersive X-ray spectroscopy (EDS) by using a Phenom Pro microscope from Phenom World. High resolution images were obtained by High resolution (Schottky) Environmental Scanning Electron Microscope with X-Ray Microanalysis and Backscattered Electron Diffraction Pattern Analysis (FEG-ESEM/EDS/EBSD) using a FEI Quanta 400 FEG ESEM / EDAX Genesis X4M.

FT-IR spectra were recorded in a FT-IR BOMEN (model MB 104) in transmittance mode by using the KBr pellet technique at a concentration of about 1% (w/w). Scanning was carried out between 500 and 4000 cm^{-1} at a resolution of 4 cm^{-1} and co-adding sixty-four scans. The characterization of the n-HApCS-5.5 and n-HApCS-7.0 microparticles was achieved by analogy with the spectra of HAp and chitosan standard samples. Thermal characterization was obtained by thermogravimetry (TG) using a TG 209 F3 Tarsus® and differential scanning calorimetry (DSC) using a DSC 200 F3 Maia. The reproducibility of the experimental procedure was checked based on 3 replicas.

4.3 Results and discussion

4.3.1 Preparation and characterization of the hybrid dispersions

Particle size distributions in volume obtained for the n-HAp/CS dispersions prepared by fast stirring and ultrasonication are presented in Figure 4.3. In accordance with the results discussed in Chapter 3, HAp nanoparticles form aggregates in the presence of chitosan at the studied concentration, $C_{HAp} = 20$ g/l, but with zeta potential values larger than +30 mV. Small differences are observed in terms of particle size depending on the mixing device used. When comparing n-HAp/CS dispersions produced at the same pH (5.5), the nanodispersion prepared by fast stirring (n-HApCS-5.5 sample) exhibited slightly smaller particle sizes than the n-HApCS-5.5-ultrasonication sample. However, no considerable differences in zeta potential are observed, as shown in Figure 4.4; for different storage times, a good electrostatic stability, with zeta potential values between +36 mV and +42 mV, was obtained for both samples with pH 5.5, independently of the used mixing device, either ultraturrax (fast stirring) or ultrasonicator.

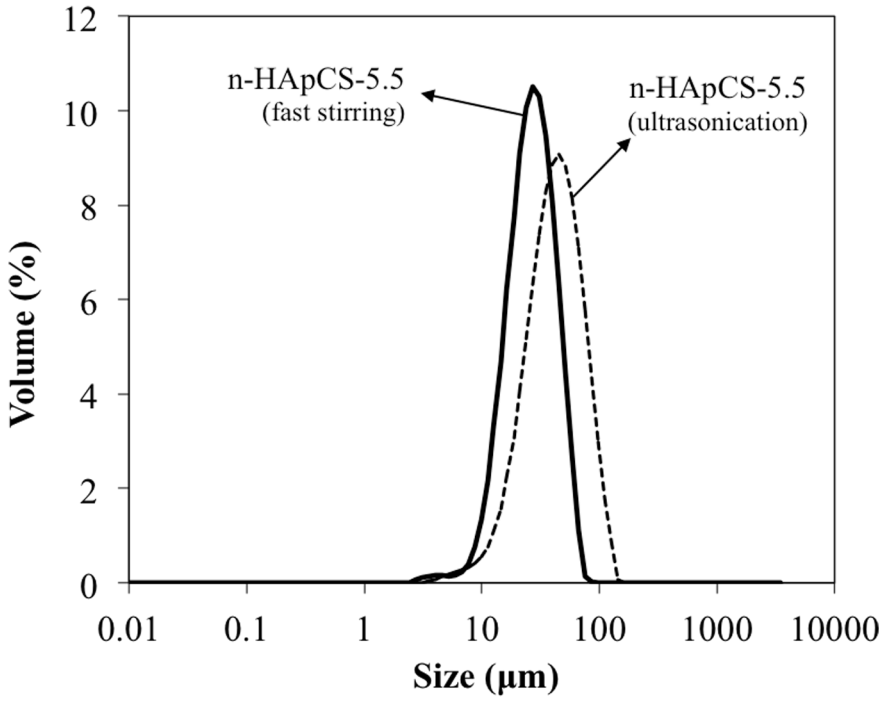

Figure 4.3. Particle size distributions in volume of the n-HApCS-5.5 sample prepared by fast stirring, and of the n-HApCS-5.5-ultrasonication sample.

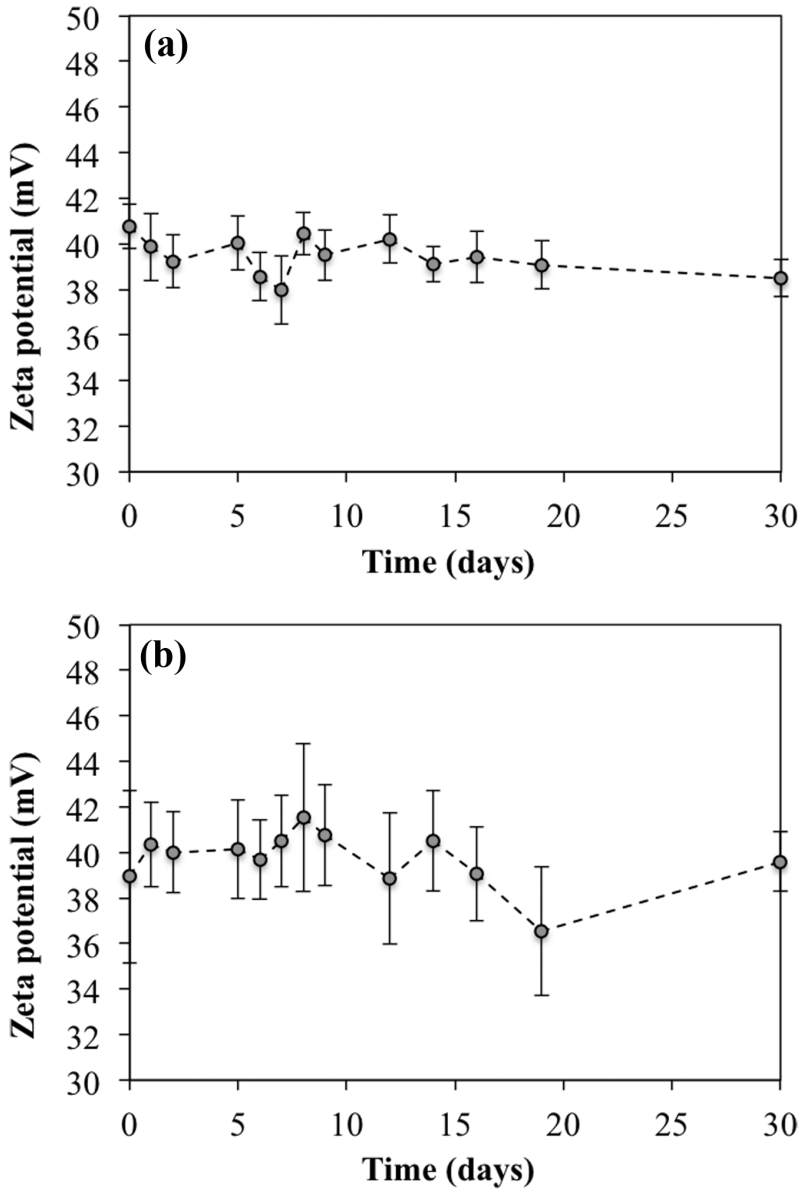

Figure 4.4. Zeta potential measured at different storage times for: (a) n-HApCS-5.5 sample prepared by fast stirring; and (b) n-HApCS-5.5-ultrasonication sample
(For both samples, pH 5.5 at room temperature)

In addition, energy efficiency was considered. The n-HApCS-5.5-ultrasonication sample was prepared using an optimum energy input of 50 J/g of sample, which is notably higher than the energy input obtained for the fast stirring device, estimated in less than 2.1 J/g of sample (see Appendix B). Therefore, the fast stirring set up used is energetically more efficient than ultrasonication, allowing the production of n-HAp/CS dispersions with smaller particle sizes, and similar zeta potential values if compared with the n-HApCS-5.5-ultrasonication sample.

Relative to the presence of KCl, Table 4.1 shows the number mean particle size and zeta potential values obtained for the n-HAp dispersions produced at pH of 5.5, alone and in the presence of chitosan, both with and without KCl. Monodispersed distributions were obtained in all cases, with larger particle sizes for the hybrid ones when compared with the n-HAp alone, but with no significant differences derived from the presence of KCl. In terms of charge stability, the n-HAp dispersions containing KCl presented higher zeta potential values (>30 mV), which indicate that the salt improves the stability of the n-HAp dispersion. In the case of n-HApCS-5.5 dispersions with KCl a good zeta potential value (>30 mV) was obtained, but an even higher zeta potential value was obtained for the n-HApCS-5.5 sample without KCl, which shows that chitosan also acts as an effective stabilizer besides providing the aforementioned list of desirable properties for bone repair and regeneration.

Table 4.1. Zeta potential and number mean particle size values obtained for nanodispersions of n-HAp with and without KCl

Sample	**Zeta potential (mV)**	**Number mean (nm)**
n-HAp-5.5 without KCl	24.1 ± 0.6	43.0 ± 3.1
n-HAp-5.5 with KCl	31.2 ± 0.3	42.7 ± 4.8
n-HApCS-5.5 without KCl	33.7 ± 0.2	198 ± 25
n-HApCS-5.5 with KCl	32.8 ± 0.2	222 ± 20

Particle sizes obtained by laser diffraction for samples n-HApCS-5.5 and n-HApCS-7.0 are summarized in **Table 4.2**; n-HAp/CS nanodispersions prepared at pH 5.5 presented a Dv50 of 28.4 μm, while the ones produced at higher pH (7.0) presented a Dv50 of 72.2 μm suggesting not only that HAp nanoparticles remain as clusters when dispersed in chitosan solutions, but also that the higher-pH condition produces larger clusters. Relative to zeta potential measurements, nanodispersions of n-HAp alone with an initial pH of approximately 9.0 and a zeta potential of +29 mV, showed a tendency of zeta potential to decrease as the pH decreases (see Figure 4.5). However, with the use of chitosan, a high zeta potential was obtained even at low pH values and, in contrast to what happens with n-HAp alone, a linear tendency of zeta potential to decrease with the increase of pH is observed (Figure 4.5).

Table 4.2. Particle size percentiles obtained for n-HApCS-5.5 and n-HApCS-7.0 samples from laser diffraction measurements

Sample	Dv10	Dv50	Dv90
n-HApCS-5.5	14.8	28.4	50.2
n-HApCS-7.0	23.5	72.2	165

4.3.2 Characterization of the n-HAp/CS hybrid microparticles

Nano-hydroxyapatite/chitosan hybrid microparticles were successfully produced by spray drying with average yields of 62 and 52% for the n-HApCS-5.5 and n-HApCS-7.0 samples, respectively. Figure 4.6 shows SEM images of microparticles obtained with the unwashed, i.e. with KCl, HAp paste. The formation of mushroom and doughnut-like microparticles was observed for the n-HApCS-5.5 sample. This type of morphology is ruled by hydrodynamics, both in- and outside the droplet, causing a droplet-transformation phenomenon going from a spherical to mushroom-like, to a final doughnut shape, as described by some authors [9, 27]. When compared to analogous spherical microparticles, studies have found that particles with torus geometry (doughnut) present advantages such as a higher stability for long-term storage in an aqueous environment and after undergoing processes such as freeze-drying [28].

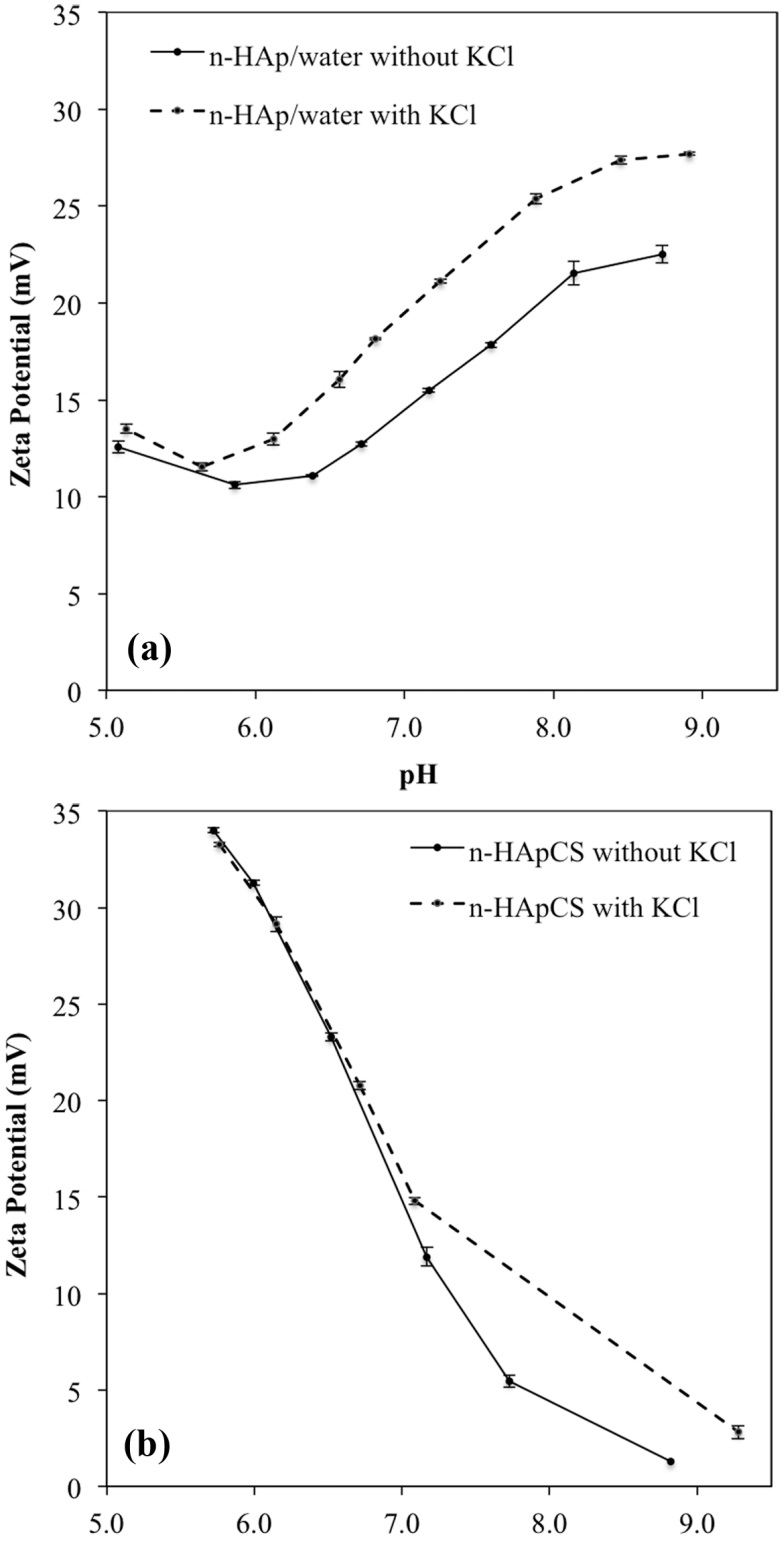

Figure 4.5. Zeta potential evolution with changing pH for:
(a) n-HAp dispersion (CH_3COOH 0.25 M as titrant);
and (b) n-HAp/CS nanodispersion (NaOH 0.25 and 1 M solutions as titrants)

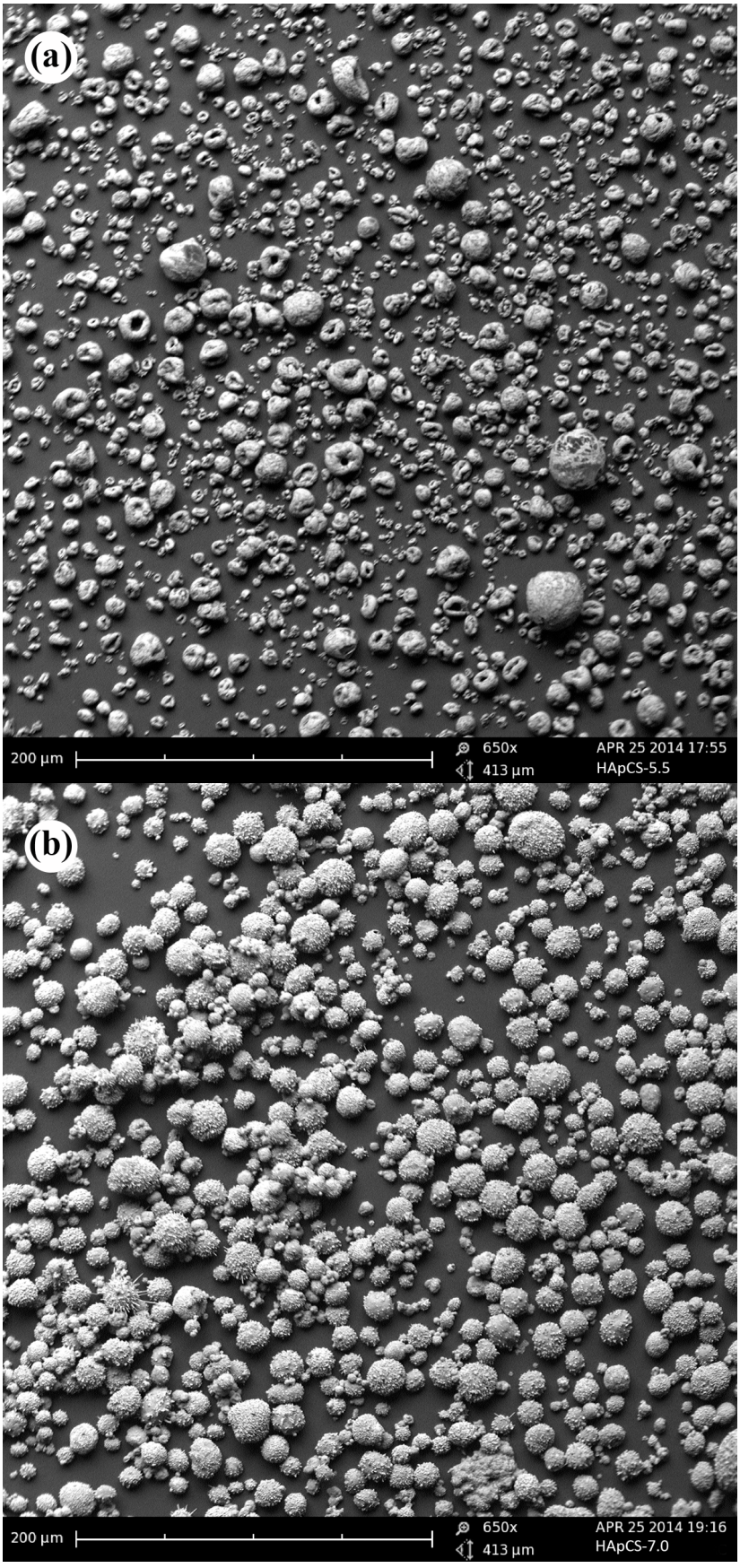

Figure 4.6. High-resolution SEM images of n-HAp/CS microparticles obtained with unwashed HAp paste (i.e. with KCl):
(a) n-HApCS-5.5 microparticles; (b) n-HApCS-7.0 microparticles

The n-HApCS-7.0 derived powder, on the other hand, presents better-defined spherical shape with spikes on the surface (see Figure 4.7). The maximum structural stability of spheres is the main reason why this shape is typically produced by spray drying. Drying temperature and velocity of the carrier gas are the main parameters influencing hydrodynamics of the droplets, but variables such as viscosity, density and concentration of the dispersions, as well as size of the nanoparticles are also fundamental factors influencing the final morphology of the microparticles [9, 27].

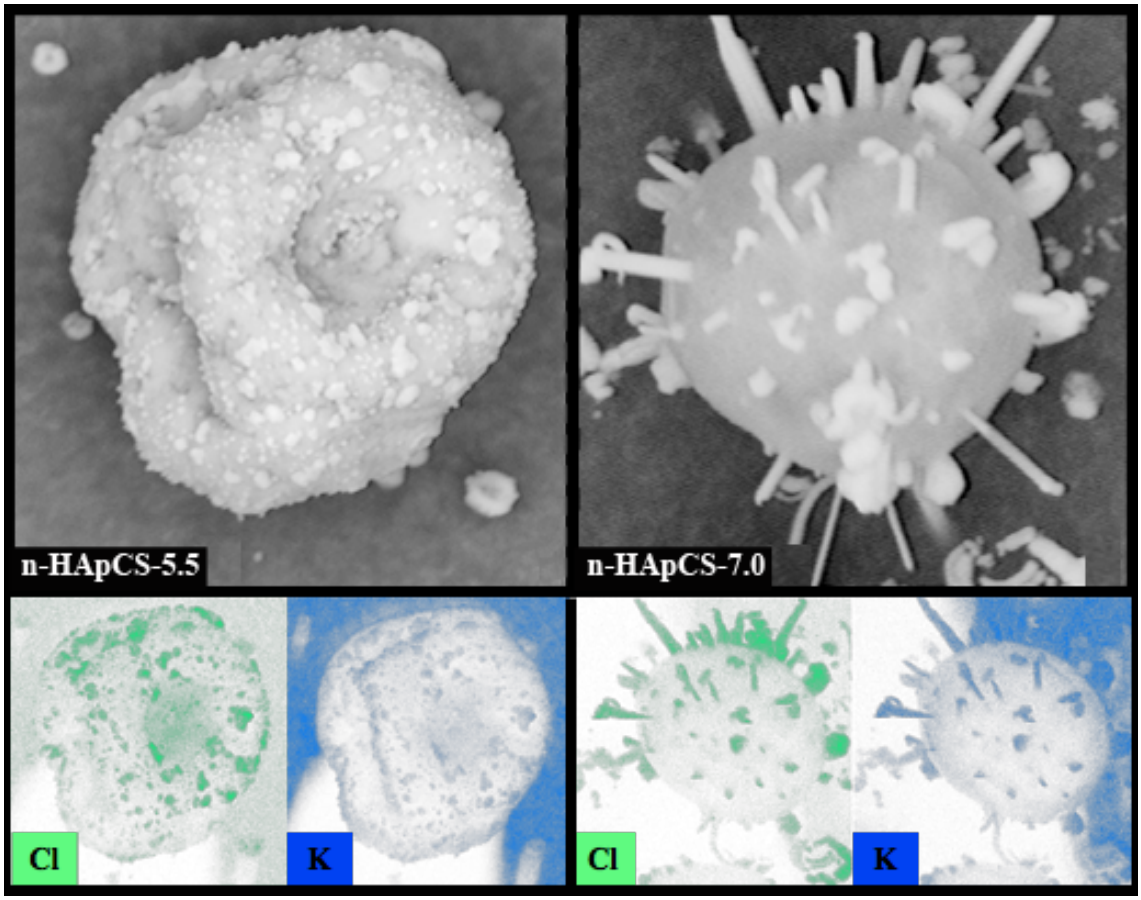

Figure 4.7. Elemental mapping by EDS of HAp/CS microparticles obtained with unwashed, with KCl, HAp paste, Cl is shown in green and K is shown in blue.

Elemental mapping by EDS (Figure 4.7) allowed the identification of the spikes observed in the n-HApCS-7.0 microparticles as KCl microcrystals. The salt was also detected in the n-HApCS-5.5 microparticles, even the crystals were significantly smaller and presented quite distinct morphology. As it is desired to produce microparticles with high purity, containing mainly HAp and chitosan, KCl appears as a contaminant in large quantities as seen in the

SEM images. In addition, it was proven that it has no beneficial effect on the stability of the n-HAp/CS dispersions and it could eventually create a hypertonic environment that could cause an inhibitory effect on cells metabolism [29].

High-resolution images of the microparticles produced from the nanodispersions prepared with the washed HAp paste are shown in Figure 4.8 and Figure 4.9. The n-HApCS-7.0 microparticles (Figure 4.9) seem to have a tendency to form strong agglomerates; this phenomenon is not observed in the case of the n-HApCS-5.5 microparticles (Figure 4.8). No traces of KCl salts were detected by EDS, and HAp rod-like particles of nanometer sizes can be observed at the surface of the microparticles, for both samples. The n-HApCS-5.5 microparticles present a rough surface that can be beneficial for biomedical applications, since it has been proven non-smooth surfaces can enhance cell adhesion and proliferation [30]. Particle sizes of the microparticles were obtained by image analysis; very similar number mean values, corresponding to 6.83 μm and 6.67 μm for n-HApCS-5.5 and n-HApCS-7.0 respectively, were obtained for both samples. In terms of Dv50, n-HApCS-7.0 sample presented a slightly smaller value of 12.4 μm based on the circle equivalent diameter of 1493 particles, compared to a Dv50 of 15.6 μm for the n-HApCS-5.5 sample based on the circle equivalent diameter of 1072 particles. These results suggest that n-HApCS-5.5 presented a few particles with larger sizes when compared to n-HApCS-7.0 sample, but also large amount of particles with small sizes. It is important to point out as well that n-HApCS-7.0 microparticles formed agglomerates of up to approximately 170 μm.

The IR spectra of n-HApCS-5.5 and n-HApCS-7.0, and the spray-dried HAp paste and chitosan, used as standard samples, are shown in Figure 4.10. Spray-dried HAp-paste spectra presented the typical bands of phosphate group, PO_4. Peaks at 1093 and 1032 cm^{-1} correspond to a triply degenerated asymmetric stretching mode vibration of the P–O bond of the phosphate group. A non-degenerated symmetric stretching mode of the P–O bond of the phosphate group is observed at 962 cm^{-1}. Peaks at 603 and 566 cm^{-1} correspond to a triply degenerated bending mode of the O–P–O bond. Peak at 632 cm^{-1} is assigned to the hydroxyl group deformation mode and it is considered to be overlapped with asymmetric P–O stretching vibration of PO_4^{3-}. Band at 3567 cm^{-1} was attributed to the stretching mode of the hydroxyl group, OH, while bands at 3421 and 1653 cm^{-1} are assigned to absorbed water, which appeared even when precautions were taken to eliminate moisture from the samples before analysis.

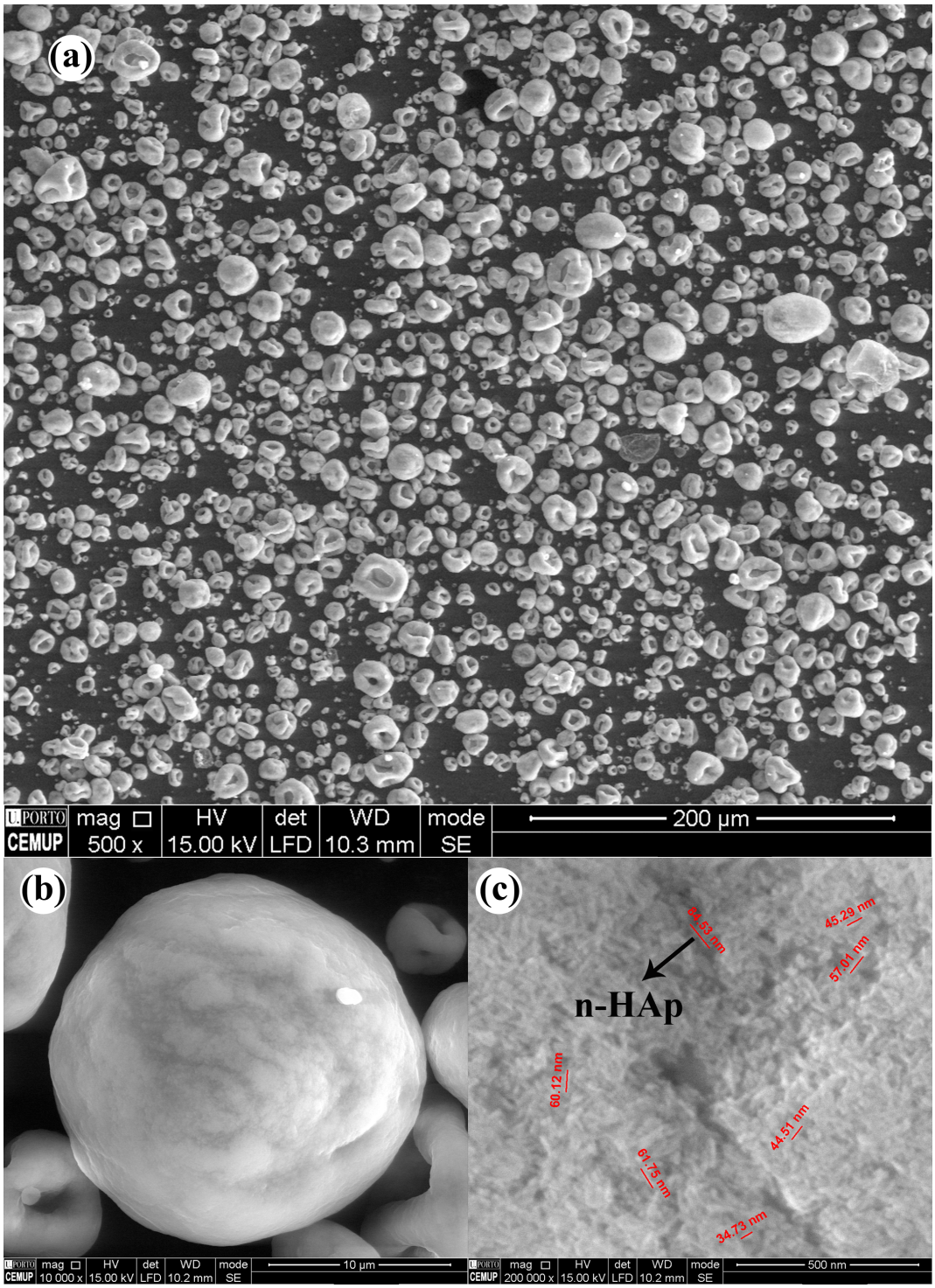

Figure 4.8. High-resolution SEM images of n-HApCS-5.5 microparticles obtained with washed, HAp paste (i.e without KCl) at magnifications of:
(a) 500X; (b) 10 000X; (c) 200 000X

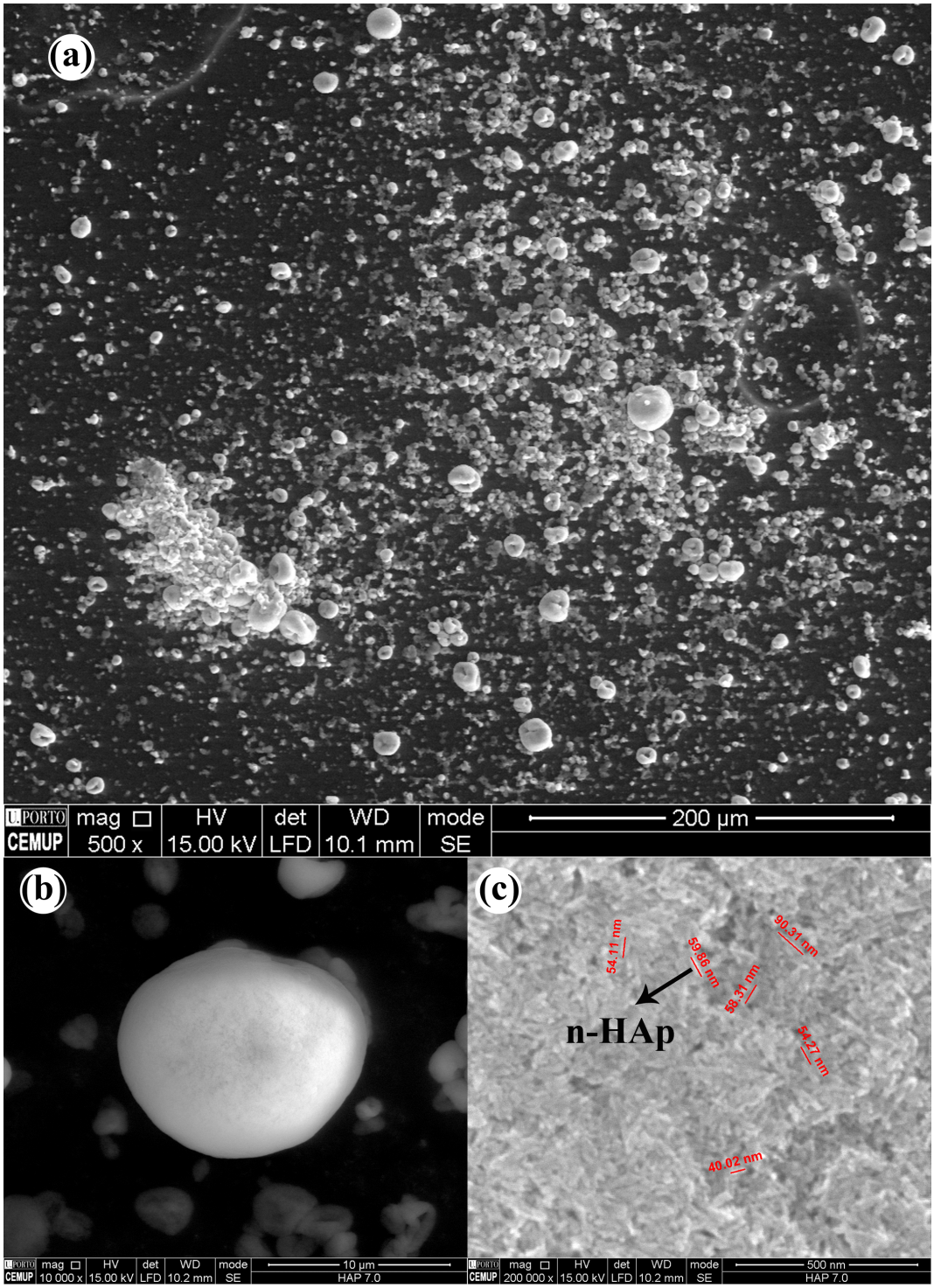

Figure 4.9. High-resolution SEM images of n-HApCS-7.0 microparticles obtained with washed, HAp paste (i.e. without KCl) at magnifications of:
(a) 500X; (b) 10 000X; (c) 200 000X

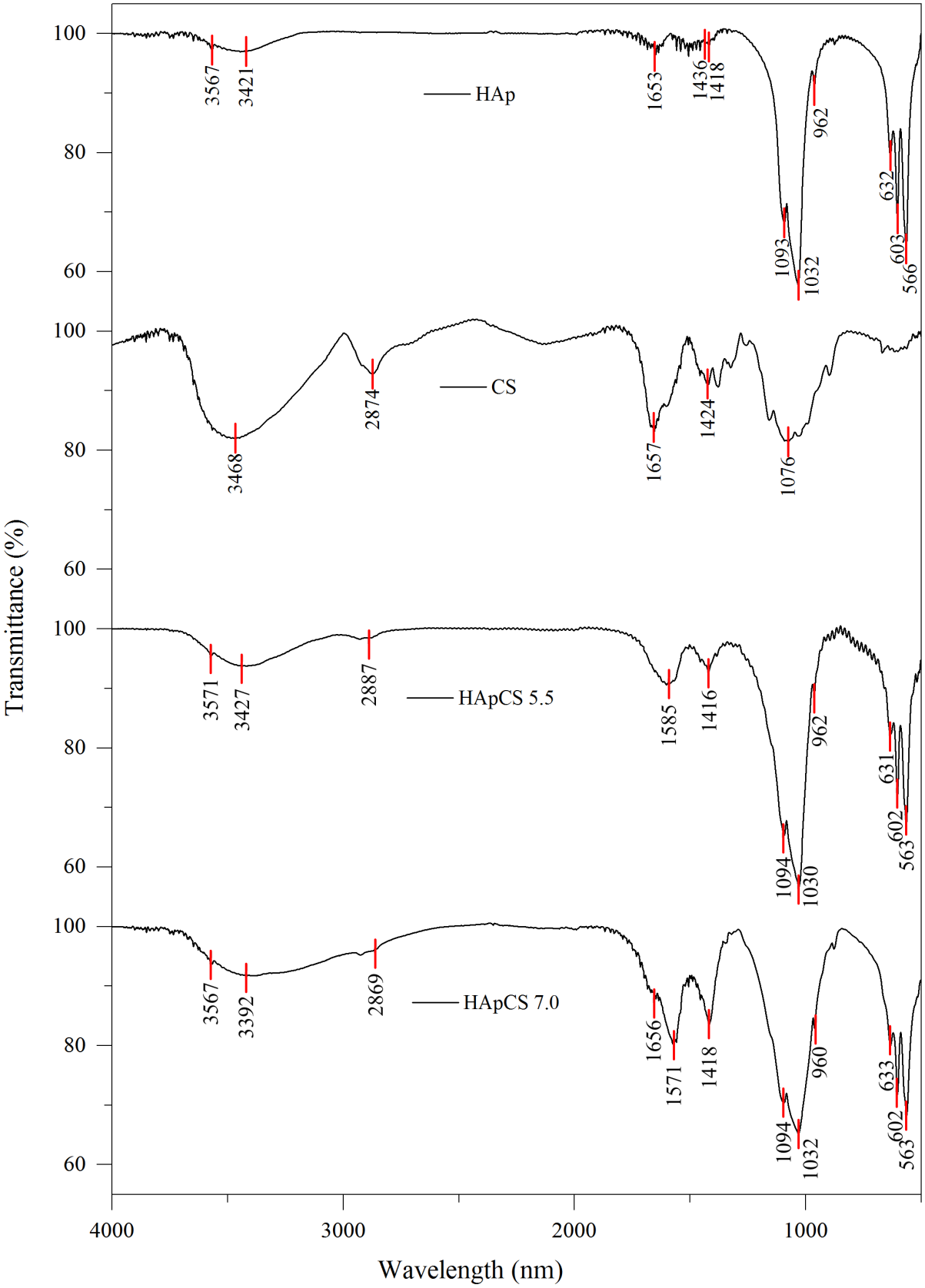

Figure 4.10. Infrared spectra of standards HAp and chitosan, n-HApCS-5.5 and n-HApCS-7.0

The characteristic groups of chitosan were also confirmed in the corresponding chitosan spectrum. The band at 3468 cm^{-1} was assigned to the stretching mode of the OH group, overlapped with the stretching mode of NH. Peaks at 1300-1450 cm^{-1} may correspond to a combination of CN-NH, CH_2-OH and CH_3 bands [31]. Bands at 2874 and 1424 cm^{-1} can be attributed to CH stretching and bending vibrations respectively, while peaks at 1657 and 1076 cm^{-1} correspond to NH, and C–O–C groups correspondingly.

IR spectra of both hybrid microparticles, n-HApCS-5.5 and n-HApCS-7.0, presented all typical bands of the characteristic groups of HAp and chitosan, proving that the HAp nanoparticles were successfully incorporated into the chitosan solution. For primary amines, the N–H bending (scissoring) vibration is observed in the region 1650-1580 cm^{-1} of the spectrum. This band of medium-strong intensity appears at slightly higher frequencies when the primary amine is associated with other groups. In particular, when the amine is protonated, the NH_3^+ group can form ionic bonds with opposite charged groups. In this case the NH_3^+ group of the primary amine will give rise to absorptions in the regions 1600-1575 and 1550-1504 cm^{-1}, close to the corresponding bands of the CH_3 group [32].

Particularizing, n-HApCS-5.5 spectrum shows only one peak at 1585 cm^{-1}, while n-HApCS-7.0 spectrum shows two peaks in this region (1656 and 1571 cm^{-1}). The peak at 1656 cm^{-1} can be attributed to the N–H of the NH_2 group due to the neutralization of the amine groups when increasing the pH of the nanodispersions. The peaks observed near 1580 cm^{-1}, in both n-HApCS-5.5 and n-HApCS-7.0, can be attributed to a possible formation of ionic bonds between the NH_3^+ groups from chitosan and the PO_4^{3-} groups from hydroxyapatite. These differences show that the pH at which the nanodispersions were prepared affected the chemical interactions between HAp and chitosan, leading to final products with different properties.

Results obtained from TG/DTG analysis of all the prepared samples are shown in Figure 4.11. For comparative purposes, solutions of chitosan in acetic acid were prepared and the pH was adjusted above and below 6.5, labelled CS-5.5 and CS-7.0, followed by spray-drying to obtain microparticles of such solutions. The first mass loss is observed between 30-100°C for all cases and it is attributed to water evaporation. Another peak is observed between 100 and 170°C in the curves of both CS-5.5 and n-HApCS-5.5, which can be related to the degradation of the acid used in the preparation of such samples. This peak is substantially

smaller in the thermograms of the samples prepared at higher pH since the acid was neutralized by the addition of base to increase the pH. The peak observed around 730°C in the n-HApCS-7.0 thermograms can be related to the degradation of the base used to increase the pH of this dispersion.

Finally, a mass loss observed between 200-310°C can be attributed to the thermal degradation of chitosan. This degradation step appears approximately at the same temperature (240°C) for all samples analyzed. Moreover, the n-HApCS-5.5 curves present what seems to be a retardation of the decomposition of the polymer at 400°C. It is noteworthy to point out that the hybrid samples show different patterns of degradation for chitosan that could be associated with differences in the interactions between chitosan and HAp depending on the pH at which the dispersions were prepared.

Both hybrids, n-HApCS-5.5 and n-HApCS-7.0, presented similar composition to that one of natural bone (see **Table 4.3**). Residual masses near 70% were attributed to HAp since the acid and base used in sample preparation were degraded below 800°C. The residual mass obtained agrees with the used HAp content.

Table 4.3. Comparative table of the composition of natural bone relative to the composition of n-HApCS-5.5 and n-HApCS-7.0 based on thermal degradation (TG/DTG analysis)

Component	**Natural Bone**	**HApCS-5.5**	**HApCS-7.0**
Inorganic	60-70% n-HAp	72% n-HAp	71.5% n-HAp
Organic	25-30% collagen	22% chitosan	21% chitosan
Water	5-10%	6% water and acetic acid	7.5% water and residual acid and base

The TG-DTG plots obtained for freeze-dried samples, n-HApCS-5.5-FD and n-HApCS-7.0-FD, are also shown in Figure 4.11. No significant differences are observed when compared to the thermograms of the analogous samples, the spray-dried n-HApCS-5.5 and n-HApCS-7.0 samples respectively, which proves that the chitosan was not degraded during the spray-drying process at the used conditions.

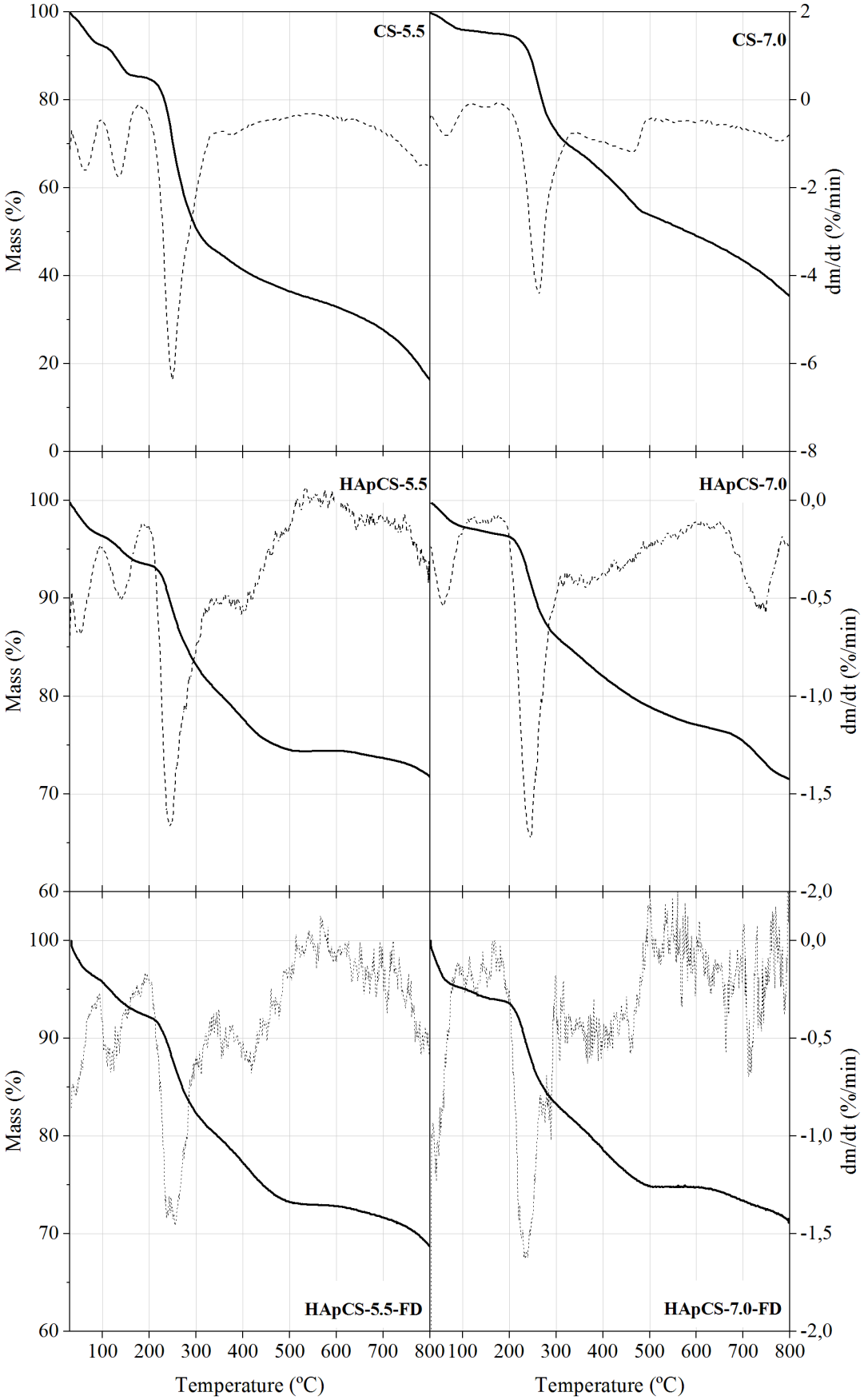

Figure 4.11. TG and DTG (dm/dt) of spray-dried n-HApCS-5.5, n-HApCS-7.0, CS-5.5, CS-7.0 and freeze-dried samples n-HApCS-5.5-FD and n-HApCS-7.0-FD (From 30 to 800°C at 10°C/min; N_2 atmosphere)

The DSC plots (Figure 4.12) confirm the results obtained by TG-DTG in terms of thermal degradation of chitosan, which has an exothermic peaks near 300°C. For both, TG and DSC analysis, a good reproducibility was observed since all transitions obtained coincide between batches of the same type of sample, either for n-HApCS-5.5 or n-HApCS-7.0.

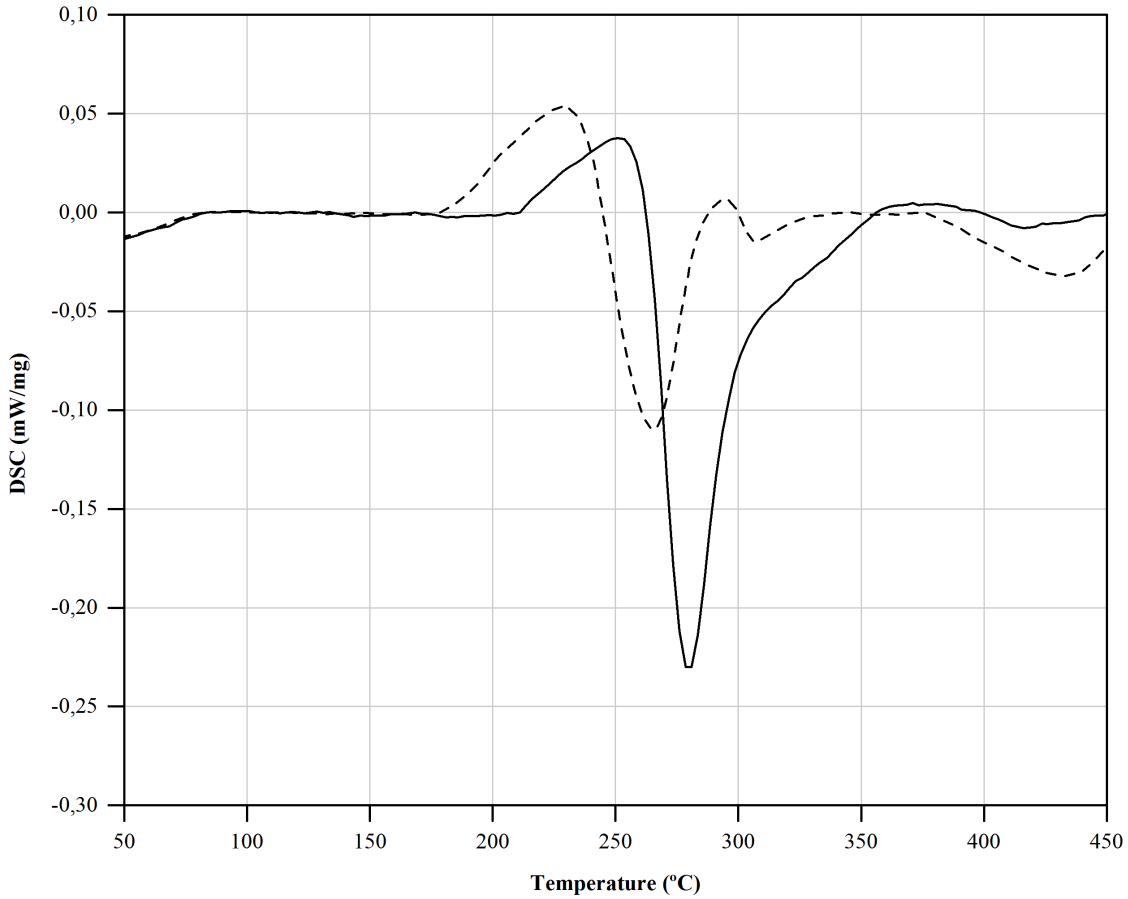

Figure 4.12. DSC of n-HApCS-5.5 (continuous line) and n-HApCS-7.0 (dotted line); from 50 to 450°C at 10°C/min; N_2 atmosphere

4.4 Conclusions

In this study, it was observed that different types of spray-dried microparticles are produced depending on the pH at which the initial nanodispersions were prepared. Dispersions with smaller particle sizes and higher zeta potential values are produced with the n-HAp/CS dispersions with pH $<$ 6.5, compared to dispersions with pH $>$ 6.5. The presence of KCl, a component of the original HAp paste used, has no beneficial effect on the stability of the n-HAp/CS dispersions, and its removal can be easily achieved by a prewashing procedure.

Differences on the spray-dried microparticles due to the effect of pH conditions were also evident from a morphological point of view. Doughnut-like n-HApCS-5.5 microparticles, with 15.8 μm average size in volume comprising n-HAp particles homogenously distributed, are preferred over n-HApCS-7.0 microparticles, which require an extra step in the productive process and also presented a tendency to form large agglomerates.

FTIR analysis of both n-HApCS-5.5 and n-HApCS-7.0 showed all typical bands of the characteristic groups of HAp and chitosan, proving that the HAp nanoparticles were successfully incorporated into the chitosan solution. Evidence of formation of ionic bonds of the primary amine groups, NH_3^+, was observed which is compatible with ionic bonds formation between NH_3^+ from chitosan and PO_4^{3-} from hydroxyapatite.

The spray-dried microparticles presented different thermal degradation behaviour that can be related with differences in HAp-CS interactions depending on the pH at which the products were prepared. The residual mass from TG results was near 70%, attributed to hydroxyapatite in accordance with the weight ratio pretended. No significant differences were observed between spray-dried and freeze-dried samples, which evidences that chitosan was not degraded during the spray-drying process at the used conditions. The reproducibility of the experimental procedure was checked based on 3 replicas.

Most importantly, hybrid n-HAp/CS microparticles containing 50 nm HAp nanoparticles were produced successfully by spray drying; such microparticles can potentially be used for biomedical applications, such as bone repair and drug delivery systems.

4.5 References

[1] Ruphuy, G., et al. Spray drying as a viable process to produce nano-hydroxyapatite/chitosan (n-HAp/CS) hybrid microparticles mimicking bone composition. Advanced Powder Technology,

[2] Kong, L., et al. Preparation and characterization of nano-hydroxyapatite/chitosan composite scaffolds. Journal of Biomedical Materials Research Part A, 75A, 275-282 (2005).

[3] Oliveira, J.M., et al. Novel hydroxyapatite/chitosan bilayered scaffold for osteochondral tissue-engineering applications: Scaffold design and its performance when seeded with goat bone marrow stromal cells. Biomaterials, 27, 6123-6137 (2006).

[4] Thein-Han, W.W. and R.D.K. Misra. Biomimetic chitosan–nanohydroxyapatite composite scaffolds for bone tissue engineering. Acta Biomaterialia, 5, 1182-1197 (2009).

[5] Silva, G., P. Ducheyne, and R. Reis. Materials in particulate form for tissue engineering. 1. Basic concepts. Journal of Tissue Engineering and Regenerative Medicine, 1, 4-24 (2007).

[6] Silva, G., et al. Materials in particulate form for tissue engineering. 2. Applications in bone. Journal of tissue engineering and regenerative medicine, 1, 97-109 (2007).

[7] Oliveira, M.B. and J.F. Mano. Polymer-based microparticles in tissue engineering and regenerative medicine. Biotechnology Progress, 27, 897-912 (2011).

[8] Okuyama, K., et al. Preparation of functional nanostructured particles by spray drying. Advanced Powder Technology, 17, 587-611 (2006).

[9] Nandiyanto, A.B.D. and K. Okuyama. Progress in developing spray-drying methods for the production of controlled morphology particles: From the nanometer to submicrometer size ranges. Advanced Powder Technology, 22, 1-19 (2011).

[10] Dias, M.I., I.C.F.R. Ferreira, and M.F. Barreiro. Microencapsulation of bioactives for food applications. Food & Function, 6, 1035-1052 (2015).

[11] Ribeiro, A., et al. Spray-drying microencapsulation of synergistic antioxidant mushroom extracts and their use as functional food ingredients. Food Chemistry, 188, 612-618 (2015).

[12] Sollohub, K. and K. Cal. Spray drying technique: II. Current applications in pharmaceutical technology. Journal of pharmaceutical sciences, 99, 587-597 (2010).

[13] Song, Y., et al. Synthesis and Sustained-Release Property of Drug-Loaded Chitosan Microspheres by Spray Drying Technique. American Journal of Macromolecular Science, 2, 1-10 (2015).

[14] C., L.A., P. S., and M.J. F. Production methodologies of polymeric and hydrogel particles for drug delivery applications. Expert Opinion on Drug Delivery, 9, 231-248 (2012).

[15] Peniche, C., et al. Chitosan/hydroxyapatite-based composites. Biotecnología Aplicada, 27, 202-210 (2010).

[16] Supova, M. Problem of hydroxyapatite dispersion in polymer matrices: a review. J Mater Sci Mater Med, 20, 1201-13 (2009).

[17] Wilson, O.C. and J.R. Hull. Surface modification of nanophase hydroxyapatite with chitosan. Materials Science & Engineering C-Biomimetic and Supramolecular Systems, 28, 434-437 (2008).

[18] Croisier, F. and C. Jérôme. Chitosan-based biomaterials for tissue engineering. European Polymer Journal, 49, 780-792 (2013).

[19] Levengood, S.K.L. and M. Zhang. Chitosan-based scaffolds for bone tissue engineering. J. Mater. Chem. B, 2, 3161 (2014).

[20] Operation Manual. Mini Spray Dryer B-290. BÜCHI Labortechnik AG.

[21] Başargan, T. and G. Nasün-Saygılı. Spray Dried Mesoporous Hydroxyapatite-Chitosan Biocomposites. Polymer-Plastics Technology and Engineering, null-null (2015).

[22] Ding, C.-C., S.-H. Teng, and H. Pan. In-situ generation of chitosan/hydroxyapatite composite microspheres for biomedical application. Materials Letters, 79, 72-74 (2012).

[23] Reverchon, E. and R. Adami. Supercritical assisted atomization to produce nanostructured chitosan-hydroxyapatite microparticles for biomedical application. Powder Technology, 246, 441-447 (2013).

[24] Granja, P., et al. Preparation and characterization of injectable chitosan-hydroxyapatite microspheres. Book of 573-576 Key Engineering Materials, 2004.

[25] Chen, J., et al. Preparation of chitosan/nano hydroxyapatite organic–inorganic hybrid microspheres for bone repair. Colloids and Surfaces B: Biointerfaces, 134, 401-407 (2015).

[26] Sivakumar, M., I. Manjubala, and K. Panduranga Rao. Preparation, characterization and in-vitro release of gentamicin from coralline hydroxyapatite–chitosan composite microspheres. Carbohydrate Polymers, 49, 281-288 (2002).

[27] Iskandar, F., L. Gradon, and K. Okuyama. Control of the morphology of nanostructured particles prepared by the spray drying of a nanoparticle sol. Journal of Colloid and Interface Science, 265, 296-303 (2003).

[28] Ungphaiboon, S., et al. Materials for microencapsulation: what toroidal particles ("doughnuts") can do better than spherical beads. Soft Matter, 6, 4070-4083 (2010).

[29] Hata, R.-i. Age-dependent changes in collagen metabolism and response to hypertonic culture conditions of rat aortic smooth muscle cells and skin fibroblasts. Cell Biology International Reports, 14, 25-33 (1990).

[30] Huang, S. and X. Fu. Cell behavior on microparticles with different surface morphology. Journal of Alloys and Compounds, 493, 246-251 (2010).

[31] Fadeeva, I.V., et al. Interactions of calcium phosphates with chitosan. Doklady Chemistry, 441, 387-390 (2011).

[32] Silverstein, R.M., et al., Spectrometric identification of organic compounds. 2014: John Wiley & Sons.

5 Production of nano-hydroxyapatite/chitosan (n-HAp/CS) hybrid scaffolds

Since long, it has been proven that hybrid scaffolds composed of hydroxyapatite (HAp) and chitosan (CS) are suitable for non-load-bearing bone graft applications. However, the productive process of such materials still faces challenges limiting process scalability and their commercialization. The main constraints comprise the need of final steps for purification/neutralization, as well as, sterilization that may be critical in view of achieving adequate properties. The purification/neutralization stage, needed to eliminate the residual acetic acid used to solubilize the chitosan, and thus make viable cell growth, can compromise the scaffold structural features. On the other hand, conventional sterilization procedures, can cause thermal degradation of the material, affect its chemical properties, and/or leave toxic residues on material's surface.

In this context, this chapter presents a process to produce n-HAp/CS scaffolds mimicking bone composition and structure, where an innovative step based on supercritical CO_2 extraction, was used as both, a purification step to eliminate the residual acetic acid, and as a potential sterilization step for thermosensitive materials. Process parameters such as temperature (40 and 75 ^{o}C) and number of extraction cycles (1 and 2) were tested. The pressure was kept constant at 8.0 MPa. With the best-achieved conditions (T = 75 ^{o}C and

P = 8.0 MPa) it was possible to remove 80% of the residual acetic acid (i.e. of the acid remaining after the freeze-drying step). The produce scaffolds exhibited adequate interconnected porous structure with a mean pore size of (72 ± 35) μm, fast swelling, and a storage modulus of (20.5 ± 2.9) kPa at 1 Hz frequency. Furthermore, the obtained scaffolds were sterile (microbiological assay revealed no microbial growth) and showed cytocompatibility, osteoconductivity, allowing the adhesion of osteoblast-like cells to its surface. Thus, the proposed process, which comprises 3-steps (n-HAp/CS dispersion preparation, freeze-drying stage to fix scaffold shape and supercritical CO_2 extraction to remove acetic acid and promote sterilization) is a simple and straightforward technique, allowing the successful production of n-HAp/CS scaffolds, exhibiting desirable properties for the treatment of small, non-load-bearing bone defects.

5.1 Introduction

Bone tissue engineering is an expanding research area due to its promising contributions to achieve materials that, in comparison with orthodox treatments, have great potential to improve bone regeneration, or ensure replacement when damaged, with the advantage of enabling customization to satisfy particular requirements [1, 2]. However, the design of bone grafts can be very challenging due to the specificities an ideal graft should fulfil; it must be biocompatible, biodegradable, exhibit appropriate mechanical properties, and present interconnected porous structure with adequate micro- and macro porosity, among others [1, 3]. In addition, off-the-shelf availability of the grafts is highly desirable and, therefore, an easily scalable manufacturing process is a key requirement as well [3].

The production of bone grafts based on hydroxyapatite ($Ca_{10}(PO_4)_6(OH)_2$, HAp) and chitosan (CS) has been widely studied and proven to be a suitable combination for bone tissue engineering applications [4]. HAp by itself is highly brittle and chitosan on its own does not induce the deposition of bone minerals even though it does promote osteogenic cells attachment and proliferation. However, when combining both components, HAp provides the required bioactivity while chitosan adds elasticity to the final material, resulting in a great candidate for non-load-bearing bone graft applications [4, 5]. In this sense, the production of n-HAp/CS hybrid materials in the form of scaffolds is of great interest.

Taking advantage of the remarkable ability of bone self-regeneration, the idea behind a scaffold is to act as a 3D template that once implanted in the bone defect, allows cell migration, adhesion, proliferation and eventually, the formation of new bone tissue. To achieve this goal, the scaffold's microstructure is critical; it should be highly porous with interconnected pores allowing cells mobility, diffusion of nutrients and vascularization. Besides the scaffolds architecture, the manufacturing process is another major factor to consider; the final product should be clinically and commercially viable, therefore, the process must be reproducible and scalable to industrial production. Additionally, from a clinician's point of view, a bone graft should be, preferably, an off-the shelf product able to be easily adapted into different shapes and with few or non-extra surgical procedures prior to implantation [3, 6].

In order to obtain the scaffolds, first the hydroxyapatite nanoparticles are introduced into a chitosan solution, resulting in an n-HAp/CS aqueous dispersion. This dispersion preparation is a key step that can be done in a number of ways. One of the most commonly used methods, because it is simple and straightforward, is the so-called *simple mixing* method. It consists in physically mixing HAp particles, micro- or nanometer sized, into a chitosan solution [4, 7]. Afterwards, the scaffolds are obtained, frequently by freeze-drying, a simple technique in which phase separation is induced by the formation of ice crystals upon freezing, followed their sublimation [4, 8]. Many authors working with the preparation of n-HAp/CS based hybrid scaffolds by freeze-drying reported the achievement of materials with desirable high porosity and pores interconnectivity [9-16].

In most cases, n-HAp/CS scaffolds prepared by freeze-drying from dispersions obtained by simple mixing still contain residual acetic acid remaining from the one used to solubilize chitosan. Therefore, a purification/neutralization step is needed since acidification of the medium can cause structure disruption upon contact with water or deviate culture medium pH from the ideal range (7.2-7.4) thus inhibiting cell growth and proliferation [8, 17]. Typically, purification/neutralization of the scaffold is carried out by immersion in an alkaline solution, washing with ultrapure water, and drying usually through another freeze-drying step [4, 10, 12-14, 18]. This neutralization process to remove the residual acetic acid is time consuming and can lead to low purity materials, i.e. materials with residual salts remaining from the used alkaline solution, as well as with compromised structural integrity, e.g. the second freeze-drying step applied to the already formed scaffold can damage its

porous structure. In fact, it has been reported that chitosan-based scaffolds undergo shrinkage and distortion after neutralization with NaOH solutions [19, 20].

Furthermore, when designing n-HAp/CS hybrid materials, sterilization is an important procedure to consider. Given that chitosan is a thermo-sensitive material, common sterilization techniques, such as dry heat and steam, are not appropriate since they can cause thermal degradation of the material. Ethylene oxide and *gamma* irradiation, on the other hand, can affect its chemical properties; the use of ethylene oxide risks the deposition of toxic residues on the materials surfaces and high-energy *gamma* irradiation can cause material degradation as well [21].

In this context, the use of $scCO_2$ as an innovative sterilization technique [21-26] has attracted great attention since it gathers a large amount of advantages; it is environmentally benign, nontoxic, non-flammable, non-corrosive, readily available, and inexpensive solvent [27, 28]. This supercritical fluid has been well known for its outstanding solvent capacities due to its high diffusivity; it has been widely used in food industry as an extraction medium, but also for processing pharmaceuticals due to its low critical temperature [29]. However, no reports were found regarding the effects of $scCO_2$ extraction using sterilizing conditions on the structural, physicochemical, and mechanical properties of scaffolds for bone tissue engineering.

In this work, a 3-step process to produce n-HAp/CS scaffolds mimicking bone composition and structure is presented, where an innovative step based on supercritical CO_2 extraction, is introduced for the purification and potential sterilization of the scaffolds. The advantages of this method were studied over other currently used procedures, often based on neutralization steps. The obtained scaffolds were characterized in what concerns morphology, porosity and pore size distribution, swelling capacity, and mechanical properties. A microbiological test was performed in order to evaluate if the scaffolds were sterilized, and biological assays were also carried out in order to assess cytotoxicity of the produced scaffolds.

5.2 Materials and methods

5.2.1 Materials

Hydroxyapatite aqueous paste *nanoXIM-HAp102,* supplied by Fluidinova S.A., was used to prepare the n-HAp/CS dispersions. It is composed of 15.0 ± 1.0% wt. of HAp rod-like nanoparticles suspended in pure water, with particle size <50 nm. Chitosan brand 90/200/A1, with deacetylation degree and dynamic viscosity of 91.9% and 128 mPa·s (1% at 20ºC in 1% acetic acid solution) respectively, was purchased from Biolog-Biotechnologie GmbH (Germany). Solutions were prepared using glacial acetic acid and sodium acetate tri-hydrate, both of analytical grade, 8 M sodium hydroxide solution brand Fluka, trypsin, EDTA, resazurin sodium salt, and PBS, all acquired from Sigma Aldrich. Brain heart infusion (BHI) was acquired from Liofilchem® s.r.l. Eagle, while minimum essential medium (MEM), alpha modification (α-MEM), fetal bovine serum, penicillin, streptomycin, and amphotericin B brand Gibco™ were acquired from Thermo Fisher Scientific Inc.

5.2.2 Dispersions preparation

Hydroxyapatite nanoparticles were incorporated in the chitosan solution by simple mixing, with rigorous control of the mixing and pH conditions, as described elsewhere [30]. Briefly, the n-HAp paste was pumped at 240 rpm (approximately 32 ml/min) and dispersed into the chitosan solution with a high speed dispersing and homogenizing device Miccra D-9 at its minimum speed rate (11 000 rpm), using a set up designed to achieve mixing times lower than 100 ms. The n-HAp/CS dispersions were prepared with a n-HAp concentration of 20 g/l and a final pH value of approximately 5.5 (room temperature). Typical bone composition, n-HAp/CS weight ratio of 70/30, was considered for the produced dispersions.

5.2.3 Scaffolds preparation

A schematic representation of the process used to produce the scaffolds, from dispersion preparation to purification steps, is shown in Figure 5.1. The hybrid n-HAp/CS scaffolds were obtained by freeze-drying. Samples of 10 ml of the n-HAp/CS dispersions were firstly frozen in 55 mm diameter polystyrene petri dishes by storing in a freezer at -20 ºC overnight. Then, scaffolds were obtained by freeze-drying during 24 h using a VirTis BenchTop 6K

Freeze Dryer (model nº6KBTEL). The samples obtained in this step are referred as *n-HApCS-5.5-untreated*.

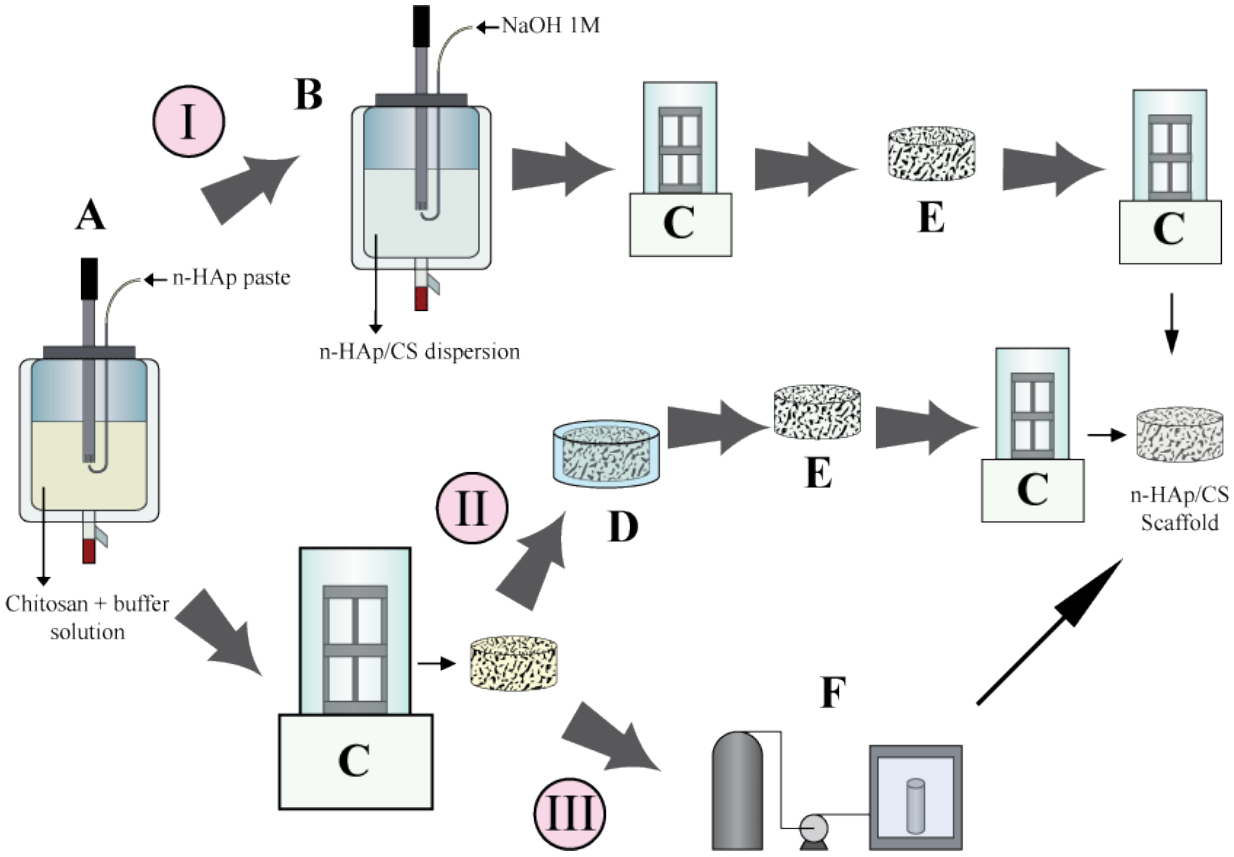

Figure 5.1. Schematic representation of the three studied procedures (I, II and III) for the production of n-HAp/CS scaffolds, that comprise the following steps: (A) Dispersion preparation; (B) Neutralization of acetic acid by dropwise addition of NaOH 1M; (C) Freeze drying; (D) Neutralization by immersion in NaOH/ethanol solution; (E) Washing with ultrapure water; (E) Acetic acid extraction with $scCO_2$.

5.2.4 Scaffolds purification

Two different purification methodologies based on acetic acid neutralization were first attempted: one consisted in neutralizing the dispersion before the formation of the 3D porous structure by freeze-drying (Figure 5.1, 5-step procedure I); and the other one consisted in immersing the formed 3D structure in an alkaline solution (Figure 5.1, 5-step procedure II). A third and innovative approach comprising the extraction of the acetic acid through $scCO_2$, was also tested (Figure 5.1, 3-step procedure III).

5.2.4.1 Procedure I

Procedure I comprises sequentially the following stages: dispersion preparation, neutralization of acetic acid, freeze drying, washing and freeze-drying again. In the neutralizing step the n-HApCS-5.5 dispersion, was neutralized by dropwise addition of NaOH (1 M) until a pH of 7.0 was reached (room temperature). After freeze-drying, the scaffolds were washed thrice with ultrapure water and freeze-dried again. Scaffolds subjected to this neutralization procedure are referred to as *n-HApCS-7.0*.

5.2.4.2 Procedure II

Procedure II comprises, sequentially, the following stages: dispersion preparation, freeze-drying, neutralization of acetic acid, washing and freeze-drying again. In this second approach (samples referred as *n-HApCS-NaOHEtOH*), neutralization was performed directly on the scaffolds obtained by freeze-drying, by immersion in a solution containing NaOH and ethanol according to the procedure described by He et al. (2011) [18]. The scaffolds were also washed thrice with ultrapure water and freeze-dried again.

5.2.4.3 Procedure III

Procedure III comprises sequentially the following stages: dispersion preparation, freeze-drying, and supercritical CO_2 extraction. The extraction of the residual acetic acid was carried out using a supercritical fluid extraction unit previously described by Gomes et al. (2007) [31]. Concisely, samples were placed equally distributed inside the 1 L extraction cell. Afterwards, CO_2 from a standard cylinder was cooled down, pumped into the cell and compressed until reaching the desired pressure. Temperature was then increased to reach the supercritical state. Experiments were carried out in static mode for 5 samples per experiment. In order to find the best conditions to remove acetic acid from the produced n-HAp/CS scaffolds, different experimental conditions were tested, as summarized in Table 5.1. The objective was to guarantee that the scaffold presents viability to support cell attachment and proliferation.

Table 5.1. Experimental conditions tested for the $scCO_2$ extraction process

Sample	Extraction time (h)		Temperature (°C)	
	Cycle 1	**Cycle 2**	**Cycle 1**	**Cycle 2**
(A) n-HApCS-$scCO_2$-40	2	-	40	-
(B) n-HApCS-$scCO_2$-75	2	-	75	-
(C) n-HApCS-$scCO_2$-75/75	2	2	75	75

All experiments were carried out at a pressure of 8.0 MPa and an extraction time of 2 h per cycle. Each experiment varied according to the number of cycles (1 and 2 cycles) and temperature (40 and 75°C). For the first experiment (A), mild conditions right above the critical pressure and temperature were chosen (T = 40°C, P = 8.0 MPa). For experiments B and C, sterilization conditions were chosen, with a temperature of 75°C, selected based on Spilimbergo et al. (2003) [32] who reported total inactivation of *Bacillus subtilis* spores using $scCO_2$ treatment at 75°C for 2 hours. Table 5.2 shows the ratio, mass of CO_2 per mass of scaffold, used in each experiment, estimated based on the CO_2 density under the used conditions, the volume of the extraction cell and the mean scaffold mass (0.3105 ± 0.0011) g. Supercritical CO_2 density data based on NIST Reference Fluid Thermodynamic and Transport Properties Database [33] is presented in Appendix C.

Table 5.2. Estimated mass of CO_2 per mass of scaffold for each experiment

Sample	Mass of CO_2 / mass of scaffold (g/g)
(A) n-HApCS-$scCO_2$-40	179.0
(B) n-HApCS-$scCO_2$-75	107.3
(C) n-HApCS-$scCO_2$-75/75	214.6 (107.3+107.3)

Subsequently to each cycle, a first depressurization step at 4 MPa, and a second one at 0.2 MPa were carried out. After each experiment, samples were taken out of the extraction chamber under a sterile environment, and store in sterile bags until characterization.

5.2.5 Characterization of the dispersions

The produced n-HAp/CS dispersions were characterized by using a Zetasizer Nano ZS from Malvern instruments (particle size and zeta potential). The final pH was measured using a microprocessor pH-mV-meter, brand pH-538 from WTW GmbH.

5.2.6 Characterization of scaffolds

5.2.6.1 Thermal degradation and extraction yield

All samples were subjected to thermogravimetric analysis using a TG 209 F3 Tarsus® under nitrogen atmosphere, and with a temperature ramp increasing from 30 to 700 °C at a rate of 10°C/min. The peak attributed to the degradation of acetic acid was analysed and the content of residual acetic acid (wt.%) in each sample was estimated relative to the scaffold weight. The extraction yield obtained for each sample was calculated relative to the content of acetic acid of an untreated sample, i.e. a sample not subjected to any purification/neutralization procedure, designated as *n-HApCS-untreated*.

5.2.6.2 Morphological characterization and elemental analysis

The produced scaffolds were analysed by scanning electron microscopy (SEM) coupled with Energy-dispersive X-ray spectroscopy (EDS) using a Phenom Pro microscope from Phenom World. Based on the acquired SEM images, mean pore size and pore size distributions were obtained by image analysis using the public domain software ImageJ developed by Wayne Rasband at the National Institute of Health (NIH). A minimum of 200 pores was analysed for each sample. Elemental analysis was used to inspect the Ca/P ratio, as well as the presence of impurities (e.g. salts derived from applied neutralization procedures).

5.2.6.3 Swelling tests

Samples were weighted dried (W_d) and swollen (W_s) after immersion in PBS solution (pH 7.4 at room temperature). These weights were used to calculate the swelling capacity (C_w) as a mass-swelling ratio [34, 35]:

$$C_w\left(g \cdot g^{-1}\right) = \frac{W_s - W_d}{W_d} \tag{5.1}$$

The samples had dimensions of 2 cm diameter and 4 mm thickness. Measurements were carried out at immersion times ranging from 0 to 60 min. Special care was taken to gently remove the excess of PBS using filter paper before measuring the weight of the swollen sample. Results are reported as mean ± SD based on 3 replicas.

5.2.6.4 Porosity determination

Total porosity, ϕ, of the n-HAp/CS scaffolds was estimated as:

$$\phi = 1 - \frac{\rho_{apparent}}{\rho_{real}} \tag{5.2}$$

where $\rho_{apparent}$ and ρ_{real} are the apparent and real densities respectively. The apparent density was determined experimentally for 3 specimens of each sample by measuring, in triplicate, their height and diameter using a *vernier caliper*, and their weight using an analytical balance. The real density was determined experimentally by carrying out measurements per triplicate using a gas pycnometer (in-house made equipment).

5.2.6.5 Mechanical properties

The mechanical behaviour of the produced scaffolds was characterized by dynamic mechanical analysis (DMA) in wet state under dynamic compression solicitation following the procedure used in the work of Rodrigues et al. (2013) [34]. The samples were cylinders with 9 mm diameter and 4 mm thickness immersed in PBS solution (pH 7.4 at room temperature) for 60 minutes before measurements. Afterwards, the samples were carried out in compression mode following cycles of increasing frequency from 0.1 to 10 Hz. The measurements were carried out in triplicate at 20 ºC using a DMA 242 E Artemis, dynamic mechanical analyser by NETZSCH-Gerätebau GmbH.

5.2.6.6 Microbiological assay

A microbiological assay was carried out in order to test sterility of the n-HAp/CS-scCO_2-75/75 scaffolds after the scCO_2 extraction. Samples of approximately 5x5x5 mm were cut in sterile conditions, avoiding cross contamination, and placed in individual sterile eppendorfs. Afterwards, 1 ml of brain heart infusion (BHI) broth was added to each eppendorf, which

was then sealed and incubated at 37 °C. Samples from 3 different batches were tested in triplicate. Additionally, two extra eppendorfs were prepared in the same conditions, without n-HAp/CS-scCO_2-75/75 samples, and used as negative controls.

The presence or absence of turbidity was verified after 24, 48 and 120 hours of incubation. At the end of the 120 hours, each eppendorf was vortexed for a few seconds, and 20 µl of the BHI suspension, per duplicate, were plated into a non-selective trypticase soy agar (TSA) culture medium. Bacterial growth was assessed after 24 hours of incubation at 37 °C, by colony forming units (CFU) counting in the TSA plates.

5.2.6.7 In-vitro cell culture

To infer the viability of the produced scaffolds for *in-vitro* cell culture, a preliminary test was preformed to check if the pH of the culture medium in contact with the scaffold suffers deviations from the optimal range (7.2-7.4). The test comprises the contact of the scaffold with culture medium. For that, samples of 5x5x5 mm (approximately 5.29×10^{-3} g), were placed in 48-well plates in sterile conditions, and 0.5 ml of culture medium were added. If pH changes from the optimal range, a change in colour due to the presence of phenol red will be noticed. In the case of acidification, a change from red colour (neutral pH) to yellow (acid pH) is observed; in the case of alkalinisation, a change from red to pink colour (alkaline pH) is observed. Only samples passing this test were subjected to the cell culture assays.

Osteoblast-like cells (MG63 cell line, ATCC number CRL-1427™) were seeded in Eagle minimum essential medium (MEM), alpha modification (α-MEM) supplemented with 10% fetal bovine serum, 100 IU/ml penicillin, 2.5 µg/ml streptomycin, and 2.5 µg/ml amphotericin B, and incubated in a humidified atmosphere of 5% CO_2 at 37 °C. The culture medium was replaced 2 to 3 times a week. At 70 – 80% confluence, cells were removed from the culture plates by enzymatic digestion, using 1 ml of 0.05% trypsin in 0.25% EDTA for 10 min in standard culture conditions, and the cell suspension was used in the experiments. The cell culture was sub-cultured at least for 2 passages before the experiments.

Without subjecting samples to further traditional disinfection or sterilization methods, samples of approximately 5x5x5 mm were cut with a scalpel blade in sterile conditions and incubated 15 minutes at 37 °C in fresh supplemented α-MEM for swelling. The wet samples were placed in 48-well plates and seeded with MG63 cells (1.25 x 10^5 cells/cm^2) in standard

conditions. Seeded scaffolds were cultured for up to 21 days, and characterized for cell viability/proliferation by the Alamar blue assay and SEM observation. Cultures performed in the absence of material samples were used as control in order to assess the suitability of this cell culture model. In addition, a parallel experiment was run as a blank with culture medium alone, using the same protocol as the cell cultures.

5.2.6.8 Alamar blue assay

Seeded scaffolds were monitored for cell viability/proliferation at time-points 1, 3, 7, 10, 14, 17 and 21 days by the non-toxic Alamar blue dye assay. In this assay, the redox activity by intracellular enzymes within the cytosol of the viable cells was assessed through the reduction of Alamar blue dye, also known as resazurin, into a fluorescent, red compound called resorufin [34]. At the first time-point, 1 day, the culture medium (supplemented α-MEM without resazurin) was removed from the wells, the seeded samples were transferred to a different well, and fresh supplemented α-MEM with 10 vol.% of resazurin solution was added. The seeded samples were incubated for 4 hours in standard conditions; then 100 µl of the medium (α-MEM with resazurin) were collected from each well, transferred to a black opaque 96-well plate, and resorufin content was determined by measuring fluorescence intensity. The fluorescence was read at a 530 nm and 590 nm wavelengths, for excitation and emission respectively, with a microplate reader brand Synergy HT, from BioTek Instruments, Winoosky, VT, USA.

The remaining medium was removed from the 48-well plates, the samples were washed with sterile PBS to remove any residual rezasurin and fresh supplemented α-MEM was added to the wells. Finally, the plates were incubated in standard conditions until the next time point. The assay was carried out based on 6 replicates.

5.2.6.9 Sample preparation for SEM observation

Samples were fixed by immersion in 1.5% glutaraldehyde in 0.14 M sodium cacodylate buffer for 10 minutes (pH = 7.3) and preserved in sodium cacodylate buffer at 4 °C. Before SEM observation, samples were washed in deionized water for 30 minutes and dehydrated in graded ethanol (50, 60, 70, 80, 90, 100%) for 30 minutes in each solution. Finally, samples were dried using a CO_2 critical point dryer, brand CPD 7501 from Polaron Range, and analyzed using a Phenom ProX scanning electron microscopy (SEM) from Phenom World.

5.3 Results and discussion

5.3.1 Dispersions stability and macroscopic analysis of the produced scaffolds

The produced n-HAp/CS dispersions were highly homogeneous and stable, with a number mean size of 230 ± 89 nm, a zeta potential > +30 mV, measured at the dispersion's final pH of 5.5 at room temperature. Therefore, even when the presence of chitosan in HAp dispersions caused an increase in particle size by particle aggregation, it had a positive impact on the stability of the dispersions, which is a desirable characteristic.

5.3.2 Thermal degradation and extraction yield

Figure 5.2 shows the TG plots obtained for the n-HAp/CS-untreated sample, and the samples exposed to $scCO_2$ extraction under the different tested conditions. Figure 5.3 presents the TG plots obtained for the n-HAp/CS-untreated sample, and the samples subjected to different purification/neutralization treatments, including the one subjected to CO_2 extraction under the best-achieved conditions (n-HApCS-scCO2-75/75). In all cases, the first mass loss observed between 30 °C and 100 °C is assigned to water evaporation. From 100 °C to approximately 190 °C, a second peak is observed and attributed to the evaporation of acetic acid. The mass loss starting from 200 °C corresponds to the degradation of chitosan. Finally, the residual mass, between 65 to 70 wt.%, is attributed to the mass of n-HAp, which is in accordance with bone composition [36] and used in the present work.

By quantifying the mass loss identified as the evaporation of acetic acid, it was possible to calculate the extraction yield by $scCO_2$. From the TG analysis it was determined that the n-HApCS-untreated sample contained about 4.1% of acetic acid (designated in this work as residual acetic acid), which corresponds to a significant reduction; based on the acetic acid present in the used base dispersion a content of 11% is expected to remain in the final scaffold. Therefore, about 63% of the acid was eliminated during the freeze-drying step.

After purification with $scCO_2$ extraction at 40 °C (n-HApCS-$scCO_2$-40 sample), with a CO_2/scaffold mass ratio of approximately 179.0 $g_{CO2}/g_{scaffold}$, about 44% of the residual acid was successfully eliminated (the acetic acid content reached 2.4%). By using a higher temperature of 75 °C (n-HApCS-$scCO_2$-75 sample), CO_2/scaffold mass-ratio of 107.3 $g_{CO2}/g_{scaffold}$, no considerable differences were observed in the obtained extraction yield

(46%). By carrying out two cycles, a noticeably increase in the extraction yield was obtained. With a total 214.6 $g_{CO2}/g_{scaffold}$ ratio (107.3+107.3) almost complete elimination of residual acetic acid was obtained in the n-HApCS-scCO$_2$-75/75 sample (80% in total corresponding to an acid content of 0.8%).

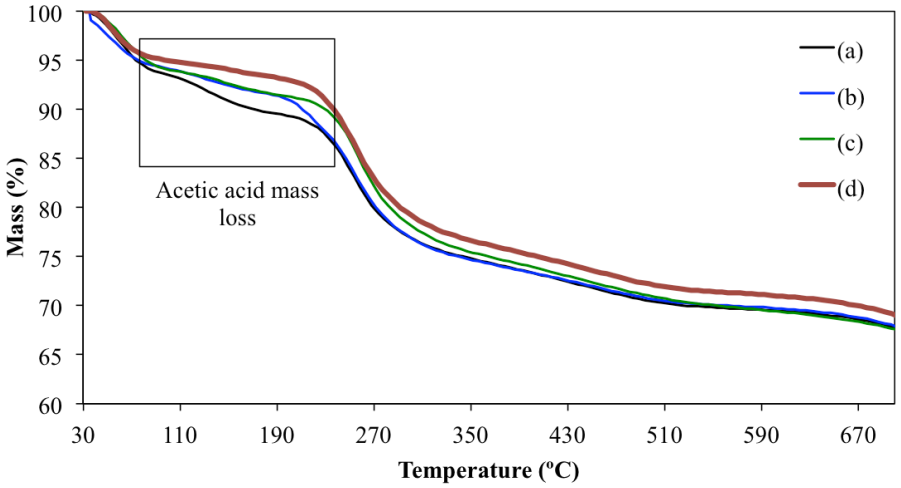

Sample	Acetic acid content (wt.%)	Extraction yield (%)
(a) n-HApCS-untreated	4.1	-
(b) n-HApCS-scCO$_2$-40	2.4	44%
(c) n-HApCS-scCO$_2$-75	2.2	46%
(d) n-HApCS-scCO$_2$-75/75	0.8	80%

Figure 5.2. Thermograms of: (a) n-HApCS-5.5-untreated; (b) n-HApCS-scCO$_2$-40; (c) n-HApCS-scCO$_2$-75; and (d) n-HApCS-scCO$_2$-75/75 (From 30 to 700°C at 10°C/min; N_2 atmosphere)

Based on the preliminary test used to evaluate the viability of cell growth and proliferation, only this last sample did not influence the pH of the culture medium, which was maintained within the required range for cell growth. For all the other samples treated with scCO$_2$, a change of culture medium to yellow (acidic) was observed. Therefore, these tested conditions, 2 cycles of 2 hours each in static mode at a temperature of 75°C and a pressure of 8.0 MPa, were considered suitable. Samples prepared using these conditions were further characterized and examined in what concerns microbial growth and cytotoxicity.

Relative to the different purification/neutralization procedures, the yield of residual acetic acid extraction corresponds to 80%, 70% and 80% for n-HApCS-5.5-NaOHEtOH, n-HApCS-7.0 and n-HApCS-scCO$_2$-75/75 samples respectively. Based on these results the neutralization

with an alkaline solution, under the used conditions of sample n-HApCS-5.5-NaOHEtOH (conventional purification/neutralization procedures), leads to a final acetic acid content in the sample of 0.8%, the same level as the one achieved with sample n-HApCS-scCO$_2$-75/75. Thus, using the best-achieved conditions of scCO$_2$ extraction, it is possible to extract as much residual acetic acid as with the most conventional purification/neutralization procedures. Nevertheless, the sample n-HApCS-5.5-NaOHEtOH did not pass the preliminary test of viability for *in-vitro* cell culture, since culture medium exhibited deviations from ideal pH (culture medium turned pink indicating the presence of alkaline residual salts) when it entered in contact with the sample.

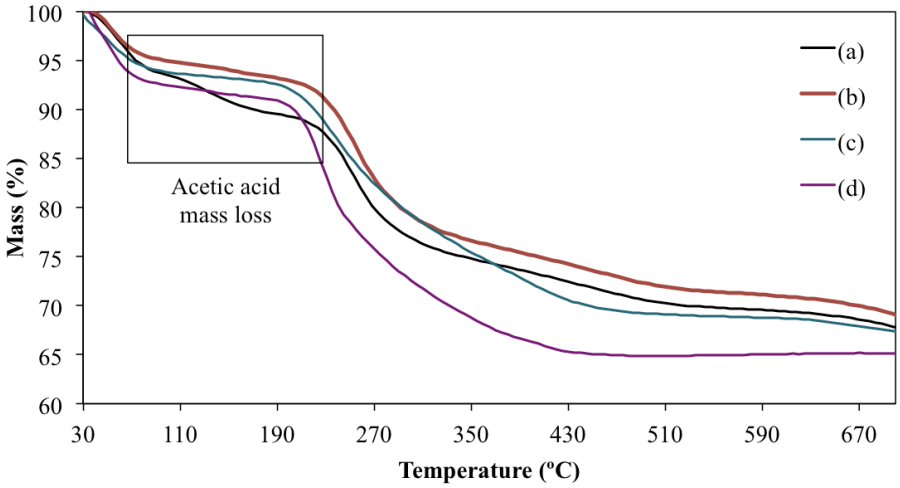

Sample	Acetic acid content (wt.%)	Extraction yield (%)
(a) n-HApCS-untreated	4.1	-
(b) n-HApCS-scCO$_2$-75/75	0.8	80%
(c) n-HApCS-NaOHEtOH	0.8	80%
(d) n-HApCS-7.0	1.2	70%

Figure 5.3. Thermograms of: (a) n-HApCS-5.5-untreated; (b) n-HApCS-scCO$_2$-75/75; (c) n-HApCS-5.5-NaOHEtOH and; (d) n-HApCS-7.0
(From 30 to 700°C at 10°C/min; N_2 atmosphere)

5.3.3 Morphological characterization and elemental analysis

Photographs of the produced scaffolds are shown in Figure 5.4, where differences deriving from the purification procedure used may be already observed at a macro scale. The n-HApCS-5.5-untreated sample (Figure 5.4a) generated homogeneous, porous and elastic 3D

structures, characteristics that were maintained after $scCO_2$ extraction (n-HApCS-5.5-$scCO_2$-75/75 sample, Figure 5.4b). The n-HApCS-NaOHEtOH sample also showed a porous and elastic-like structure; nevertheless some deterioration was noticed (Figure 5.4c). Finally, the main difference observed at a macro-scale level was for the n-HApCS-7.0 sample (Figure 5.4d), even though its integrity in terms of shape was preserved, the sample became highly brittle.

SEM micrographs (Figure 5.5) and pore size distribution plots, deriving from image analysis (Figure 5.6), were obtained for the produced scaffolds samples. Microstructure is a key factor to be evaluated when producing scaffolds for bone regeneration. A combination of adequate pore sizes and interconnectivity allows the motion of cells throughout the scaffolds and the required nutrients and metabolites diffusion for cells survival and proliferation [3]. Several studies have been conducted regarding the relationship between pore size and cell activity, showing that pores larger than 100 μm allow angiogenesis and contribute to nutrient and waste transport, whereas pores smaller than 50 μm can improve osteointegration and generate cell anchoring sites [1, 37-41].

The n-HApCS-untreated sample (Figure 5.5a) exhibits the desired interconnected porous structure, with a mean pore size of (86 ± 40) μm (Figure 5.6a). The pore interconnectivity is also observed in the n-HApCS-$scCO_2$-75/75 sample (Figure 5.5b), with (72 ± 35) μm mean pore size (Figure 5.6b), showing that the obtained desired morphology is not affected by the $scCO_2$ extraction at the best-achieved conditions. In what concerns the HApCS-5.5-NaOHEtOH sample, with a mean pore size (63 ± 27) μm, modifications in structure's architecture were observed after the second freeze drying step, as seen in the SEM image (Figure 5.5c), affecting not only the morphology but also pore size distribution (Figure 5.6c). All these three samples, n-HApCS-untreated, n-HApCS-$scCO_2$-75/75, and HApCS-5.5-NaOHEtOH, present adequate pore sizes; pores sizes larger than 100 μm and smaller than 50 μm are present, however in different proportions. The n-HApCS-NaOHEtOH sample presented the least amount of pores >100 μm (14%), and the n-HApCS-untreated sample the larger amount (42%), whereas the n-HApCS-$scCO_2$-75/75 sample presented pores >100 μm and pores pores <50 μm in a similar proportion of about 30%.

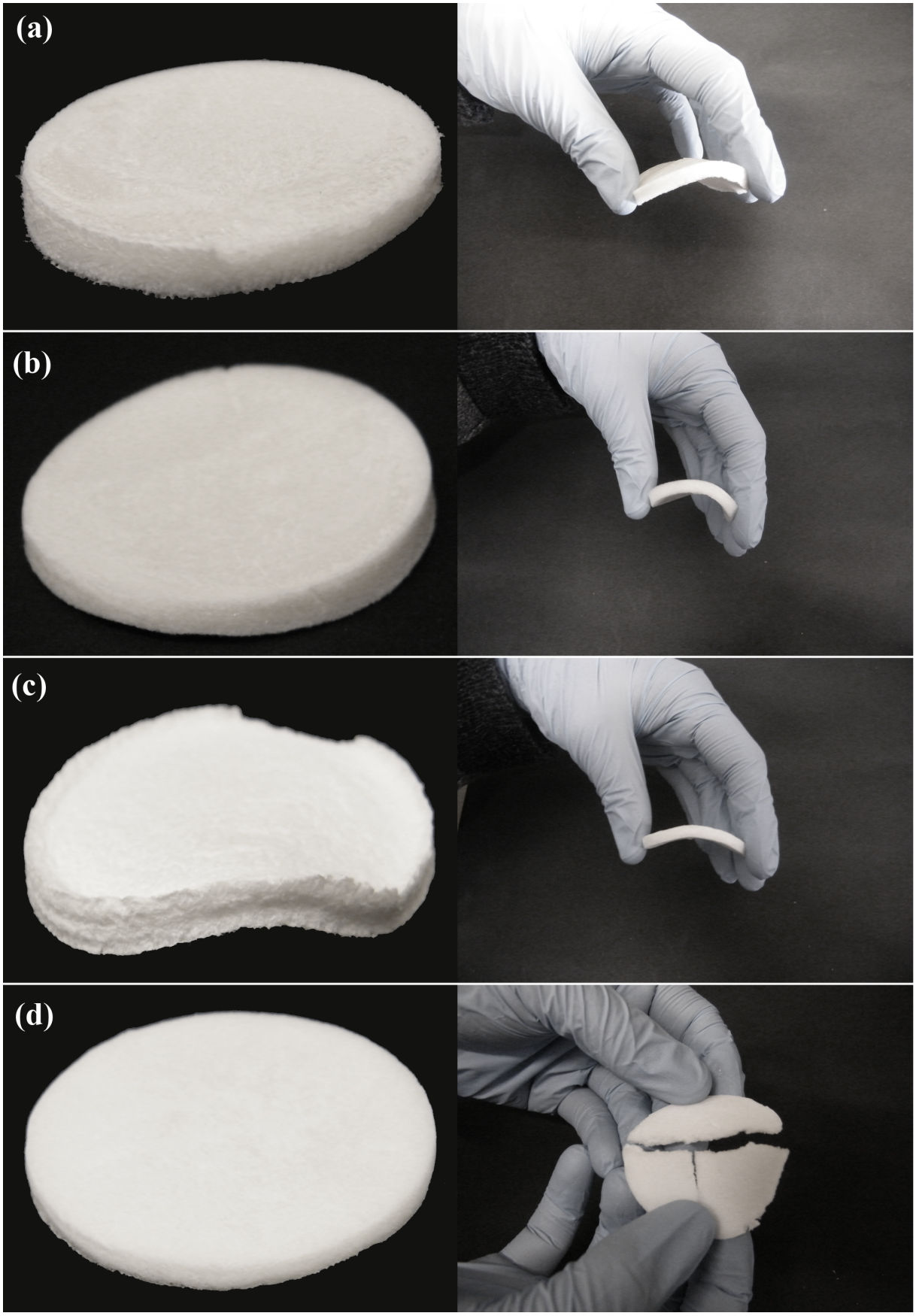

Figure 5.4. Images of the produced scaffolds: (a) n-HApCS-5.5-untreated; (b) n-HApCS-5.5-scCO$_2$; (c) n-HApCS-5.5-NaOH/EtOH; (d) n-HApCS-7.0.

Finally, for the n-HApCS-7.0 sample (Figure 5.5d) a brittle structure was obtained right after its preparation, even before the washing and second freeze-drying steps, showing that the pH at which the hybrid dispersion was prepared affected the structure of the final scaffold. Due to the evident high brittleness and structural disruption of n-HApCS-7.0 sample, it is not further considered for analysis. The observed distortion of the samples neutralized with a basic solution has been attributed by other authors to base-induced changes in crystallinity and associated structural stresses [19, 20, 42].

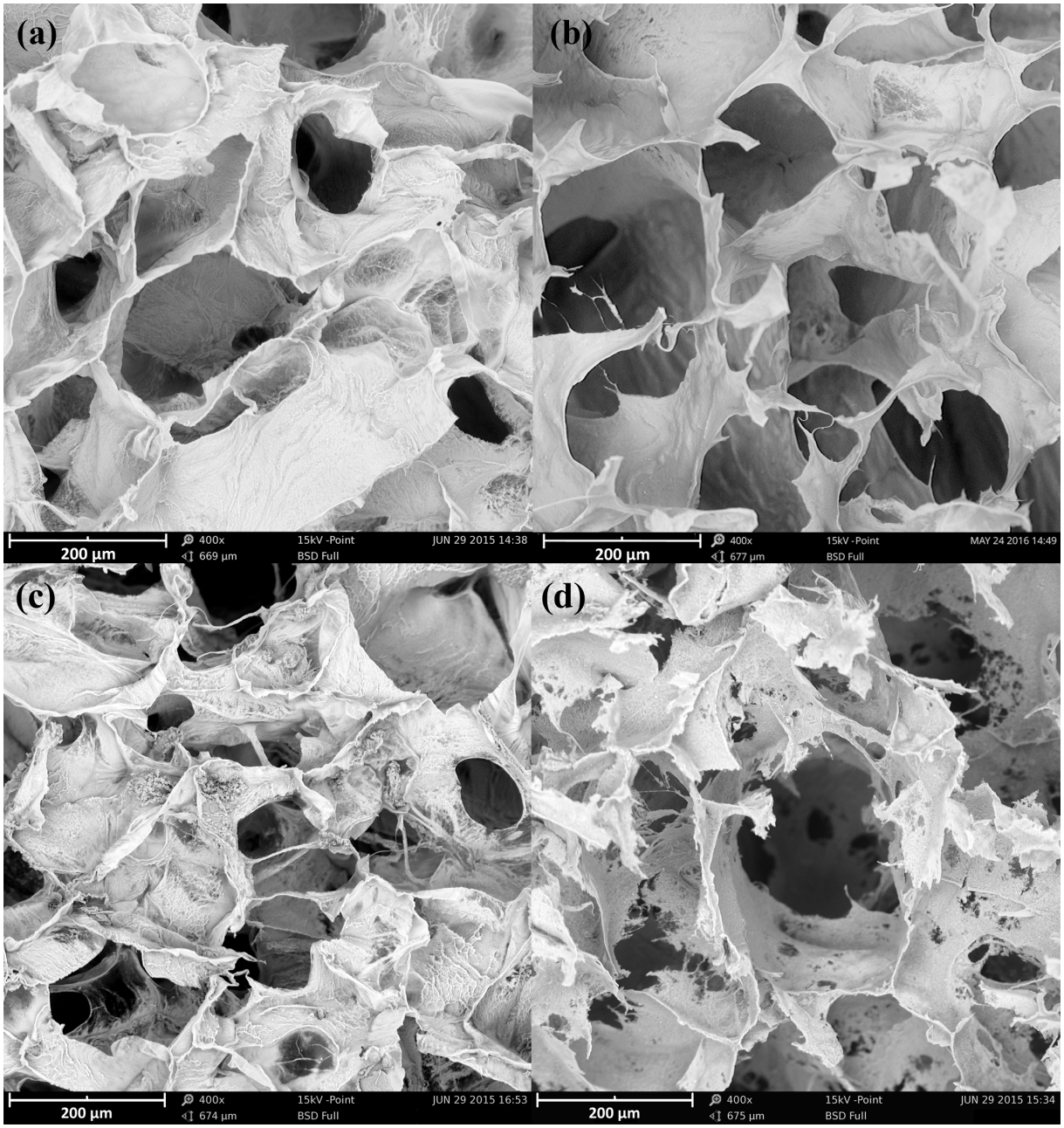

Figure 5.5. SEM micrographs (400X) of a cross-section of: (a) n-HApCS-5.5-untreated; (b) n-HApCS-5.5-scCO$_2$-75/75; (c) n-HApCS-5.5-NaOHEtOH; (d) n-HApCS-7.0.

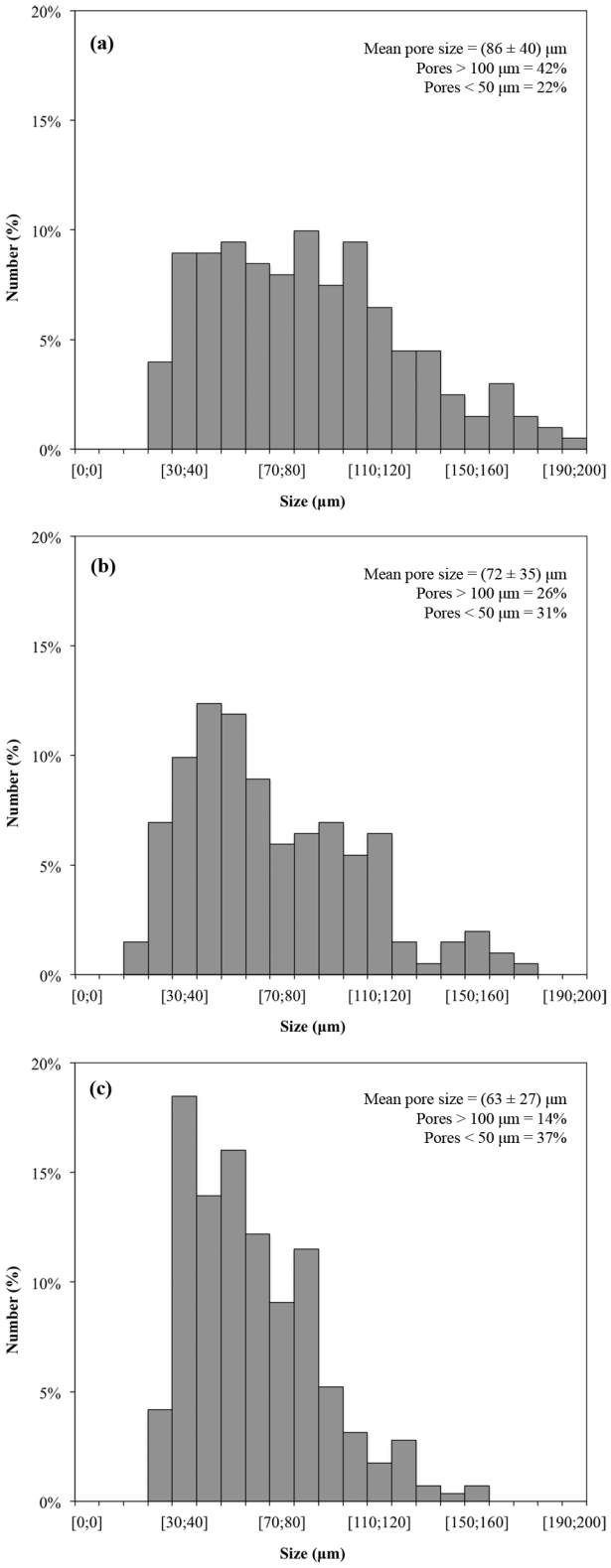

Figure 5.6. Particle size distributions of: (a) n-HApCS-untreated; (b) n-HApCS-scCO$_2$-75/75; (c) n-HApCS-NaOHEtOH.

In addition to the morphological study, elemental analysis of the samples was performed. Results presented in Figure 5.7 show that despite the repeated washing steps, impurities were detected in the n-HApCS-NaOHEtOH sample. Such impurities were identified as sodium salts, whose origin can be the alkaline solution used during the neutralization step (Figure 5.7c, cross symbol 1). Salt impurities were not observed in the SEM image of n-HApCS-untreated (Figure 5.7a) and n-HApCS-scCO$_2$-75/75 (Figure 5.7b) samples and the respective EDS analysis showed predominantly the presence of Ca and P from HAp.

Elemental analysis was also used to quantify the atomic concentrations of Ca and P present in the produced samples (Table 5.3) in order to estimate the Ca/P ratios, reported as the mean values of measurements carried out in two different spots (represented as a cross symbol and a square in Figure 5.7) of the same sample. Ca/P ratios of 1.70 and 1.68 were obtained for n-HApCS-untreated and n-HApCS-scCO$_2$-75/75 scaffolds respectively, very close to the Ca/P ratio of 1.67 of stoichiometric HAp. However, non-stoichiometric Ca/P ratio was obtained for n-HApCS-5.5-NaOHEtOH, with 2.0±0.18, showing that this neutralization procedure using alkaline solution can compromise the purity of the n-HAp used, due to the potential chemical interactions involved.

Table 5.3. Atomic concentrations of Ca and P obtained by EDS

Sample	**Ca (%)**	**P (%)**	**Ca/P atomic ratio**
Stoichiometric HAp	10	6	1.67
(a) n-HApCS-5.5-untreated	14.4	8.45	1.70 ± 0.06
(b) n-HApCS-5.5-scCO$_2$-75/75	17.7	10.6	1.68 ± 0.08
(c) n-HApCS-5.5-NaOHEtOH	10.6	5.20	2.00 ± 0.18

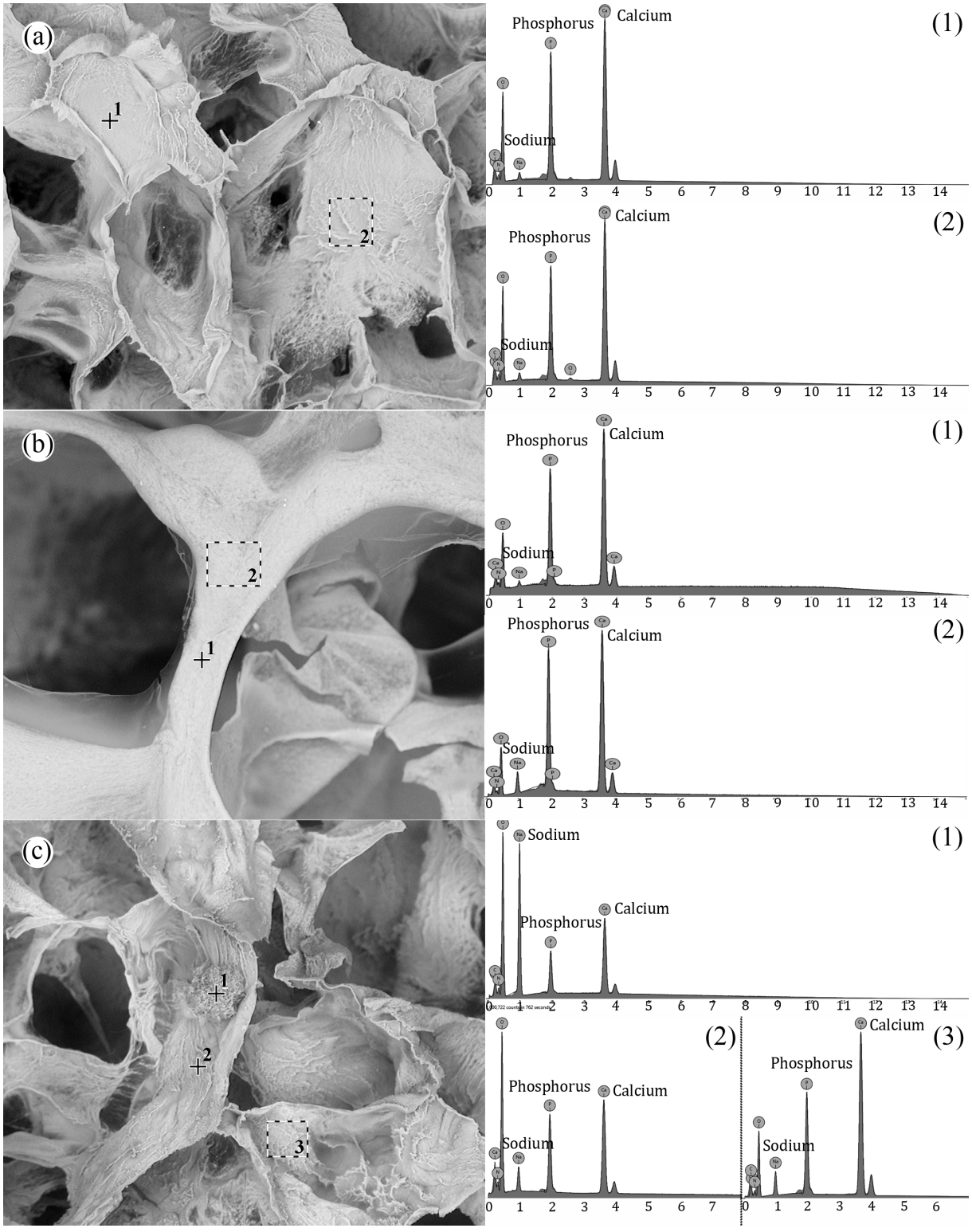

Figure 5.7. SEM micrographs and EDS analysis spectra of:
(a) n-HApCS-untreated; (b) n-HApCS-scCO$_2$-75/75; (c) n-HApCS-NaOHEtOH.
The cross symbol and the square in the images represent the areas analysed by EDS.

5.3.4 Swelling tests

When implanted *in vivo*, scaffolds are introduced in an aqueous environment, influencing their overall properties; therefore, it is essencial to evaluate their swelling behaviour in aqueous medium in order to determine their suitability for bone regeneration. Swelling performance of a scaffold allows the evaluation of both, its water-binding ability and its pore interconnectivity. First, the structural integrity of the scaffolds during swelling was assessed by immersing the samples in PBS during 60 min. Fast swelling was observed for all samples, since sample enlargement was observed right after immersion in PBS, which is typical of highly hydrophilic materials and/or microstructures with a large range of pore interconnectivity that allow a fast circulation of nutrients throughout the scaffold [34].

After 60-min immersion, as it may be observed in Figure 5.8, the n-HApCS-untreated sample exhibited the major enlargement, which can be attributed to the amount of protonated amino groups. According to Berger et al. (2004) [43], for chitosan-containing scaffolds swelling is highly influenced by ionic interactions, moreover, it is favoured by the protonation and repulsion of chitosan free ammonium groups. The content of residual acetic acid present in the n-HApCS-untreated sample induces the protonation of free amino groups favouring swelling; however, at the same time it promotes dissolution, causing a significant structural disruption as observed in Figure 5.8a.

In the case of n-HApCS-scCO$_2$-75/75 and n-HApCS-NaOHEtOH samples, they both presented similar swelling behaviour. However, while n-HApCS-scCO$_2$-75/75 preserved its structural integrity (Figure 5.8b), the n-HApCS-NaOHEtOH sample suffered from a slight disruption after 60-min immersion (Figure 5.8c). These differences can be attributed mainly to structural changes produced by the purification/neutralization procedure used; the second freeze-drying step used to obtain n-HApCS-NaOHEtOH sample causes structural damage, making the scaffold easily vulnerable to disruption. For the n-HApCS-scCO$_2$-75/75 case, it presented a controlled swelling (Figure 5.9), with no substantial changes observed in swelling capacity after 10 min immersion so that, at this time point, it is considered that swelling equilibrium is reached ($C_w = 24.5 \pm 2.7\ g \cdot g^{-1}$ at 60-min immersion). Due to the experimental difficulties from the mass loss caused by structural disruption of samples n-HApCS-5.5-untreated and n-HApCS-NaOHEtOH, the swelling capacity at different immersion times was determined only for n-HApCS-scCO$_2$-75/75 sample.

Based on these results, $scCO_2$ extraction appears as a favourable process that promotes the extraction of the acid without interfering on the equilibrium protonated/free amino groups, thus promoting swelling without inducing dissolution, and without compromising its structural integrity. Thereby, $scCO_2$ extraction allows the production of scaffolds with desirable swelling behaviour.

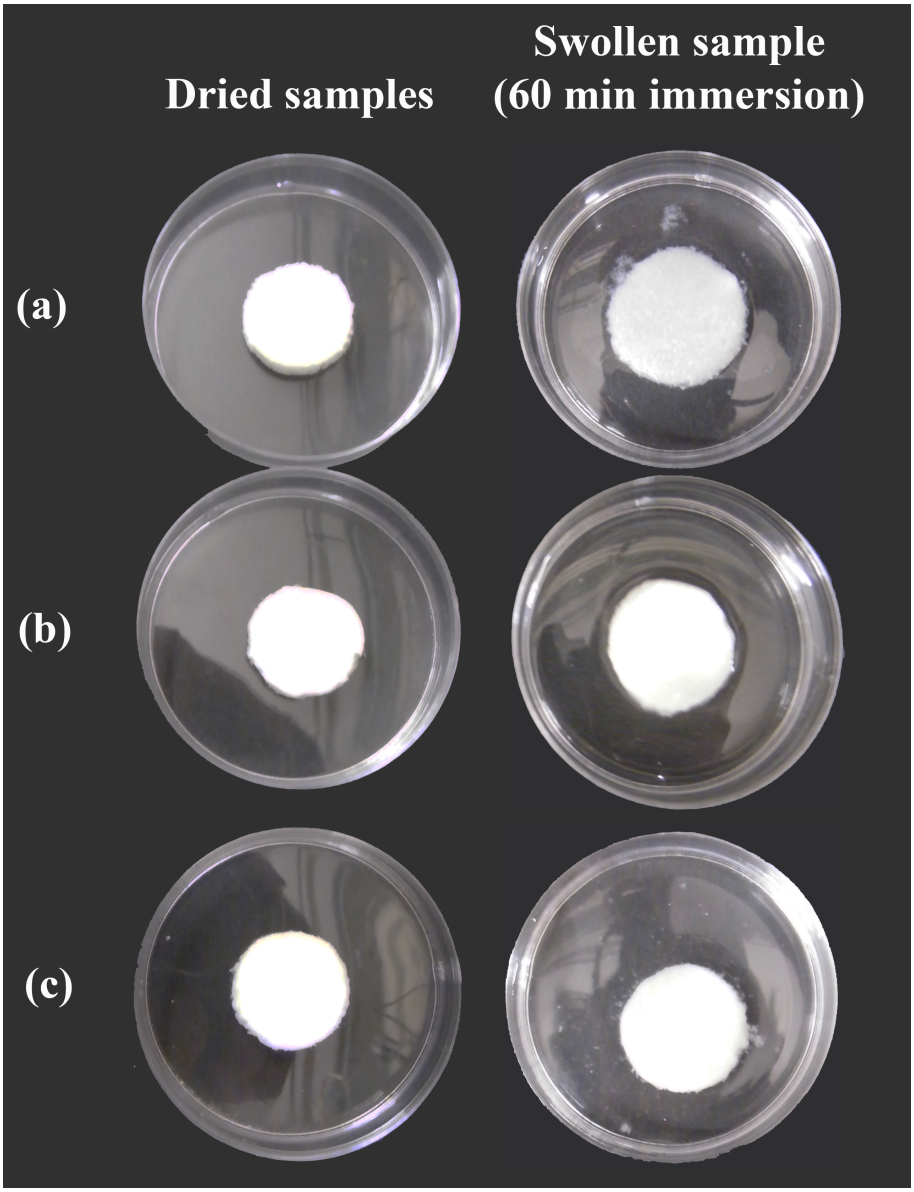

Figure 5.8. Dried and swollen samples, after 60 min of immersion in PBS, of: (a) n-HApCS-untreated; (b) n-HApCS-$scCO_2$-75/75; (c) n-HApCS-NaOHEtOH

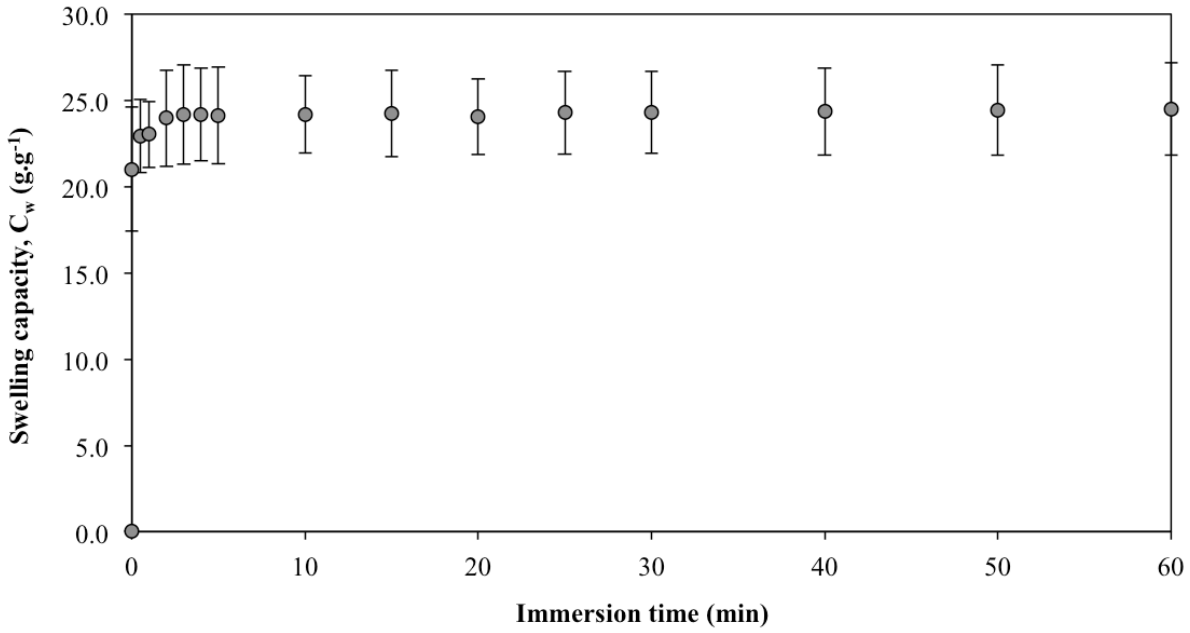

Figure 5.9. Swelling capacity at different immersion times of sample n-HApCS-scCO$_2$-75/75

5.3.5 Porosity determination

Structurally, natural bone is composed of a hard and very dense outer layer known as *cortical bone*, and a spongy inner layer known as *cancellous bone*. Depending on the surgical requirements, bone grafts can be either cortical, cancellous, or a combination of both, each one exhibiting different mechanical and structural properties [44]. Cancellous bone lacks of mechanical strength due to its high porosity (30-90% porosity) but it is characterized for inducing osteogenesis [1, 4, 8]. Thus, bone grafts mimicking cancellous bone are frequently used for small defects such as non-union fractures, maxillofacial and dental defects, and spinal fusion [44].

Following the implantation of a scaffold *in vivo*, the mechanism of bone regeneration comprises the attachment and penetration of cells from the surrounding hard tissue, as well as the process of angiogenesis; therefore, it is expected that higher porosities induce enhanced osteogenesis [45]. Accordingly, it has been reported that ideal overall porosity of a bone graft ranges from 60 to 99% [46]. All the produced scaffolds exhibit high desirable porosity, as shown in Table 5.4. No substantial difference is observed in the determined theoretical porosity between the n-HApCS-5.5-untreated and n-HApCS-scCO$_2$-75/75 samples, showing that the purification with scCO$_2$ extraction does not compromises the structural integrity of

the scaffold in what concerns its overall porosity. However, an increase of approximately 10% in porosity is obtained when the scaffold is subjected to the neutralization process by immersion in alkaline solution (n-HApCS-5.5-NaOHEtOH sample), probably caused by the microstructural changes that the scaffold undergoes mainly due to the second freeze-drying step.

Table 5.4. Total porosity and apparent density obtained for the produced scaffolds

Sample	Total Porosity (%)	Apparent density (g/cm^3)
n-HApCS-5.5-untreated	83%	0,0347 ± 0,0009
n-HApCS-scCO$_2$-75/75	81%	0,0423 ± 0,0028
n-HApCS-5.5-NaOHEtOH	93%	0,0720 ± 0,0010

5.3.6 Mechanical properties

In order to mimic *in vivo* conditions, the mechanical performance of the produced scaffolds was evaluated by DMA in wet state and within the physiological frequency range in load-bearing applications, ranging from 1 to 10 Hz [47, 48]. The variation of storage modulus (E') and the loss factor (tan δ) as a function of frequency are shown in Figure 5.10. The storage modulus represents the stiffness of a material and is proportional to the energy stored during a loading cycle [34, 49]. The loss factor, also known as specific loss or specific damping capacity, is a measure of the energy lost, expressed in terms of the recoverable energy and represents mechanical damping or internal friction in a system. The loss factor is expressed as a dimensionless number (tan δ = E''/E', where E'' is the loss modulus, a measurement proportional to the energy dissipated during one cycle) [49, 50].

The obtained values for the storage component at a reference frequency of 1 Hz, reported as (mean±SD), were (6.75±0.72) kPa, (13.3±1.5) kPa, and (20.5±2.9) kPa, for n-HApCS-untreated, n-HApCS-NaOHEtOH, and n-HApCS-scCO$_2$-75/75 samples respectively. A previous study of n-HAp/CS materials by Thein-Han and Misra (2009) [10] reported values in the same order of magnitude, ranging from 4 to 10 kPa, for chitosan and n-HAp/CS

scaffolds with 0.5-2.0 wt.% of n-HAp. Considering that the compression modulus of natural cancellous bone ranges from 50 to 500 MPa, scaffolds exhibiting compression modulus below 25 MPa are only suitable for non-load-bearing applications. The low compression modulus values are attributed to the high porosity of the scaffolds, generally >80%, which is essential for bone ingrowth as previously discussed [46].

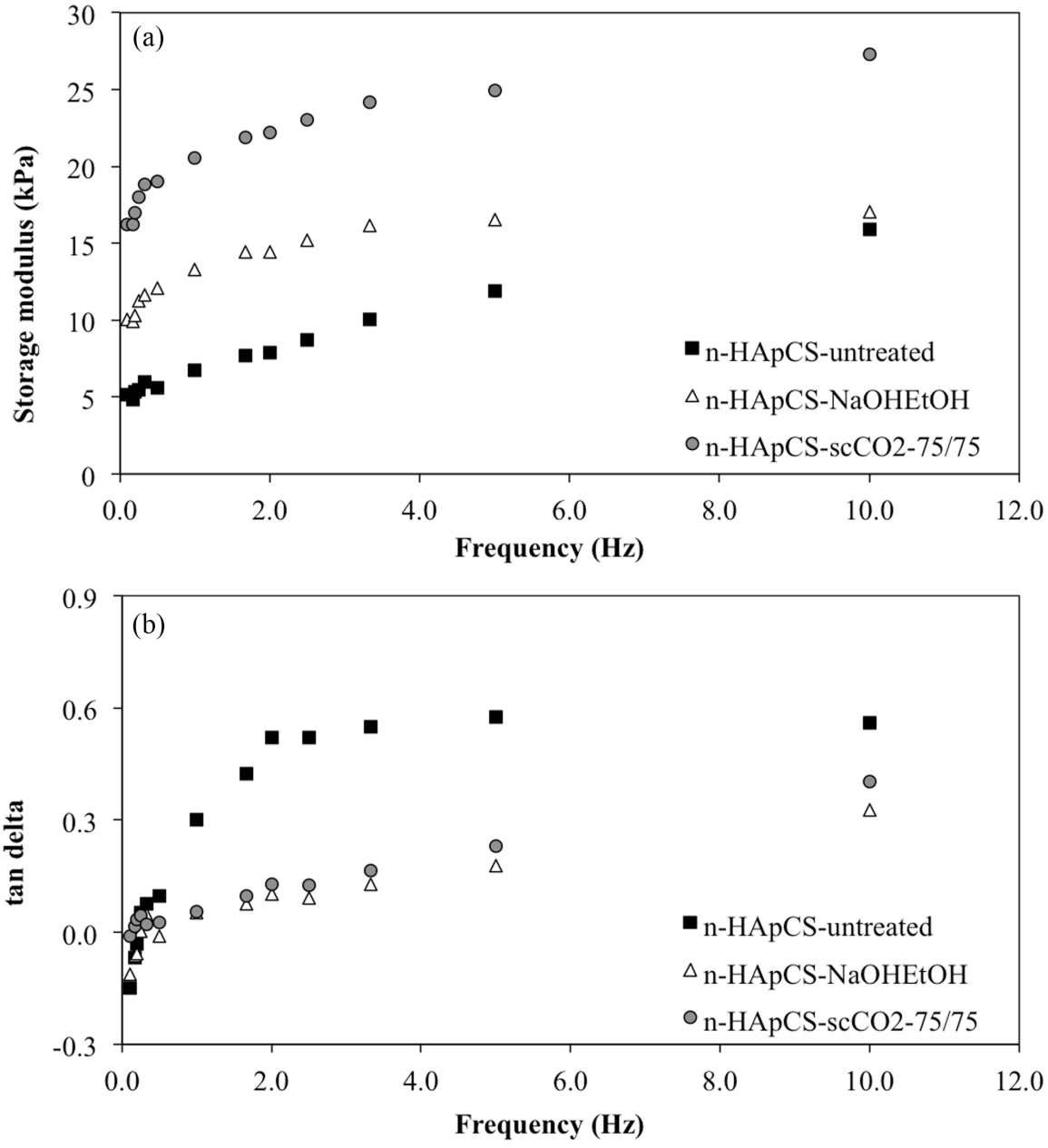

Figure 5.10. Storage modulus (a) and loss factor, tan delta, (b) under dynamic compression solicitation as a function of frequency, increasing from 0.1 to 10 Hz

Figure 5.10a shows data obtained for storage modulus, representative of measurements carried out in triplicate with less than 20% deviation. A tendency of storage modulus to increase with frequency was observed for all samples. The n-HApCS-untreated sample exhibits the lowest storage modulus values, which can be attributed to the disruption of this scaffold in aqueous medium, as observed during the swelling test, due to the presence of residual acetic acid. After subjecting the scaffolds to the tested purification/neutralization procedures, the scaffolds display an increase in storage modulus relative to the untreated scaffold, but with differences depending on the used procedure.

The n-HApCS-scCO$_2$-75/75 sample exhibits considerably higher compression strength than the n-HApCS-NaOHEtOH, dissimilarity that can also be attributed to the microstructural changes due to the purification/neutralization procedure. As previously discussed, the n-HApCS-NaOHEtOH sample suffers microstructural changes, increasing its overall porosity in about 10%, and consequently affecting its mechanical properties. It has been reported that, with a 10 to 20% increase in total porous volume, mechanical strength decreases up to a factor four [45]. On the other hand, when using scCO$_2$ extraction to purify the scaffolds, microstructural properties of the n-HApCS-scCO$_2$-75/75 sample are preserved, and the scaffold does not undergo disruption induced by dissolution, thus its mechanical properties are improved. These results are in accordance with the observations from the swelling tests.

Relative to the loss factor, presented in Figure 5.10b, an increase of tan δ with increasing frequency is observed for all cases, indicating that the samples tend to lose elasticity while their viscous properties become more relevant. The loss of elasticity is more evident for the n-HApCS-5.5-untreated scaffold, evidencing that the scaffold solubilizes due to the presence of residual acetic acid, and thus becomes more viscous. No substantial difference is observed in the loss factor values obtained for n-HApCS-NaOHEtOH and n-HApCS-scCO$_2$-75/75 samples, showing that the purification process does not affect the viscoelastic properties of the scaffolds. Moreover, the viscous contribution exhibited by the scaffolds depicts the damping properties of the specimens, which is pertinent for biomedical applications because it allows the scaffolds to partially dissipate inputted mechanical energy without suffering disruption [50].

5.3.7 *In-vitro* biological studies

After 24, 48 and 120 hours of incubation of the material samples in BHI suspension, the culture medium was clean and comparable to the negative controls. Furthermore, no UFCs were counted after culturing the medium in TSA medium, evidencing that the n-HApCS-$scCO_2$-75/75 scaffolds were sterile. Therefore, the cell viability test was carried out with the n-HApCS-$scCO_2$-75/75 scaffolds without any further disinfection or sterilization treatment after $scCO_2$ extraction. The sterility of the n-HApCS-$scCO_2$-75/75 samples was also verified through the observation of the attachment and proliferation of cells to the scaffolds.

When cells enter in contact with the surface of a biomaterial, they start a process of attachment, growth and proliferation that can be assessed by the morphological changes that cells experience throughout such process. The main stages that cells undergo after attachment are radial growing of filopodia, cytoplasmatic networking, and a sequential flattening of the cell mass [51, 52]. Figure 5.11 shows the SEM micrographs of osteoblast-like MG63 cells cultured on n-HApCS-$scCO_2$-75/75 samples after 1, 7, 14 and 21 days. It can be observed how the cells changed from a roundish morphology from day 1 to a spindle-like shape on day 7. At day 14, flattening of the cells is evident. Moreover, it is observed how the cells presented good adherence to the scaffold, as well as filopodial-like growth along the 21 days. At day 7 the cells already started forming continuous cell layers, and by days 14 and 21 the scaffold was almost completely covered by cell layers, spreading in its surface and inside the pores.

Cell viability and proliferation results evaluated by resazurin assay are shown in Figure 5.12, given in terms of fluorescence intensity, which is proportional to resorufin content. Despite a slight drop registered at the third day, which can be considered a normal phenomenon, cells exhibited good viability and proliferation, with a gradual increase in fluorescence intensity. Moreover, a 5-fold increase in the cell proliferation was registered from day 3 to day 21, which is a promising outcome. Thus, the n-HApCS-$scCO_2$-75/75 scaffolds appear to be cytocompatible, osteoconductive and allow the adhesion of osteoblast-like cells to its surface.

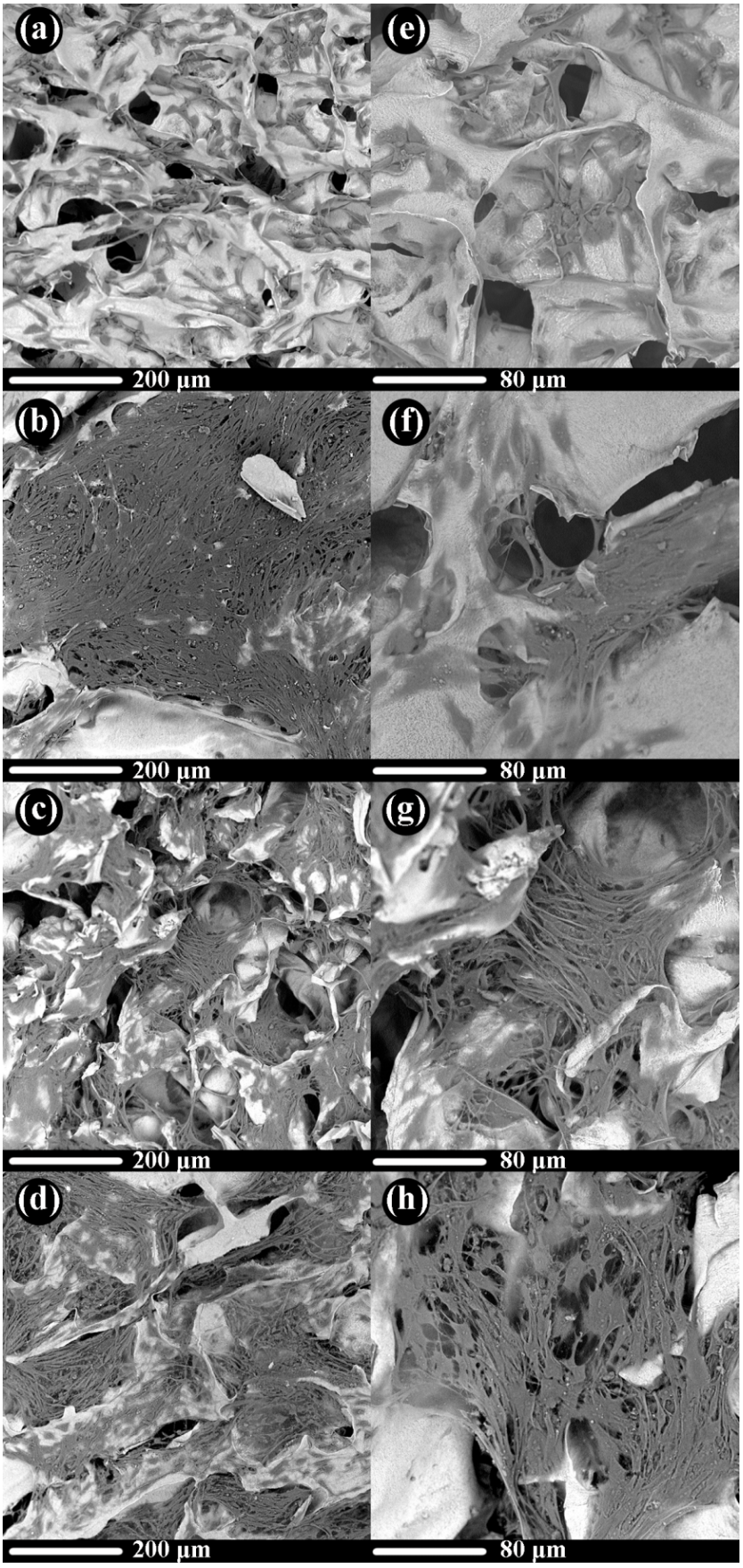

Figure 5.11. SEM micrographs of osteoblast-like MG63 cells cultured on n-HApCS-scCO$_2$-75/75 samples after 1 day (a, e); 7 days (b, f); 14 days (c, g); 21 days (d, h). Magnification: 410X (a, b, c and d); 1000X (e, f, g and h)

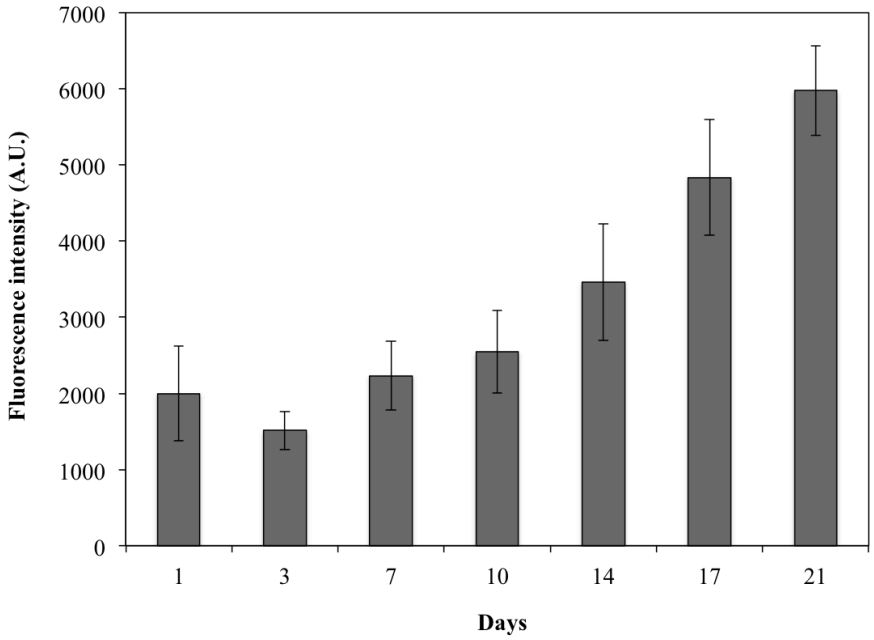

Figure 5.12. Fluorescence intensity obtained through rezasurin assay indicating cell proliferation of osteoblast-like MG63 cells in control and n-HApCS-scCO$_2$-75/75 culture for time-points ranging from 1 to 21 days

Similar results were published recently by Qasim *et al.* (2015) [53], who seeded MG63 osteoblasts on a CS/HAp (50:50) porous membrane and evaluated cellular viability by Alamar blue assay, showing a significant increase from 1 to 7 days culture. Lai *et al.* (2015) [54] also reported a gradual enhancement on the number of viable cells of human bone marrow-derived mesenchymal stem cells (hMSCs) seeded on CS/silk fibroin/n-HAp nanofibrous membranes (10 or 30 wt.% n-HAp). In the reports described the proportion of n-HAp in the biomaterial composition is lower than the n-HAp/CS ratio (70/30) of the present study; however, they evidence that materials combining n-HAp and chitosan are cytocompatible, osteoconductive and allow the adhesion of osteoblast-like cells to the biomaterial surface. Furthermore, it is worth noting that in both reports samples were disinfected by immersion in ethanol solution prior the cytotoxicity test, whereas in the present study, the rezasurin assay was carried out with the n-HApCS-scCO$_2$-75/75 sample without any disinfection or sterilization treatment, confirming its sterility.

5.4 Conclusions

In this work, a simple 3-step process to produce HAp/CS hybrid scaffolds was developed. Sterilization conditions were considered for the optimization of the process; thus, with an extraction yield of 80%, it was determined that the optimal $scCO_2$ extraction conditions are two 2-hour cycles in static mode at temperature 75 °C and pressure 8.0 MPa. The produced scaffolds presented a storage modulus of (20.5 ± 2.9) kPa at 1 Hz frequency and elastic properties. Moreover, the scaffolds contained highly pure nanocrystalline HAp, and mimic the structure and composition of bone extracellular matrix, exhibited adequate micro- and macroporosity, interconnected structure, and fast swelling, which are highly desirable features for bone regeneration.

Based on the results obtained from this study it was shown that, opposed to the other purification procedures used, it was possible to preserve the structure fixed by the first freeze-drying step, and the salt impurities derived from the neutralization procedures with NaOH were avoided using the $scCO_2$ extraction. Also, the final freeze-drying step required with the alternative neutralization procedures was, in this case, eliminated. To reinforce the potential of the developed process, it must be highlighted that the use of $scCO_2$ as an innovative sterilization technique has been recently studied and proven viable [21-26].

Even though additional studies are necessary to validate the used $scCO_2$ extraction conditions for the sterilization of the scaffolds, preliminary results presented in this work are promising. Results from the microbiological assay showed no microbial growth, evidencing that the produced n-HApCS-$scCO_2$-75/75 scaffolds were sterile, enabling the adhesion and proliferation of osteoblastic cells. The biomaterial allowed cellular proliferation, which increased gradually along the experimental period. Moreover, cells with normal morphology, a tendency for pores colonization and the existence of organized cell groups, increasing in extension along the culture period, were observed.

Therefore, sterile n-HAp/CS scaffolds, with desirable properties for the treatment of small, non-load-bearing bone defects, were successfully produced by a simple 3-step process, consisting of: (1) preparation of homogeneous and stable n-HAp/CS dispersion by fast stirring; (2) freeze-drying for the elimination of the solvent and fixation of the microstructure; and (3) purification, with potential sterilization capacity, of the scaffolds using supercritical CO_2 ($scCO_2$) extraction.

5.5 References

[1] Bose, S., M. Roy, and A. Bandyopadhyay. *Recent advances in bone tissue engineering scaffolds.* Trends in Biotechnology, 30, 546-554 (2012).

[2] Brydone, A., D. Meek, and S. Maclaine. *Bone grafting, orthopaedic biomaterials, and the clinical need for bone engineering.* Proceedings of the Institution of Mechanical Engineers, Part H: Journal of Engineering in Medicine, 224, 1329-1343 (2010).

[3] O'Brien, F.J. *Biomaterials & scaffolds for tissue engineering.* Materials Today, 14, 88-95 (2011).

[4] Levengood, S.K.L. and M. Zhang. *Chitosan-based scaffolds for bone tissue engineering.* J. Mater. Chem. B, 2, 3161 (2014).

[5] Dorozhkin, S.V. *Biocomposites and hybrid biomaterials based on calcium orthophosphates.* Biomatter, 1, 3-56 (2011).

[6] Dhandayuthapani, B., et al. *Polymeric Scaffolds in Tissue Engineering Application: A Review.* International Journal of Polymer Science, 2011, (2011).

[7] Peniche, C., et al. *Chitosan/hydroxyapatite-based composites.* Biotecnología Aplicada, 27, 202-210 (2010).

[8] Costa-Pinto, A.R., R.L. Reis, and N.M. Neves. *Scaffolds based bone tissue engineering: the role of chitosan.* Tissue Eng Part B Rev, 17, 331-47 (2011).

[9] Wei, G. and P.X. Ma. *Structure and properties of nano-hydroxyapatite/polymer composite scaffolds for bone tissue engineering.* Biomaterials, 25, 4749-57 (2004).

[10] Thein-Han, W.W. and R.D.K. Misra. *Biomimetic chitosan–nanohydroxyapatite composite scaffolds for bone tissue engineering.* Acta Biomaterialia, 5, 1182-1197 (2009).

[11] Zhao, F., et al. *Preparation and histological evaluation of biomimetic three-dimensional hydroxyapatite/chitosan-gelatin network composite scaffolds.* Biomaterials, 23, 3227-3234 (2002).

[12] Jiang, L., et al. *Preparation and properties of nano-hydroxyapatite/chitosan/carboxymethyl cellulose composite scaffold.* Carbohydrate Polymers, 74, 680-684 (2008).

[13] Kong, L., et al. *Preparation and characterization of nano-hydroxyapatite/chitosan composite scaffolds.* Journal of Biomedical Materials Research Part A, 75A, 275-282 (2005).

[14] Kong, L., et al. *A study on the bioactivity of chitosan/nano-hydroxyapatite composite scaffolds for bone tissue engineering.* European Polymer Journal, 42, 3171-3179 (2006).

[15] Oliveira, J.M., et al. *Novel hydroxyapatite/chitosan bilayered scaffold for osteochondral tissue-engineering applications: Scaffold design and its performance when seeded with goat bone marrow stromal cells.* Biomaterials, 27, 6123-6137 (2006).

[16] Sultana, N., et al. *Chitosan-based nanocomposite scaffolds for tissue engineering applications.* Materials and Manufacturing Processes, 30, 273-278 (2015).

[17] Barile, F.A., *Principles of Toxicology Testing, Second Edition.* 2013: CRC Press.

[18] He, Q., et al. *Preparation of chitosan films using different neutralizing solutions to improve endothelial cell compatibility.* Journal of Materials Science: Materials in Medicine, 22, 2791-2802 (2011).

[19] Madihally, S.V. and H.W.T. Matthew. *Porous chitosan scaffolds for tissue engineering.* Biomaterials, 20, 1133-1142 (1999).

[20] Seda Tığlı, R., A. Karakeçili, and M. Gümüşderelioğlu. *In vitro characterization of chitosan scaffolds: influence of composition and deacetylation degree.* Journal of Materials Science: Materials in Medicine, 18, 1665-1674 (2007).

[21] Checinska, A., et al. *Sterilization of biological pathogens using supercritical fluid carbon dioxide containing water and hydrogen peroxide.* Journal of Microbiological Methods, 87, 70-75 (2011).

[22] Hemmer, J.D., et al. *Sterilization of bacterial spores by using supercritical carbon dioxide and hydrogen peroxide.* Journal of Biomedical Materials Research Part B: Applied Biomaterials, 80B, 511-518 (2007).

[23] White, A., D. Burns, and T.W. Christensen. *Effective terminal sterilization using supercritical carbon dioxide.* Journal of Biotechnology, 123, 504-515 (2006).

[24] Zani, F., et al. *Sterilization of corticosteroids for ocular and pulmonary delivery with supercritical carbon dioxide.* International Journal of Pharmaceutics, 450, 218-224 (2013).

[25] Zhang, J., et al. *Sterilizing Bacillus pumilus spores using supercritical carbon dioxide.* Journal of Microbiological Methods, 66, 479-485 (2006).

[26] Zhang, J., et al. *Sterilization using high-pressure carbon dioxide.* The Journal of Supercritical Fluids, 38, 354-372 (2006).

[27] Duarte, A.R.C., J.F. Mano, and R.L. Reis. *Perspectives on: supercritical fluid technology for 3d tissue engineering scaffold applications.* Journal of Bioactive and Compatible Polymers, 24, 385-400 (2009).

[28] Quirk, R.A., et al. *Supercritical fluid technologies and tissue engineering scaffolds.* Current Opinion in Solid State and Materials Science, 8, 313-321 (2004).

[29] Duarte, A.R.C., J. Mano, and R. Reis. *Supercritical fluids in biomedical and tissue engineering applications: a review.* International Materials Reviews, 54, 214-222 (2009).

[30] Ruphuy, G., et al. *Spray drying as a viable process to produce nano-hydroxyapatite/chitosan (n-HAp/CS) hybrid microparticles mimicking bone composition.* Advanced Powder Technology, 27, 575-583 (2016).

[31] Gomes, P.B., V.G. Mata, and A.E. Rodrigues. *Production of rose geranium oil using supercritical fluid extraction.* The Journal of Supercritical Fluids, 41, 50-60 (2007).

[32] Spilimbergo, S., et al. *Inactivation of Bacillus subtilis spores by supercritical CO2 treatment.* Innovative Food Science & Emerging Technologies, 4, 161-165 (2003).

[33] *NIST Reference Fluid Thermodynamic and Transport Properties Database. REFPROP version 7.* 2016, U.S. Secretary of Commerce on behalf of the United States of America.

[34] Rodrigues, S.C., et al. *Preparation and characterization of collagen-nanohydroxyapatite biocomposite scaffolds by cryogelation method for bone tissue engineering applications.* Journal of Biomedical Materials Research Part A, 101A, 1080-1094 (2013).

[35] Zhu, J. and R.E. Marchant. *Design properties of hydrogel tissue-engineering scaffolds.* Expert review of medical devices, 8, 607-626 (2011).

[36] Amit, S.M., S. Xinfeng, and G.M. Antonios, *Nanocomposite Scaffolds for Tissue Engineering*, in *Tissue Engineering and Artificial Organs*, J.D. Bronzino, Editor. 2006, CRC Press. p. 40-1-40-11.

[37] Agrawal, C. and R.B. Ray. *Biodegradable polymeric scaffolds for musculoskeletal tissue engineering.* Journal of biomedical materials research, 55, 141-150 (2001).

[38] Lan Levengood, S.K., et al. *The effect of BMP-2 on micro- and macroscale osteointegration of biphasic calcium phosphate scaffolds with multiscale porosity.* Acta Biomaterialia, 6, 3283-3291 (2010).

[39] Polak, S.J., et al. *Analysis of the roles of microporosity and BMP-2 on multiple measures of bone regeneration and healing in calcium phosphate scaffolds.* Acta Biomaterialia, 7, 1760-1771 (2011).

[40] Woodard, J.R., et al. *The mechanical properties and osteoconductivity of hydroxyapatite bone scaffolds with multi-scale porosity.* Biomaterials, 28, 45-54 (2007).

[41] Klenke, F.M., et al. *Impact of pore size on the vascularization and osseointegration of ceramic bone substitutes in vivo.* Journal of Biomedical Materials Research Part A, 85A, 777-786 (2008).

[42] Rathke, T.D. and S.M. Hudson. *Review of chitin and chitosan as fiber and film formers.* Journal of Macromolecular Science, Part C: Polymer Reviews, 34, 375-437 (1994).

[43] Berger, J., et al. *Structure and interactions in covalently and ionically crosslinked chitosan hydrogels for biomedical applications.* European Journal of Pharmaceutics and Biopharmaceutics, 57, 19-34 (2004).

[44] Oryan, A., et al. *Bone regenerative medicine: classic options, novel strategies, and future directions.* Journal of Orthopaedic Surgery and Research, 9, 1-27 (2014).

[45] Hannink, G. and J.J.C. Arts. *Bioresorbability, porosity and mechanical strength of bone substitutes: What is optimal for bone regeneration?* Injury, 42, Supplement 2, S22-S25 (2011).

[46] Pilia, M., T. Guda, and M. Appleford. *Development of Composite Scaffolds for Load-Bearing Segmental Bone Defects.* BioMed Research International, 2013, 15 (2013).

[47] Garner, E., et al. *Viscoelastic Dissipation in Compact Bone: Implications for Stress-Induced Fluid Flow in Bone.* Journal of Biomechanical Engineering, 122, 166-172 (1999).

[48] Malafaya, P.B., et al. *Morphology, mechanical characterization and in vivo neo-vascularization of chitosan particle aggregated scaffolds architectures.* Biomaterials, 29, 3914-3926 (2008).

[49] Mano, J.F. *Viscoelastic properties of bone: Mechanical spectroscopy studies on a chicken model.* Materials Science and Engineering: C, 25, 145-152 (2005).

[50] Mano, J.F. *Viscoelastic Properties of Chitosan with Different Hydration Degrees as Studied by Dynamic Mechanical Analysis.* Macromolecular Bioscience, 8, 69-76 (2008).

[51] Rajaraman, R., et al. *A scanning electron microscope study of cell adhesion and spreading in vitro.* Experimental Cell Research, 88, 327-339 (1974).

[52] Tao, C.-T. and T.-H. Young. *Polyetherimide membrane formation by the cononsolvent system and its biocompatibility of MG63 cell line.* Journal of Membrane Science, 269, 66-74 (2006).

[53] Qasim, S.B., et al. *Freeze gelated porous membranes for periodontal tissue regeneration.* Acta Biomaterialia, 23, 317-328 (2015).

[54] Lai, G.-J., K.T. Shalumon, and J.-P. Chen. *Response of human mesenchymal stem cells to intrafibrillar nanohydroxyapatite content and extrafibrillar nanohydroxyapatite in biomimetic chitosan/silk fibroin/nanohydroxyapatite nanofibrous membrane scaffolds.* International Journal of Nanomedicine, 10, 567-584 (2015).

6 Final remarks

In this work, hybrid materials based on highly pure nano-hydroxyapatite were successfully produced. For that, HAp nanoparticles were embedded in an organic component, chitosan, in order to generate materials mimicking bone composition and with suitable properties. Due to the similarity with the mineral phase of the bone, together with the exceptional biocompatibility and bioactivity with respect to bone cells and surrounded tissues, hydroxyapatite has been studied, since long, for bone tissue engineering applications. Its combination with chitosan presents several advantages imparted by this polymer's particular features, which add value to the resulting hybrid materials. Among the most outstanding properties of chitosan, its hydrophilic character can promote osteoblast adhesion and proliferation leading to better material-cell interactions. In addition, chitosan exhibits bio-adhesiveness (of special interest for drug delivery systems), antimicrobial capacity, can be processed under mild conditions, generates non-toxic biodegradation products, and is available in large quantities and adequate commercial grades.

Three forms of n-HAp/CS hybrid materials, having in view different potential applications, were produced: dispersions, powders (microparticles), and scaffolds. In order to obtain such products, the following main processing stages were considered: (1) dispersion preparation in which n-HAp is incorporated into the chitosan solution; (2) phase separation/solvent elimination in which the fixation of structural forms as microparticles and scaffolds takes

place; and (3) purification and potential sterilization procedures. Different compositions, parameters and processing conditions were evaluated in order to achieve adequate properties of the final products.

The dispersion preparation was carried out by physically mixing the HAp nanoparticles with the chitosan solution. Even though this is a simple and straightforward approach, the incorporation of HAp nanoparticles into an acidic environment (chitosan solution) can influence HAp solubility, phase stability and surface chemistry. Therefore, in a first study, dispersions of HAp nanoparticles were prepared by ultrasonication, alone or in the presence of chitosan, aiming to study the effect of different parameters (pH, chitosan content, presence of KCl and storage time) on the resulting dispersion's particle size and electrostatic stability (zeta potential).

One of the most important parameters, affecting particle size and zeta potential, is the pH. It was determined that in an alkaline environment (pH 9-10), dispersions of n-HAp alone exhibited good zeta potential values (+29 mV), but decreasing as the pH decreases. This behavior was mainly attributed to changes on surface charge by differential ion dissolution mechanism induced by pH variations. In the presence of chitosan, the opposite behavior was observed. In this case, the observed tendency was attributed to both, the changes on HAp surface charge by differential ion dissolution mechanism and the adsorption of positively charged chitosan molecules onto HAp nanoparticles surface. Therefore, in slightly acidic environment (pH 5.5) the electrostatic stability of n-HAp particles dispersed in water was poor (zeta potential +10 mV), but improving with the incorporation of chitosan (zeta potential >+30 mV).

Additionally, results indicated that n-HAp dispersions in the presence of chitosan (pH 5.5) result in, comparatively with their aqueous counterparts, larger particle sizes, and that particle size increases with chitosan content. However, zeta potential also increases with chitosan content showing that, even when its presence promotes particle agglomeration, chitosan acts as a good stabilizer of HAp nanoparticles in slightly acidic environment (pH 5.5). Such good stability was proven to be consistent along time, since zeta potential remained nearly constant along 30 days of storage time. Relative to KCl, while no significant influence on particle size was observed, an improvement on zeta potential due to its presence

was observed in the n-HAp aqueous dispersions. Nevertheless, the stabilizing effect of chitosan appeared to be better without the interference of salts.

Taken into consideration these results, a method for the preparation of n-HAp/CS dispersions by fast stirring (ultraturrax) was developed. With mixing times <100 ms, the used fast stirring set up is energetically more efficient than ultrasonication, allowing the production of n-HAp/CS dispersions (pH 5.5) with smaller particle sizes, and similar zeta potential values (>+30 mV). The produced dispersions were highly homogeneous and stable and, the ones using HAp/CS weight ratio of 70/30 and n-HAp concentration of 20 g/l, were found suitable materials for the production of n-HAp/CS hybrids in different forms, the topic of this work. Additionally, they have potential to be used in other applications such as coating of implants by electrophoretic deposition, for example. The developed method and formulation can be adapted to further produce the n-HAp/CS dispersions in continuous mode using technologies such as the NETmix reactor. This is an interesting perspective having in view a future industrialization of the process.

The production of n-HAp/CS microparticles was carried out by spray drying. This technique is advantageous due to its easy industrialization, cost-effectiveness and continuous production; however, it was found to be underexploited in what respects the production of n-HAp/CS microparticles. The effect of pH of the n-HAp/CS dispersion (5.5 and 7.0), as well as the presence of KCl, on the final n-HAp/CS microparticle's properties were studied. SEM images showed that KCl appeared as a contaminant on the formed microparticles, exhibiting different morphology depending on the pH of the n-HAp/CS dispersion, microcrystals in sample n-HApCS-5.5 and spikes in sample n-HApCS-7.0. In addition, it was confirmed that KCl has no beneficial effect on the stability of the n-HAp/CS dispersions; even risks creating a hypertonic environment able to cause an inhibitory effect on cells metabolism. Thus, removal of KCl was achieved by a simple washing procedure of the n-HAp original paste, before preparing the n-HAp/CS dispersions.

The generated microparticles presented differences depending on the pH at which the n-HAp/CS dispersion was prepared. Doughnut-like n-HApCS-5.5 microparticles, with 15.8 μm average size in volume incorporating n-HAp particles homogenously distributed, were found preferred over n-HApCS-7.0 microparticles; the late ones require one step more in the productive process and presented a tendency to form large agglomerates. Finally,

thermogravimetric analysis evidenced that chitosan was not degraded during the spray-drying process at the used conditions; therefore, hybrid n-HAp/CS microparticles containing 50-nm HAp nanoparticles were produced successfully by spray drying. The produced microparticles are advantageous, as they allow HAp's superior properties at the nanoscale to be preserved in the form of microparticles that are easier to handle thanks to their reduced size. In addition, they can be suitable materials to develop injectable systems or be shaped into solid substrates with increased surface area that will promote chemical and biological activity. Furthermore, the produced n-HAp/CS hybrid microparticles present potential as drug delivery systems; they can be further loaded with active pharmaceutical ingredients (API), such as anti-cancer or anti-inflammatory drugs, or with bone growth factors, such as BMP-2. The resulting loaded n-HAp/CS microparticles can be used to produce embedded scaffolds with dual function, 3D structural support for cell invasion and angiogenesis, and for controlled drug delivery.

The n-HAp/CS dispersions were also used in this work to produce n-HAp/CS hybrid scaffolds. For that, a simple 3-step production process was developed and proven to be advantageous over other existing methods. The process consists in: (1) n-HAp/CS dispersion preparation; (2) freeze-drying stage to fix scaffold shape; and (3) supercritical CO_2 ($scCO_2$) extraction to remove acetic acid and promote sterilization. From the different $scCO_2$ extraction conditions tested, the best-achieved ones were two 2-hour cycles at T = 75 °C and P = 8.0 MPa. Using such conditions, 80% of residual acetic acid was successfully removed, proving that $scCO_2$ extraction is a suitable purification procedure, with the advantage of not compromising the microarchitecture achieved by freeze-drying unlike other tested methods based on neutralization with alkaline solutions.

In addition, the developed process requires fewer steps than other conventional processes, with the benefit of being able to purify and potentially sterilize the scaffolds, all in one step (using $scCO_2$ extraction). The produced n-HAp/CS scaffolds mimic bone composition, are composed of highly pure HAp nanoparticles, and displayed desirable features for bone regeneration; namely, adequate interconnected porous structure with both micro- (<50 μm) and macroporosity (>100 μm), a mean pore size of (72 ± 35) μm, and fast swelling. In addition, the scaffolds exhibited elastic properties and can be cut and shaped into different geometries. With a storage modulus of (20.5 ± 2.9) kPa at 1 Hz, the scaffolds find application as cancellous bone graft, being suitable for non-load bearing applications, e.g.

treatment of small defects such as non-union fractures, maxillofacial and dental defects, and spinal fusion. The improvement of mechanical properties can be attempted by using n-HAp/CS dispersions with higher solid content (more concentrated dispersions) to produce the scaffolds, and/or use different HAp/CS weight ratios.

The microbiological test carried out revealed no microbial growth, showing that the scaffolds were sterile; and the resazurin assay showed that the produced scaffolds were cytocompatible and osteoconductive, allowing the adhesion and proliferation of osteoblast-like cells to its surface and within the pores. Based on the obtained results, the developed 3-step process has great potential to produce ready-to-use n-HAp/CS scaffolds mimicking bone composition and structure.

A Nano-hydroxyapatite based aqueous dispersions: Solutions preparation, mean free path and energy balance

A.1 Solutions preparation

A chitosan solution 3% (w/v) in acetic acid 1% (v/v) was prepared and diluted if needed using an acetate buffer 0.05 mol/l (CH_3COOH/CH_3COONa). The buffer was prepared by mixing adequate quantities of CH_3COOH (1 mol/l) and NaOH (1 mol/l) for the desired pH, which were calculated based on Henderson-Hasselbach equation (A.1) and the chemical reaction:

$$CH_3COOH + NaOH \rightarrow CH_3COONa + H_2O$$

$$pH = pKa + \log\left(\frac{\left|CH_3COO^-\right|}{\left|CH_3COOH\right|}\right) \tag{A.1}$$

Thus, the quantities used to prepare 1000 ml of acetate buffer 0.05 mol/l (CH3COOH/CH3COONa) with different pH values are shown in Table A.1.

Table A.1. Calculated volume of reagents needed to prepare 1000 ml of acetate buffer 0.05 mol/l

Desired pH	Volume of CH_3COOH 5M (ml)	Volume of NaOH 4M (ml)
5.0	10.0	7.90
5.5	10.0	10.6
6.0	10.0	11.8

Furthermore, aqueous nanodispersions of hydroxyapatite (HAp), alone or in the presence of chitosan (CS), were prepared at different concentrations as shown in Table A.2 and Table A.3 for the corresponding free mean path $\Delta x / L$ calculated based on Fonte (2013) [1].

Table A.2. Volume of solutions added to prepare 50 ml of aqueous nanodispersion of HAp alone

Mean free path $\Delta x / L$ **(adim)**	**Concentration of HAp (g/l)**	**Volume to add (ml)**	
		HAp paste 15%	**Acetate buffer (pH~5.5)**
3.0	1.6	0.50	49.9
1.5	6.4	2.1	47.5
0.70	20	7.0	43

Table A.3. Volume of solutions added to prepare 50 ml of aqueous nanodispersion of HAp in the presence of chitosan

Mean free path $\Delta x / L$ **(adim)**	**Concentration of HAp (g/l)**	**Volume to add (ml)**		
		HAp paste 15%	**Chitosan solution 3%***	**Acetate buffer (pH~5.5)**
3.0	1.6	0.50	1.1	48
1.5	6.4	2.1	4.5	43
0.70	20	7.0	14	29

A.2 Mean free path

Rod-like HAp nanoparticles were approximated to a cylindrical shape, as shown in Figure A.1.

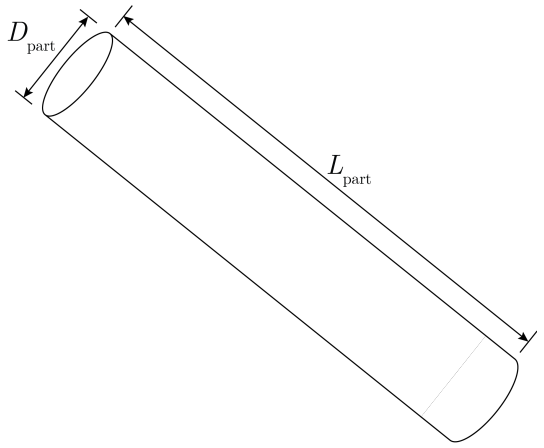

Figure A.1. Geometrical approximation considered for HAp nanoparticles (Reproduced from Fonte (2013) [1])

For a HAp nanoparticle with diameter D_{part} and length L_{part}, its volume is calculated as:

$$V_{part} = \frac{\pi}{4} D_{part}^2 L_{part} \tag{A.2}$$

By dividing the total volume of HAp nanoparticles by the volume of a single particle, the total number of particles (N_{part}) in dispersion can be estimated:

$$N_{part} = \frac{m_{HAp}}{\rho_{HAp}} \frac{4(L_{part}/D_{part})^2}{\pi L_{part}^3} \tag{A.3}$$

Where the total volume of HAp nanoparticles is obtained by dividing the total mass of HAp in dispersion (m_{HAp}) by the density of HAp (ρ_{HAp}).

Considering the volume of the dispersion (V_{dis}) the same as the volume of a cube in which the total number of particles is evenly distributed, then, the distribution of the particles in an edge of such cube is described as:

$$\left(N_{part}\right)^{1/3} L_{part} + \left(N_{part}\right)^{1/3} \Delta x_{part} = \left(V_{dis}\right)^{1/3} \tag{A.4}$$

Thus, the distance between particles, Δx_{part}, can be deduced as:

$$\begin{aligned} \frac{\Delta x_{part}}{L_{part}} &= \left(\frac{\pi}{4}\right)^{1/3} \left(\frac{V_{dis}\rho_{HAp}}{m_{HAp}}\right)^{1/3} \left(\frac{D_{part}}{L_{part}}\right)^{2/3} - 1 \\ \frac{\Delta x_{part}}{L_{part}} &= \left(\frac{\pi}{4}\right)^{1/3} \left(\frac{\rho_{HAp}}{C_{HAp} \cdot M_{HAp}}\right)^{1/3} \left(\frac{D_{part}}{L_{part}}\right)^{2/3} - 1 \end{aligned} \tag{A.5}$$

Where C_{HAp} and M_{HAp} are the concentration of HAp in the dispersion and its molar mass respectively.

A.3 Energy balance

The energy absorbed by the samples as heat was estimated using equation (A.6):

$$E_{abs} = m_{dis} \cdot C_P \cdot \Delta T \tag{A.6}$$

Where m is the mass of the sample; C_P the heat capacity of the sample, calculated using equation (A.7) in which x_i is the molar fraction of the different species present in the dispersion, and ΔT is the temperature increased estimated from the data obtained from the temperature measurements before and after ultrasonication was applied.

$$C_P = \sum \left(x_i \cdot C_{Pi}\right) \tag{A.7}$$

The mass (m_{dis}) of the sample was calculated as:

$$m_{dis} = \rho_{dis} \cdot V_{dis} \tag{A.8}$$

Where ρ_{dis} and V_{dis} are the density and volume of the n-HAp/CS hybrid dispersion respectively. The density was estimated according to the next equation:

$$\rho_{dis} = \frac{\sum m_i}{\sum \left(\frac{m_i}{\rho_i} \right)} \tag{A.9}$$

Where the symbols m_i and ρ_i correspond to the mass and density of the different species present in the dispersion, i.e. HAp, chitosan and buffer respectively. In the case of the buffer, data for water was consider.

The energy input (E_{in}), given by the energy delivered to the sample through the ultrasonication probe, was used to calculate the energy loss (E_{loss}) by doing an energy balance. The energy loss was calculated per mass of sample (m_{dis}) in J/g:

$$E_{loss} = \frac{E_{in} - E_{abs}}{m_{dis}} \tag{A.10}$$

A.4 References

[1] Pereira da Fonte, C.M., The NETmix Reactor: Application to High Added-Value Products, in Chemical and Biological Engineering. 2013, University of Porto: FEUP: Porto, Portugal.

B Dispersions preparation by fast stirring: Mixing time and energy input

B.1 Pump calibration

The pump used in the preparation of n-HAp/CS dispersions by fast stirring was calibrated by measuring per triplicate the volume and time at different flow rates. The calibration curve is shown in Figure B.1 and data obtained is presented in Table B.1.

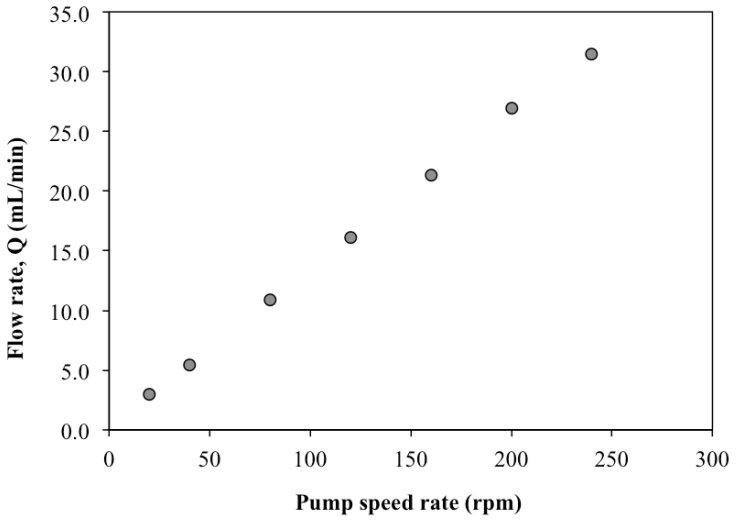

Figure B.1. Calibration curve obtained for the pump used in the preparation of n-HAp/CS dispersions by fast stirring

Table B.1. Calibration data

Speed (rpm)	Q (ml/min)
20	3.0 ± 0.3
40	5.4 ± 0.9
80	11 ± 0.8
120	16 ± 0.9
160	21 ± 0.0
200	27 ± 0.9
240	32 ± 0.0

B.2 Determination of mixing time

The mixing system was designed such that the HAp paste was injected into the solution inside the vessel as shown in Figure B.2.

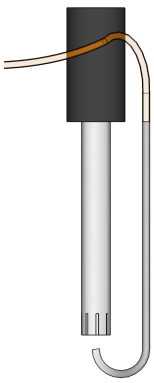

Figure B.2 Mixing scheme

A video using the same system was taken in order to estimate the mixing time. The number of frames in which one droplet comes out of the inlet tube, enters the mixing device and is dispersed (Figure B.3) was determined and related to the velocity of the movie (29,97 frames/second). Then, for a pumping rate of 120 rpm (~16 ml/min), one droplet is dispersed in the time the video runs 3 frames, which is 100 ms.

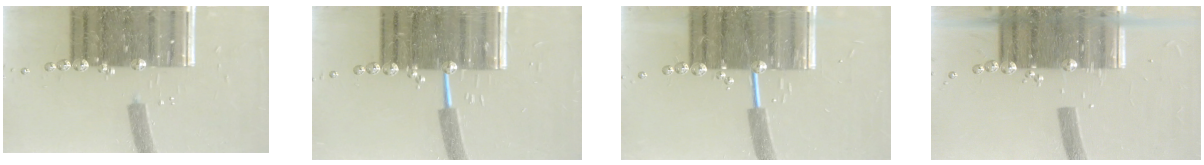

(a) (b) (c) (d)

Figure B.3 Estimation of mixing time: One droplet (a) right before coming out of the inlet tube; (b) coming out of the inlet tube; (c) entering the mixing device and; (d) being dispersed

Now, since the actual pump rate used to prepare the nanodispersions of this study was of 240 rpm (~32 ml/min), it is valid to affirm that the mixing time of the system used was less than 100 ms. The estimation of the mixing time using a pump rate of 240 rpm could not be carried out because it was not possible to observe clearly the dynamics of the drops on the video.

B.3 Energy input

The energy input, E_{in}, is the energy delivered to the sample through the fast stirring device used, Miccra D-9, in the preparation of the n-HAp/CS dispersions. It was calculated based on the power output of the device, according to the technical specifications given by the manufacturer (see Figure B.4). The time $t_{reaction}$ necessary to pump a volume of HAp paste, V_{HAp}, at a pump speed rate, $\dot{V}_{pump}$, into the reaction vessel containing the chitosan solution is:

$$t_{reaction} = \frac{V_{HAp}}{\dot{V}_{pump}} \tag{B.1}$$

6 Synopsis of technical data

Drive	MICCRA D-9	MICCRA D-15	MICCRAD-3 PA
Power input (watt)	850	1520	350
Power output (watt	495	900	200
Tension/Frequency (V/Hz)	230V AC / 50/60	230V AC / 50/60 110V AC / 50/60	12V DC (Battery)
Speed range (rpm)	11.000 - 39.000	8.800 - 33.600	18.000 (fixed)
Speed adjustment	yes	yes	no
Electronic stabilizer	yes	yes	no
Weight (kg)	1,4	2,0	1,6 (w. battery)
Dimensions (mm)	66 x 66 x 220	70 x 70 x 270	66 x 66 x 225
Protective system	IP 20	IP 20	IP 20
Safety class	II	II	II
Overload protection	Therm. sensor	Therm. sensor	no
Safety switch	yes	yes	no
Smooth start	yes	yes	no
CE	yes	yes	yes
Tools compatible with ART drives	all	all	all
Permiss. ambient temp.	5 - 50 °C	5 - 50 °C	5 - 50 °C
Permiss. ambient humid.	up to 85%	up to 85%	up to 85%
Noise level	max. 75 dB (A)	max. 75 dB (A)	max. 70 dB (A)
Warranty	5 years	5 years	5 years

Figure B.4 Technical specifications of the fast stirring device used, ultraturrax, given by the manufacturer
(Reproduced from ART Prozess & Labortechnik GmbH & Co [1])

With the speed rate of the pump, $\dot{V}_{pump}$, in given in volume per time units. Thus, the energy input, calculated per mass of sample (m_{dis}) in J/g, is:

$$E_{in} = \frac{t_{reaction} \cdot P_{output}}{V_{dis} \cdot \rho_{dis}} \qquad (A.2)$$

Where P_{output} is the power output of the device, V_{dis} and ρ_{dis} are the volume and density of the n-HAp/CS dispersion. The volume of HAp paste 15 wt.%, V_{HAp}, is determined following the calculations described in Appendix A, for $C_{HAp} = 20$ g/l and a HAp/CS mass ratio of

70/30. The density, ρ_{dis}, for a dispersion with the same characteristics is (993.7 ± 7.7) kg/m^3, expressed as (mean ± SD); it was determined experimentally per triplicate using a picnometer. Therefore, for $P_{output} = 495$ J/s, the energy input is E_{in} = 2.1 J/g of sample. Considering that the power output, $P_{output} = 495$ J/s, given by the manufacturer refers to the highest speed capacity of the device (39 000 rpm), and that the speed rate used experimentally was the lowest capacity (11 000 rpm), then the actual energy input is less than 2.1 J/g for the conditions used in this thesis.

B.4 References

[1] High-Speed Dispersion and Homogenizing Devices: Operating Manual, in MICCRA D-9, MICCRA D-15, MICCRA D-3/PA. 2010, ART Prozess & Labortechnik GmbH & Co.

C Determination of CO_2 mass

C.1 Density and mass of CO_2

Supercritical CO_2 density data was taken from NIST Reference Fluid Thermodynamic and Transport Properties Database [1]. Table C.1 shows density data for the used temperature and pressure.

Table C.1 Supercritical CO_2 density data

Temperature (ºC)	**Pressure (MPa)**	**Density (g/l)**
40	8.0	277.90
75	8.0	166.54

Determination of mass of CO_2 (m_{CO_2}) was estimated by multiplying its density (ρ_{CO_2}) times the volume (V_{CO_2}):

$$m_{CO_2} = \rho_{CO_2} \cdot V_{CO_2} \tag{C.1}$$

C.2 NIST Database

NIST National Institute of Standards and Technology | MATERIAL MEASUREMENT LABORATORY | Standard Reference Data Program | Data Gateway | Chemistry WebBook

Isobaric Properties for Carbon dioxide

- Fluid Data
- Auxiliary Data
- References
- Additional Information
- Important Information About This Data
- Notes
- **Other Data Available:**
  - View data in HTML table.
  - Download data as a tab-delimited text file.
  - Main NIST Chemistry WebBook page for this species.
  - Recommended citation for data from this page.
  - Fluid data for other species

Fluid Data

Isobaric Data for P = 8.0000 MPa

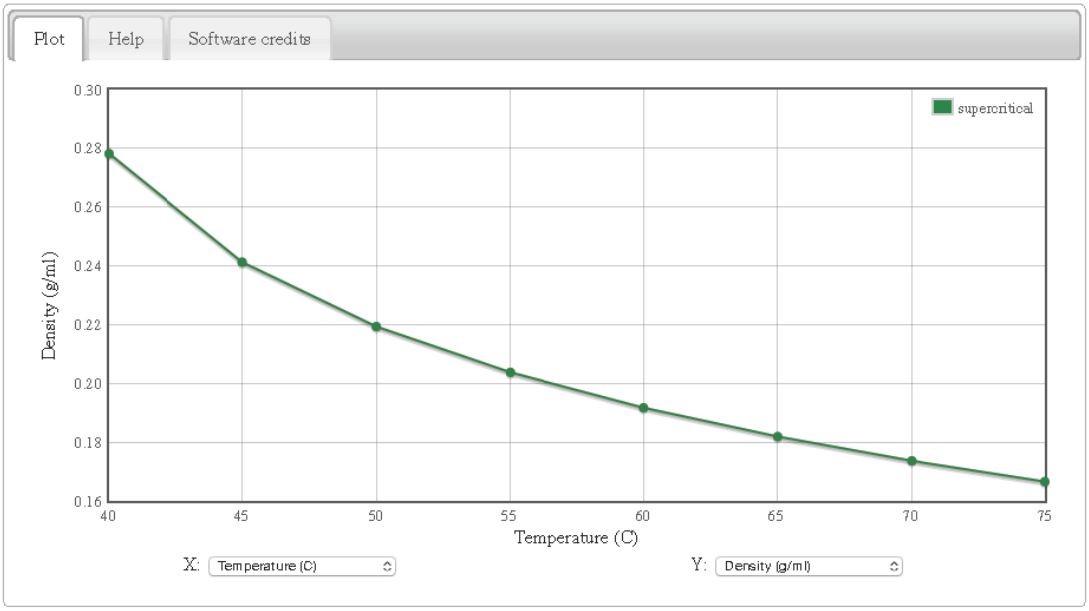

Auxiliary Data

Reference States

Internal energy	U = 0 at 273.16 K for saturated liquid.
Entropy	S = 0 at 273.16 K for saturated liquid.

Additional fluid properties

Critical temperature (T_c)	30.9782 C
Critical pressure (P_c)	7.3773 MPa
Critical density (D_c)	0.467600 g/ml
Acentric factor	0.22394
Normal boiling point	-78.40 C
Dipole moment	0.0 Debye

References

Equation of state, auxiliary model, melting curve, and sublimation curve

Span, R.; Wagner, W., *A New Equation of State for Carbon Dioxide Covering the Fluid Region from the Triple-Point Temperature to 1100 K at Pressures up to 800 MPa*, **J. Phys. Chem. Ref. Data**, 1996, 25, 6, 1509-1596. [doi:10.1063/1.555991] [all data]

Auxiliary model

Ely, J.F.; Magee, J.W.; Haynes, W.M., **Thermophysical properties for special high CO_2 content mixtures**, Research Report RR-110, Gas Processors Association, Tulsa, OK, 1987, 0. [all data]

Auxiliary model

McCarty, R.D., **Correlations for the Thermophysical Properties of Carbon Monoxide**, National Institute of Standards and Technology, Boulder, CO, 1989, 0. [all data]

Thermal conductivity

Vesovic, V.; Wakeham, W.A.; Olchowy, G.A.; Sengers, J.V.; Watson, J.T.R.; Millat, J., *The transport properties of carbon dioxide*, **J. Phys. Chem. Ref. Data**, 1990, 19, 3, 763-808. [doi:10.1063/1.555875] [all data]

Auxiliary model

Olchowy, G.A.; Sengers, J.V., *A simplified representation for the thermal conductivity of fluids in the critical region*, **Int. J. Thermophysics**, 1989, 10, 2, 417-426. [doi:10.1007/BF01133538] [all data]

Viscosity and auxiliary model

Fenghour, A.; Wakeham, W.A.; Vesovic, V., *The Viscosity of Carbon Dioxide*, **J. Phys. Chem. Ref. Data**, 1998, 27, 1, 31-44. [doi:10.1063/1.556013] [all data]

Surface tension

Rathjen, W.; Straub, J., *Temperature dependence of surface tension, coexistence curve, and vapor pressure of CO2, CClF3, CBrF3, and SF6* in **Heat Transfer in Boiling**, Academic Press, New York, 1977, 425-451. [all data]

Additional Information

Equation of state

At pressures up to 30 MPa and temperatures up to 523 K, the estimated uncertainty ranges from 0.03% to 0.05% in density, 0.03% (in the vapor) to 1% in the speed of sound (0.5% in the liquid) and 0.15% (in the vapor) to 1.5% (in the liquid) in heat capacity. Special interest has been focused on the description of the critical region and the extrapolation behavior of the formulation (to the limits of chemical stability).

Auxiliary model

Use of this Cp0 equation in conjunction with Ely's BWR will produce numbers identical to those calculated in NIST12, Version 3.0.

Thermal conductivity

Note: Vesovic et al. use a crossover equation of state to compute derivatives in the critical region; the default EOS is used here. Also, their "simplified" critical enhancement for thermal conductivity is used.

The uncertainty in thermal conductivity is less than 5%.

Viscosity

The uncertainty in viscosity ranges from 0.3% in the dilute gas near room temperature to 5% at the highest pressures.

Important Information About This Data

The data above are from an older version of the NIST Reference Fluid Thermodynamic and Transport Properties Database (REFPROP version 7). We will be updating our site to use the newer version (version 9.1) of this database in the the next couple of months. Information on REFPROP version 9.1 can be found here. REFPROP version 9.1 includes additional data and features not available from this site.

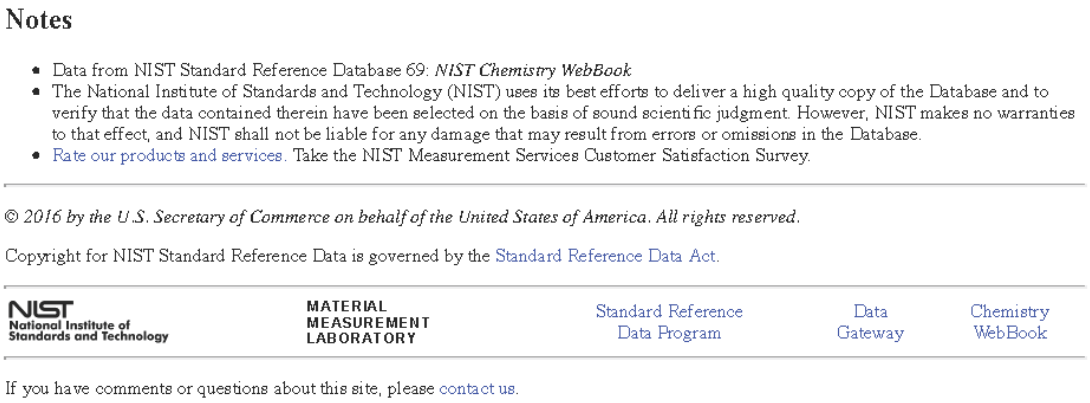

Notes

- Data from NIST Standard Reference Database 69: *NIST Chemistry WebBook*
- The National Institute of Standards and Technology (NIST) uses its best efforts to deliver a high quality copy of the Database and to verify that the data contained therein have been selected on the basis of sound scientific judgment. However, NIST makes no warranties to that effect, and NIST shall not be liable for any damage that may result from errors or omissions in the Database.
- Rate our products and services. Take the NIST Measurement Services Customer Satisfaction Survey.

NIST National Institute of Standards and Technology | MATERIAL MEASUREMENT LABORATORY | Standard Reference Data Program | Data Gateway | Chemistry WebBook

If you have comments or questions about this site, please contact us.

C.3 References

[1] NIST Reference Fluid Thermodynamic and Transport Properties Database. REFPROP version 7. 2016, U.S. Secretary of Commerce on behalf of the United States of America.